Coordination Chemistry Reviews 255 (2011) 1642–1685

Contents lists available at ScienceDirect

Coordination Chemistry Reviews

journal homepage: www.elsevier.com/locate/ccr

Review

Polyoxometalates containing late transition and noble metal atoms

Piotr Putaj, Frédéric Lefebvre*

Université Lyon 1, CPE Lyon, CNRS, UMR C2P2, LCOMS, Bâtiment CPE Curien, 43 Boulevard du 11 Novembre 1918, F-69616 Villeurbanne, France

Contents

Abbreviations: POM, polyoxometalate; Me, methyl; Et, ethyl; Bu, butyl; MeCN, acetonitrile; DMF, dimethylformamide; DMSO, dimethyl sulfoxide; COD, 1,5-cyclooctadiene; *p*-cym, *para*-cymene; Cp*, C_5Me_5; Cp, C_5H_5; OAc, CH_3COO^-; Bipym, bipyrimidyl; bipy, bipyridine; py, pyridine; 4atrz, 4-amino-1,2,4-triazole; trz, 1,2,4-triazole; 3atrz, 3-amino-1,2,4-triazole; tpyprz, tetra-2-pyridylpyrazine; Hfcz, fluconazole-[2-(2,4-difluorophenyl)-1,3-di(1*H*-1,2,4-triazol-1-yl)propan-2-ol]; phen, 1,10-phenanthroline; bhep, N,N′-bis(2-hydroxyethyl)piperazine; bppy, 5-(4-bromophenyl)-2-(4-pyridinyl)pyridine; dafo, 4,5-diazafluoren-9-one; nct, nicotinate; pz, pyrazine; phnz, phenazine.

* Corresponding author.
E-mail address: lefebvre@cpe.fr (F. Lefebvre).

0010-8545/$ – see front matter
doi:10.1016/j.ccr.2011.01.030

ARTICLE INFO

Article history:
Received 6 August 2010
Accepted 13 January 2011
Available online 3 February 2011

Keywords:
Polyoxometalate
Noble metal
Structure
Catalysis

ABSTRACT

This review describes the state of the art in the field of polyoxometalates containing noble metal atoms (ruthenium, rhodium, palladium, silver, osmium, iridium, platinum and gold). The structures of the various species are listed together with their applications (mainly in catalysis).

1. Introduction

Polyoxometalates have been known since the beginning of the XIXth century as it is generally admitted that the first compound of this class (the ammonium salt of $PMo_{12}O_{40}^{3-}$) was discovered by Berzelius in 1826 [1]. The first structural determination of the phosphotungstic anion was made by Keggin in 1934 [2] and during many years these compounds remained only laboratory curiosities. It is only at the end of the nineteen seventies that catalytic studies by many groups around the world put them in the light and now their applications have exploded in various domains such as analysis, biochemistry, non linear optics without omitting catalysis (see for example [3–19]).

From a structural point of view, the polyoxometalates can be considered as aggregates, generally anionic, with a structure

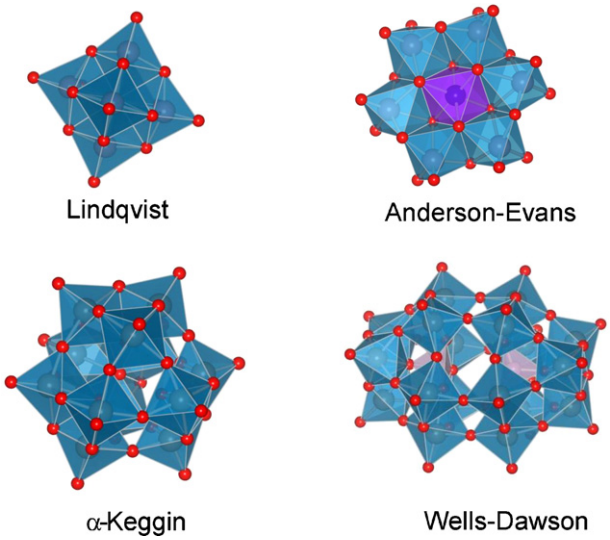

Fig. 1. Some classical structures of polyoxometalates.

formed by oxo species of transition metals with one or more bridging oxygen atoms. These structures contain at least three metal atoms, in most cases from groups 5 or 6 usually in their highest oxidation state with (heteropolyoxometalates) or without (isopolyoxometalates) heteroatoms. A lot of structures have been described, the most known being the Lindqvist, Anderson, Keggin and Dawson ones (Fig. 1). Most heteropolycompounds are based on molybdenum or tungsten while numerous isopolycompounds containing vanadium, niobium or tantalum have been described. Modification of these compounds can be made easily by removing M=O (mainly M = Mo or W) entities and replacing them by other transition metals. New structures were also obtained by joining two (or more) known structures via some transition metal ions. As a consequence, the number of compounds which can be prepared is very large and every day new structures are reported in the literature.

From the point of view of their applications in catalysis, on which we will focus more extensively in this review, polyoxometalates (and more precisely heteropolyoxometalates) are very interesting and display applications in fields such as acid catalysis and redox catalysis. Indeed, polyoxometalates with tungsten (and more particularly those displaying the Keggin structure) are highly acidic (at least as acidic as sulfuric acid) and they can then be applied in all catalytic reactions involving a strong (and naturally a weak) Brönsted acidity. Reactions such as the cracking or the isomerization of alkanes can then be catalyzed by heteropolyacids [20–25] and there are numerous reports of organic reactions catalyzed by acids which are efficiently made with polyoxometalates (see for example [26–31]). If the polyoxometalate is based on molybdenum, which can be reduced more easily than tungsten, it can be used in redox reactions as difficult as the oxidation of alkanes by oxygen or peroxides (see for example [32–38]). In order to tune these properties, other transition metal atoms are often introduced inside or outside the structure. A classical example is the replacement of one Mo=O group in the $[PMo_{12}O_{40}]^{3-}$ Keggin structure by a V=O group. The resulting $[PMo_{11}VO_{40}]^{4-}$ polyoxometalate is more active than its precursor in a lot of oxidation reactions. In this particular case the vanadium will simply modify the redox properties of the polyoxometalate but in some cases the metal atom will act by itself as a catalytic center and the polyoxometalate will serve essentially to give additional properties (redox, acidity, stabilization, etc.). One example is the titanium complex $[PW_{11}Ti(OH)O_{39}]^{4-}$ which is active for the epoxidation of alkenes with H_2O_2. In most cases, the metals used in catalysis are "noble" metals, a group which contains ruthenium, rhodium, palladium, silver, osmium, iridium, platinum and gold. When looking at the literature data, it is reasonable to say that at least one of these eight elements gives an active system whatever the catalytic reaction (if it needs a metal naturally). Their combination with polyoxometalates is not so evident and for example depending on the metal it will be possible or not to introduce a noble metal atom in a lacunary Keggin structure simply by mixing in solution these two species, and sometimes the result will be a completely different structure. As a consequence very often the syntheses are relatively difficult and lead to a lot of structures not observed with other transition metal atoms. The purpose of this review is to give an extended survey of these compounds and of their applications, mainly in catalysis.

2. Polyoxometalates containing ruthenium

A lot of polyoxometalates containing ruthenium were reported and even very recently new structures were described. For clarity we will describe them first as a function of the main metal in the polyoxometalate (vanadium, niobium, molybdenum or tungsten) and then as a function of its structure (Lindqvist, Keggin, Dawson, etc.). Quite the same scheme will be used for other paragraphs.

2.1. Polyvanadates

2.1.1. $[V_4O_{12}]^{4-}$

$[Ru^{II}(COD)(MeCN)_2(V_4O_{12})]^{2-}$ and $[Ru^{II}(COD)(MeCN)_2(HV_4O_{12})]^{-}$ were prepared by reaction of $[Ru(COD)Cl(MeCN)_3]PF_6$ with $(Bu_4N)VO_3$ or $(Bu_4N)_3HV_4O_{12}$, respectively, in acetonitrile [39]. These complexes were characterized by infrared and NMR spectroscopies and it was proposed that the polyanion acts as a bidentate ligand for the ruthenium metal, as observed for the rhodium, iridium and palladium derivatives, for which the crystal structures had been solved (see the corresponding sections).

2.1.2. Lindqvist structure $[V_6O_{19}]^{8-}$

$[\{Ru^{II}(p\text{-cym})\}_4(V_6O_{19})]$ was synthesized from $[Ru(p\text{-cym})Cl_2]_2$ and $NaVO_3$ in an aqueous solution and extracted with CH_2Cl_2 [40]. The four Ru(*p*-cym) moieties are attached on four alternate faces of the V_6O_{19} octahedron, via three bonds with three adjacent bridging oxygens (d_{Ru-O} = 2.082(4)–2.232(4) Å) (Fig. 2). Reaction with $[Ru(C_6Me_6)Cl_2]_2$ leads to the isomorphous $[\{Ru^{II}(C_6Me_6)\}_4(V_6O_{19})]$ compound. Both products are soluble in water and CH_2Cl_2. The rhodium and iridium analogues were also prepared (see below).

2.1.3. Other polyvanadates

The simple one-pot reaction of $NaVO_3$, NaH_2PO_4 and *cis*-$Ru(DMSO)_4Cl_2$ in buffer solution at pH = 4.8 resulted in a new mixed-valence polyvanadate: $[\{[Ru^{II}(DMSO)_3]_3PV^{V}{}_{11}V^{IV}Ru^{III}O_{37}(OH)_3\}_2]^{8-}$ [42]. This unprecedented open-structure consists of directly linked tetrahedra (PO_4, $V^{V}O_4$), square pyramids ($V^{V}O_5$) and octahedra ($V^{IV}O_6$, $Ru^{III}O_6$). Its outer surface is decorated with six $[Ru(DMSO)_3]^{2+}$ groups, each of them being linked to vanadium centers via 3 Ru–O bonds (Fig. 3). Note that in contrast to the above example, the interaction is made via terminal oxygen atoms.

2.2. Polyniobates

Hexaniobate clusters with 1, 2 and 4 organometallic moieties were synthesized from $[Ru(p\text{-cym})Cl_2]_2$ and $K_7HNb_6O_{19}$ in aqueous solutions [43]. It was noticed that increasing the number of grafted $[Ru(p\text{-cym})]^{2+}$ fragments led to a lower stability of the POM/Ru

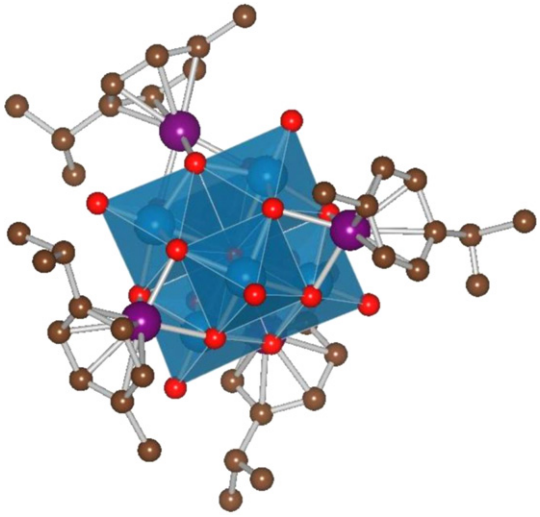

Fig. 2. Structure of $[\{Ru^{II}(p\text{-cym})\}_4(V_6O_{19})]$ (Ref. [40]). W = blue octahedra, O = red, Ru and other late transition metals in the scope of this article = violet, C = brown. All the other figures hold the same colour scheme if not indicated otherwise. Images were prepared using the VESTA crystallographic software [41].

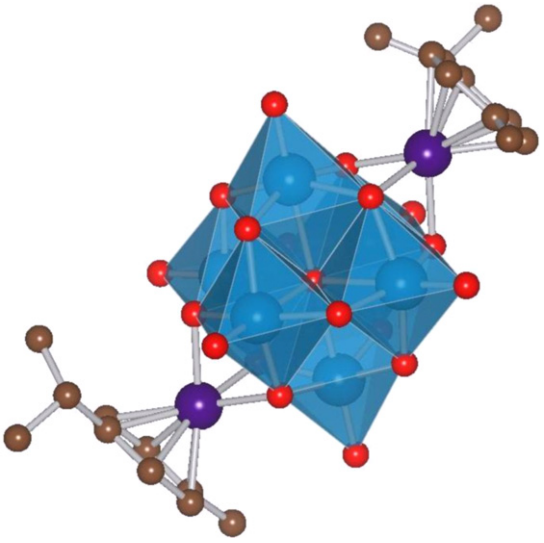

Fig. 4. Structure of $[trans\text{-}\{Ru^{II}(p\text{-cym})\}_2(Nb_6O_{19})]^{4-}$ (Ref. [43]).

hybrid. In all cases the ruthenium atom is linked to the polyoxometalate via three bonds with adjacent bridging oxygen atoms (Fig. 4). $[\{Ru^{II}(p\text{-cym})\}_2Nb_6O_{19}]^{4-}$ undergoes *trans–cis* isomerization in solution, through intramolecular rearrangement of bonds. The neutral $[\{Ru^{II}(p\text{-cym})\}_4Nb_6O_{19}]$ complex decomposes in H_2O, MeOH and CH_3Cl by loss of organometallic fragments.

2.3. Polymolybdates

2.3.1. $[Mo_4O_{16}]^{8-}$ and/or its derivatives

An aqueous solution of Na_2MoO_4 and $[Ru(p\text{-cym})Cl_2]_2$ stirred for 4 h at 25 °C and extracted with CH_2Cl_2 produces $[(Ru^{II}p\text{-cym})_4Mo_4O_{16}]$ [44]. In the solid state the cluster has a windmill-type structure (Fig. 5, on the left). The $[Ru(p\text{-cym})]^{2+}$ groups are tripodally anchored on the polyoxometalate. In chlorinated solvents, an isomerization process is observed and the presence of a second species, so-called triple-cubane (Fig. 5, on the right), is evidenced by multinuclear NMR. The inner cube is made exclusively from Mo and O atoms while the four $[Ru(p\text{-cym})]^{2+}$ species complete the outer cubes. Mo binds to 4 bridging and 2 terminal oxygens. Ru connects to three adjacent bridging oxygens: 2 triple-bridging O_{MoRu} and 1 quadruple-bridging O_{Mo_3}. Mo and Ru exhibit distorted octahedral geometries. The suggested interconversion mechanism involves synchronised movement of two organometallic moieties [45].

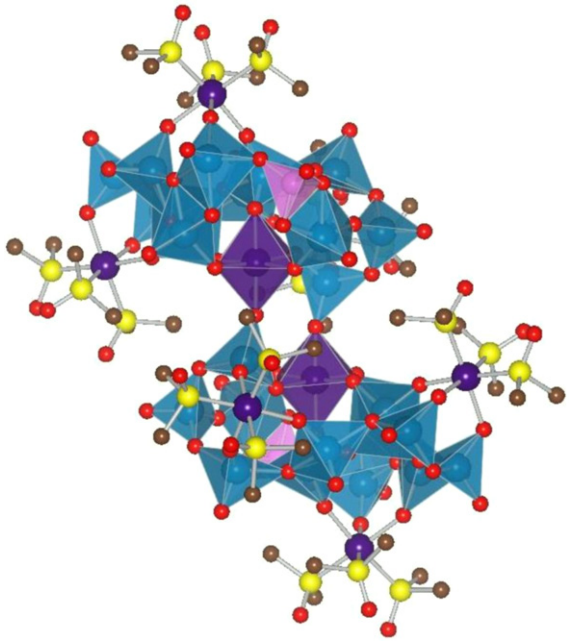

Fig. 3. Structure of $[\{[Ru^{II}(DMSO)_3]_3PV^{V}{}_{11}V^{IV}Ru^{III}O_{37}(OH)_3\}_2]^{8-}$ (Ref. [42]). V = blue polyhedra, P = pink tetrahedra, Ru = violet balls and octahedra, S = yellow balls.

The synthesis of other isomorphous $[(Ru^{II}arene)_4Mo_4O_{16}]$ clusters was reported: arene = C_6Me_6 [46]; arene = toluene, mesitylene, durene [47]. Notably, $[(Ru^{II}C_6Me_6)_4Mo_4O_{16}]$ has a windmill structure in the solid state and does not isomerize in solutions, while $[(Ru^{II}toluene)_4Mo_4O_{16}]$ is a triple-cubane compound in the solid state and isomerizes in methanol. In order to find some general trends in these experimental features, DFT calculations were performed on a series of clusters with various arene ligands. In each case, the windmill form was more stable for isolated molecules. The fluxionality was attributed to environmental effects such as the role of O···H contacts between oxo core and protons of aromatic rings (in other words – type of ligand), association with H_2O, etc. rather than to a small energy difference between isomers [47]. In a following study effects of substituting metal (Ru vs. Os) as well as of solvents (especially their dielectric properties) were addressed [48].

A moderate activity of this family of compounds was noted in the racemization of 1-phenylethanol in chlorobenzene. It was correlated with the type of cluster (higher for polytungstates than polymolybdates) and the ability to isomerize in solution (higher for fluxional moieties) [49].

A mixture of the $[Ru(p\text{-cym})Cl_2]_2$ and $[Rh(Cp^*)Cl_2]_2$ substrates with Na_2MoO_4 in water gives bi-functionalized clusters: $[(Ru^{II}p\text{-cym})(Rh^{III}Cp^*)_3Mo_4O_{16}]$ and $[(Ru^{II}p\text{-cym})_2(Rh^{III}Cp^*)_2Mo_4O_{16}]$. Based on their IR spectra, a triple-cubane structure rather than a windmill one was postulated [40]. Refluxing $[(Ru^{II}p\text{-cym})_4Mo_4O_{16}]$ in methanol in the presence of *p*-hydroquinone leads to breaking of the structure and the chair-like $[(Ru^{II}p\text{-cym})_2Mo_2O_6(OMe)_4]$ complex is isolated [50]. Another route to this compound is to react $(Bu_4N)_2Mo_2O_7$ with $[Ru(p\text{-cym})Cl_2]_2$ in methanol at room temperature [51].

Other clusters were isolated by varying the reaction conditions such as $[(Ru^{II}arene)_2Mo_6O_{20}(OMe)_2]^{2-}$ (arene=C_6Me_6,

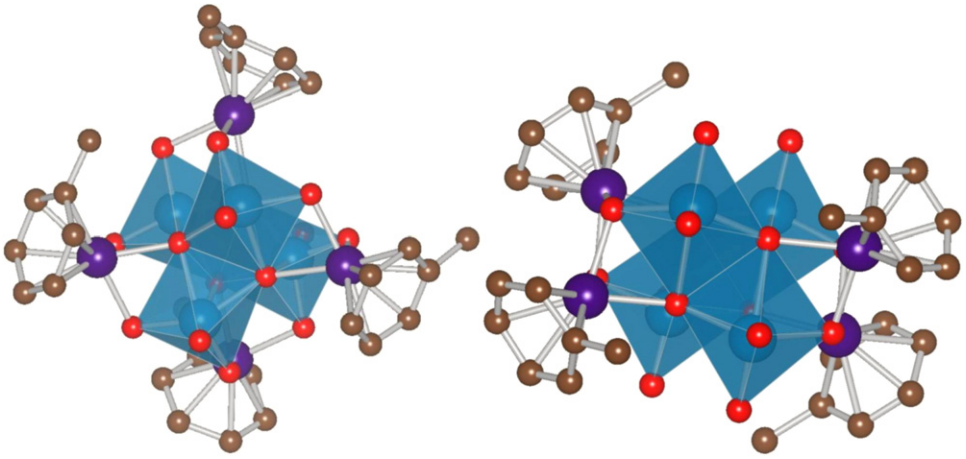

Fig. 5. Windmill (left) and triple cubane (right) isomers of $[(Ru^{II}toluene)_4Mo_4O_{16}]$ (Ref. [47]).

toluene) which is isostructural with $[(Rh^{III}Cp^*)_2Mo_6O_{20}(OMe)_2]^{2-}$ (described in Section 3.2.1), $[(Ru^{II}p\text{-cym})Mo_2O_4(MeC(CH_2O)_3)_2]$ and $[(Ru^{II}C_6Me_6)_2Mo_6O_{18}(MeC(CH_2O)_3)_2]^{2-}$ [51] (Fig. 6).

2.3.2. *Lindqvist structure $[Mo_6O_{19}]^{2-}$ and/or its derivatives*

The lacunary Lindqvist cluster $[Mo_5O_{18}]^{6-}$ (obtained by removing one Mo=O group) supports three $[Ru(C_6Me_6)]^{2+}$ groups in the structure of $[\{Ru^{II}(\eta^6\text{-}C_6Me_6)\}_2\{Ru^{II}(\eta^6\text{-}C_6Me_6)(H_2O)\}Mo_5O_{18}]$ [46]. Two of them are tripodally anchored on three adjacent bridging oxygen atoms while the third one is bipodal, with one H_2O molecule completing the coordination sphere of ruthenium. This complex was obtained by reaction of $[Ru(C_6Me_6)Cl_2]_2$ with Na_2MoO_4 in water or alternatively, with $(Bu_4N)_2Mo_2O_7$ in MeOH. It was tested, together with $[\{Ru^{II}(\eta^6\text{-}C_6Me_6)\}_2\{Ru^{II}(\eta^6\text{-}C_6Me_6)(H_2O)\}W_5O_{18}]$, $[Ru(C_6Me_6)Cl_2]_2$ and $[Ru(p\text{-cym})Cl_2]_2$, in the hydroxylation of adamantane in acidic 1,2-dichloroethane, with 2,6-dichloropyridine N-oxide as oxygen donor. High conversions (up to 94% based on the substrate) and high C^3-H/C^2-H ratios of selectivities were observed for all compounds. As a result, a high valent oxo-Ru complex created *in situ* was suggested to be the catalytically active species [52]. On the other hand, this compound was inactive in the racemization of 1-phenylethanol in chlorobenzene [49]. See also Sections 3.2.2 and 7.2 for Rh and Ag analogues (Fig. 7).

2.3.3. *Keggin structure $[XMo_{12}O_{40}]^{n-}$*

The $(Bu_4N)_4[Ru^{III}LPMo_{11}O_{39}]$ with L = H_2O or DMSO compounds were prepared from $RuCl_3$ or *cis*-$Ru(DMSO)_4Cl_2$ and $(Bu_4N)_4H_3PMo_{11}O_{39}$ in MeCN. The DMSO ligand is hardly labile making the latter complex inactive in catalysis. The $[M(H_2O)PMo_{11}O_{39}]^{n-}$ complexes (M = Ru(III), Co(II), Mn(II)) were tested in one stage aerobic epoxidation of alkenes (1-octene) using alkanes (cumene) to form oxygen transfer intermediates. They showed comparable activities and for the Ru species formation of 1-octene oxide and cumyl alcohol proceeded in a 1:1 ratio, with only traces of acetophenone [53,54]. However, problems with a reproducibility of synthesis of $(Bu_4N)_4[Ru^{III}(DMSO)PMo_{11}O_{39}]$ were reported [55].

2.3.4. *Other polymolybdates*

A polymolybdate with the formula $(NH_4)_4[Ru^{II}(DMSO)_3Mo_7O_{24}]$ crystallized from a solution of *cis*-$[Ru(DMSO)_4Cl_2]$ and $[Mo_7O_{24}](NH_4)_6$ in water [56]. In this compound the ruthenium center is in a trigonal antiprismatic coordination mode and is bound to three DMSOs via the sulfur atom and three bridging

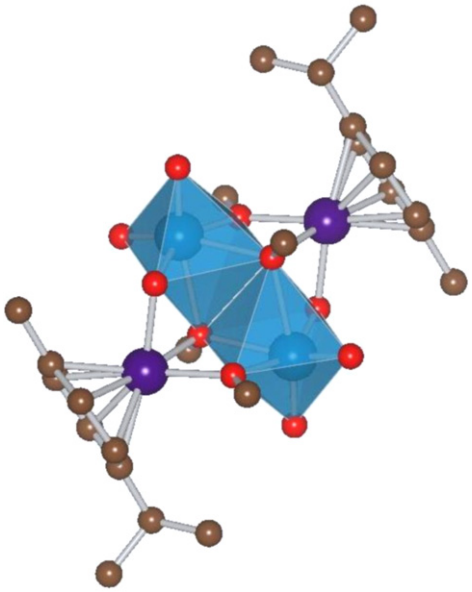

Fig. 6. Structure of $[(Ru^{II}p\text{-cym})_2Mo_2O_6(OMe)_4]$ (Ref. [50]).

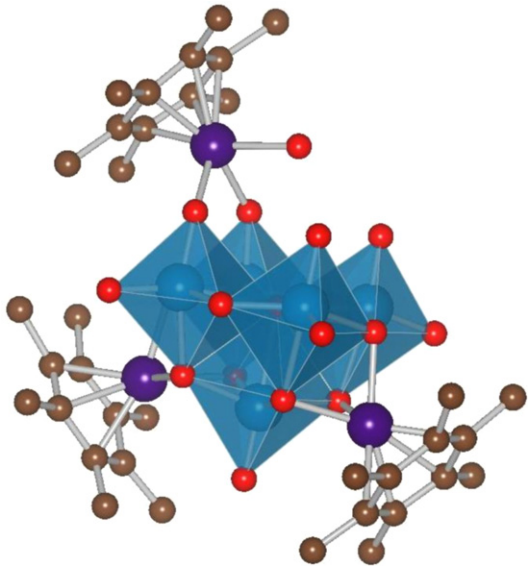

Fig. 7. Structure of $[\{Ru^{II}(\eta^6\text{-}C_6Me_6)\}_2\{Ru^{II}(\eta^6\text{-}C_6Me_6)(H_2O)\}Mo_5O_{18}]$ (Ref. [46]).

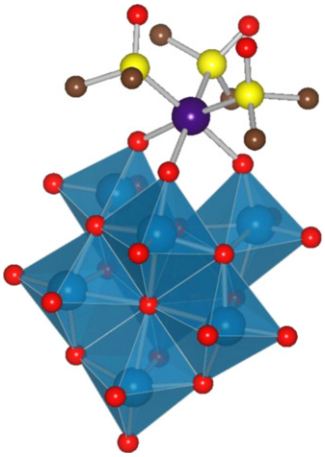

Fig. 8. Structure of $[Ru^{II}(DMSO)_3Mo_7O_{24}]^{4-}$ (Ref. [56]).

oxygen atoms of the heptamolybdate species. This complex and its Os analogue, $(NH_4)_4[Os^{II}(DMSO)_3Mo_7O_{24}]$, were tested in the liquid phase aerobic oxidation of alcohols, due to their similarity to heterobimetallic Ru–Cr and Os–Cr complexes, known to be catalytically active in this process. Benzylic alcohols were efficiently (TON ~ 500) and selectively (>99%) oxidized to the corresponding benzaldehyde derivatives, in the absence of solvent. Secondary allylic alcohols were also oxidized effectively to the corresponding β-unsaturated ketones with a generally high (>90%) chemoselectivity. On the other hand, primary aliphatic allylic alcohols were less reactive, and the formation of β-unsaturated aldehydes as products proceeded only with ~50% chemoselectivity. Simple secondary alcohols reacted more slowly, but selectively (>99.5%) to yield ketones. Ru and Os compounds show comparable activity and were stable in the reaction conditions. To explain the results, a modification of an oxometal type mechanism of oxidation was proposed (Fig. 8).

2.4. Polytungstates

2.4.1. $[W_4O_{16}]^{8-}$ and/or its derivatives

The $[(Ru^{II}L)_4W_4O_{16}]$ (L = *p*-cym, C_6Me_6) complexes were synthesized from $(Bu_4N)_2WO_4$ and $[RuLCl_2]_2$ in acetonitrile [45,46]. They have windmill-type structures, in the solid state as well as in $CHCl_3$. They display a moderate activity in the racemization of 1-phenylethanol in chlorobenzene [49].

Another double-cubane cluster, $[(Ru^{II}p\text{-cym})_4W_2O_{10}]$ was obtained as a by-product during the preparation of $[(Ru^{II}p\text{-cym})_4W_4O_{16}]$ [45,46]. The same reactions, carried out in water instead of acetonitrile, resulted in the formation of $[(Ru^{II}L)_2(\mu\text{-}OH)_3]_2[(Ru^{II}L)_2(Ru^{II}LH_2O)_2W_8O_{28}(OH)_2]$, L = *p*-cym, C_6Me_6, composed of organometallic cations and of polyanions made of two cubes joined by two *cis*-$\{WO_2\}^{2+}$ groups [46] (Fig. 9).

2.4.2. Lindqvist structure $[W_6O_{19}]^{2-}$ and/or its derivatives

$[(Ru^{II}p\text{-cym})cis\text{-}Nb_2W_4O_{19}]^{2-}$ is synthesized by reaction of $[Ru(p\text{-cym})Cl_2]_2$ with $(Bu_4N)_4[cis\text{-}Nb_2W_4O_{19}]$ in 1,2-dichloroethane at room temperature [57]. Although the syntheses are routinely performed under N_2, this compound is air-stable. Its structure, where ruthenium is tripodally fixed to the polyoxometalate via three bonds with adjacent bridging oxygen atoms, has been proposed by analogy with $[(Rh^{III}Cp^*)cis\text{-}Nb_2W_4O_{19}]^{2-}$, see Section 4.3.2. There are three possible diastereisomers of this compound but only two (types I and II illustrated in Fig. 35) are observed.

The reaction product of $(Bu_4N)_4[cis\text{-}Nb_2W_4O_{19}]$ and $[Ru(COD)Cl(MeCN)_3](PF_6)$ is thought to be dimeric $[\{Ru^{II}(COD)Cl(MeCN)\}_5(cis\text{-}Nb_2W_4O_{19})_2]^{3-}$, its structure being closely related to those of $[\{Rh^{I}(C_7H_8)\}_5(cis\text{-}Nb_2W_4O_{19})_2]^{3-}$ and $[\{Ir^{I}(COD)\}_5(Nb_2W_4O_{19})_2]^{3-}$, see Section 4.3.2. Two clusters are oriented face-to-face towards each other and linked through five Ru-organometallic moieties bound to their bridging and terminal oxygen atoms [39].

Based on similarities of their IR spectra, $[Ru^{II}(C_6H_6)(Cp^*TiW_5O_{18})]^-$ was proposed to be isostructural with $[Ir^{I}(COD)(Cp^*TiW_5O_{18})]^{2-}$, for which the crystal structure had been solved (see Section 4.3.2). It was obtained from $(Bu_4N)_3[Cp^*TiW_5O_{18}]$ and $[Ru(C_6H_6)(MeCN)_2](PF_6)_2$ in 1,2-dichloroethane, under N_2 [57]. The $[Cp^*TiW_5O_{18}]^{3-}$ polyanion is also able to create dimeric moieties, like e.g. $[\{Ru^{I}(CO)_2(Cp^*TiW_5O_{18})\}_2]^{4-}$ (Fig. 10). This light-sensitive compound is produced from $(Bu_4N)_3[Cp^*TiW_5O_{18}]$ and $[Ru_2(CO)_4(MeCN)_6](PF_6)_2$ in CH_2Cl_2. Both Ru centers are in a distorted octahedral coordination with three oxygen atoms of the polyanion and three carbon atoms from two bridging and one terminal CO molecules [58].

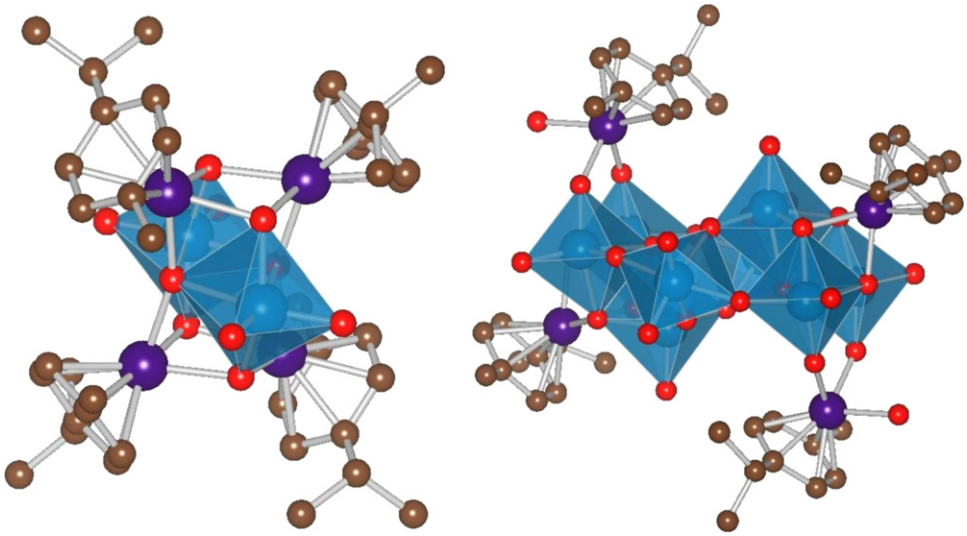

Fig. 9. Structures of $[(Ru^{II}p\text{-cym})_4W_2O_{10}]$ (left, Ref. [45]) and $[(Ru^{II}p\text{-cym})_2(Ru^{II}p\text{-cym}\ H_2O)_2W_8O_{28}(OH)_2]^{2-}$ (right, Ref. [46]).

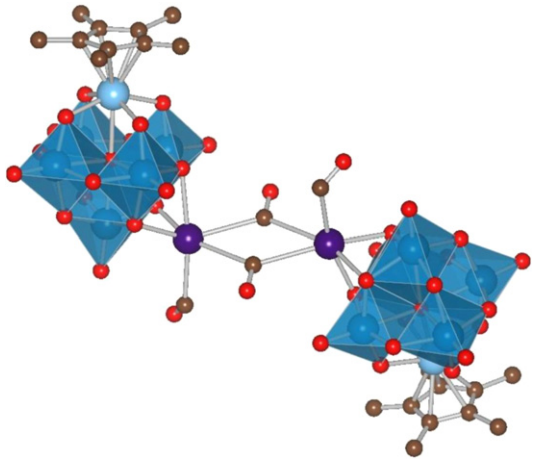

Fig. 10. Suggested structure of $[\{Ru^{I}(CO)_2(Cp^*TiW_5O_{18})\}_2]^{4-}$ (Ref. [58]). Ti = light blue.

The characterization and catalytic tests on $[\{Ru^{II}(\eta^6\text{-}C_6Me_6)\}_2\{Ru^{II}(\eta^6\text{-}C_6Me_6)(H_2O)\}W_5O_{18}]$ were described above for its polymolybdate analogue [46,52]. This compound was inactive in racemization of 1-phenylethanol in chlorobenzene [49].

2.4.3. *Keggin structure* $[XW_{12}O_{40}]^{n-}$

As there are high number of data for complexes between ruthenium and Keggin ions, we will discuss them as a function of the central heteroatom X.

2.4.3.1. Phosphorus as the central atom in the Keggin unit (X = P). $[Ru^{III}(H_2O)PW_{11}O_{39}]^{4-}$ is obtained by mixing $[PW_{11}O_{39}]^{7-}$ and $[Ru(H_2O)_6](C_7H_7SO_3)_2$ in water, under argon, followed by oxidation with O_2. This compound is electrochemically reducible in solution yielding $Ru^{II}(H_2O)$ and oxidizible to $Ru^{IV}(=O)$ and $Ru^{V}(=O)$. Its Bu_4N^+ salt catalyzes the epoxidation of *trans*-stilbene by iodosylbenzene in MeCN [59]. $[Ru^{III}(H_2O)PW_{11}O_{39}]^{4-}$ was also an efficient catalyst for the cleavage oxidation of styrene to benzaldehyde and benzoic acid with $NaIO_4$ in biphasic 1,2-dichloroethane/H_2O systems [60]. Its $Ru^{II}(H_2O)$ form undergoes various ligand exchange reactions with pyridine, sulfoxides, dialkyl sulfides or active alkenes (e.g. maleic acid) [59]. The rates of substitutions $H_2O \rightarrow$ pyridine, pyrazine, etc. for $[Ru^{II}(H_2O)PW_{11}O_{39}]^{5-}$ were measured and the decrease of lability of the aquo ligand in comparison to other Ru(II) complexes was shown. It was attributed to a weakly π-acidic character of the polyanion. The rates of oxidation of alcohols by the $Ru^{V}(=O)$ form of the complex were too low for potential applications [61].

Other procedures for ruthenium-containing phosphotungstates were introduced: $[Ru^{II}(H_2O)PW_{11}O_{39}]^{5-}$, obtained from $[PW_{11}O_{39}]^{7-}$ and *cis*-$[Ru(DMSO)_4(H_2O)_2](BF_4)_2$ in water under N_2, showed a moderate activity in the oxygenation of saturated hydrocarbons by *t*-butyl hydroperoxide and hypochlorite NaClO in biphasic CH_2Cl_2/H_2O systems [62]. $[Ru^{III}(H_2O)PW_{11}O_{39}]^{4-}$ obtained from $[PW_{11}O_{39}]^{7-}$ and $RuCl_3$ in water was characterized by EXAFS spectroscopy in the solid state and in MeCN solution [63]. The $[M(H_2O)PW_{11}O_{39}]^{n-}$, M = Ru(III), Co(II), Mn(II) complexes were tested in one stage aerobic epoxidation of alkenes (1-octene) using alkanes (cumene) to form oxygen transfer intermediates. Upon reaction with dioxygen the Ru-substituted polytungstate turned catalytically inert, though [53,54]. Reaction of $[PW_{11}O_{39}]^{7-}$ with $K_2RuOHCl_5$ in aqueous solution gave Ru-supported species with diamagnetic binuclear fragments $(Ru^{IV}L_x)_2O$ and additional ligands L. These species were active in primary alcohols and aldehydes oxygenation to carboxylic acids by $KClO_3$ in water. Acrolein was oxidized to acrylic acid, without affecting the carbon–carbon double bond [64,65]. Recently, a one pot synthesis from $H_3PW_{12}O_{40}$ and HCl-activated $RuCl_3$ in acidic aqueous solution was proposed. Crystalline $Na_5[Ru^{II}(H_2O)PW_{11}O_{39}]\cdot 13H_2O$ was collected and tested in non-solvent liquid phase oxidation of alkenes with molecular oxygen. Cyclohexene was oxidized to cyclohexane oxide with a high activity and 100% selectivity. The catalyst was stable in reaction conditions [66]. Microwave-assisted synthesis from $K_7PW_{11}O_{39}$ and $[Ru(DMF)_6](CF_3SO_3)$ in water yields the Ru(III)-incorporating lacunary polyanion $[Ru^{III}(H_2O)PW_{11}O_{39}]^{4-}$, which can be isolated as organic or inorganic salts, according to [67].

In addition to the ligand exchange reaction $H_2O \rightarrow$ DMSO described in [59], a new, fast (15 min) and selective method towards $[Ru^{II}(DMSO)PW_{11}O_{39}]^{5-}$ was described by reaction of $[PW_{11}O_{39}]^{7-}$ with *cis*-$[Ru(DMSO)_4Cl_2]$ in water, under microwave irradiation. It was proposed that the polyanion, by analogy to silicotungstate, acts as a pentadentate ligand for the Ru center. However, ^{99}Ru and ^{183}W NMR spectra alone did not allow to draw such a conclusion with certainty. This compound was catalytically active in the oxidation of cyclooctene with sodium periodate $NaIO_4$ in H_2O and in the hydroxylation of adamantane with potassium monopersulfate $KHSO_5$ in 1,2-dichloroethane/H_2O. In both cases, no reaction was observed when using 2,6-dichloro pyridine *N*-oxide $PyCl_2NO$ as oxidant. Under microwave irradiation in oxygen atmosphere $[Ru^{II}(DMSO)PW_{11}O_{39}]^{5-}$ catalyzes the oxidation of DMSO to $DMSO_2$ in water [68,69]. DFT calculations were performed on this compound (and other Ru systems) to determine the ^{99}Ru [70,71] and ^{183}W [72] nuclear shieldings and the NMR properties. Another compound with DMSO ligands, $[Ru^{II}(DMSO)_3(H_2O)PW_{11}O_{39}]^{6-}$, shows a strikingly different binding modes of the organometallic moiety to the polyanion. Indeed, Ru does not enter the lacuna of the polyanion, but is supported on it via two oxygen atoms, its coordination sphere being completed by four terminal ligands: 3 DMSO and 1 H_2O. Furthermore, these two oxygens are non-equivalent (one from complete W_3O_{13} and one from incomplete W_2O_{12} triads) and the grafting reaction leads to a loss of symmetry of a parent ion. This reaction is also fully regioselective, yielding two enantiomeric forms whatever the nature of the grafted moiety. The nature of this peculiar behaviour was addressed by means of DFT calculations [73].

EPR spectra of a series of Bu_4N salts of Ru-containing compounds: $[Ru^{III}(L)PW_{11}O_{39}]^{5-}$, where L = H_2O, py or DMSO, were recorded at 77 K and analysed. A *S*-type coordination mode of the DMSO molecule to the metal center was suggested [74].

Two types of complexes could be isolated from aqueous solutions of $[Ru(arene)Cl_2]$ and $K_7PW_{11}O_{39}$, with arene = C_6H_6, toluene, *p*-cym or C_6Me_6. In the first type, with the formula $[\{Ru^{II}(arene)(H_2O)\}PW_{11}O_{39}]^{5-}$, the organometallic moiety is bipodally grafted on the rim of the lacuna of polyanion and Ru fills up its coordination sphere with a H_2O molecule. UV irradiation of degassed solutions of these compounds stimulates the ligand substitution: arene $\rightarrow$ H_2O, DMSO, tetramethylene sulfoxide TMSO or diphenyl sulfoxide Ph_2SO. This reaction is combined with a change of the coordination mode of Ru that leaves the rim and anchors in the lacuna. Complexes of the second type with the formula $[\{Ru^{II}(arene)(PW_{11}O_{39})\}_2WO_2]^{8-}$ are built from two Ru-supporting polyanions joined by a *cis*-dioxo $\{WO_2\}^{2+}$ linker. Instead of H_2O, both Ru centers coordinate oxygen atoms of the linker. The ratio between monomeric and dimeric products was thought at first to be strongly dependent on the arene ligand – the bulkier it is, the less favourable the formation of dimeric species [75]. Subsequent studies evidenced a pH-dependent interconversion of the two types of complexes in solution, with a preferrable formation of dimers at low pH and a minor role of the steric repulsion between arene ligands [76]. $[\{Ru^{II}(p\text{-cym})(H_2O)\}PW_{11}O_{39}]^{5-}$

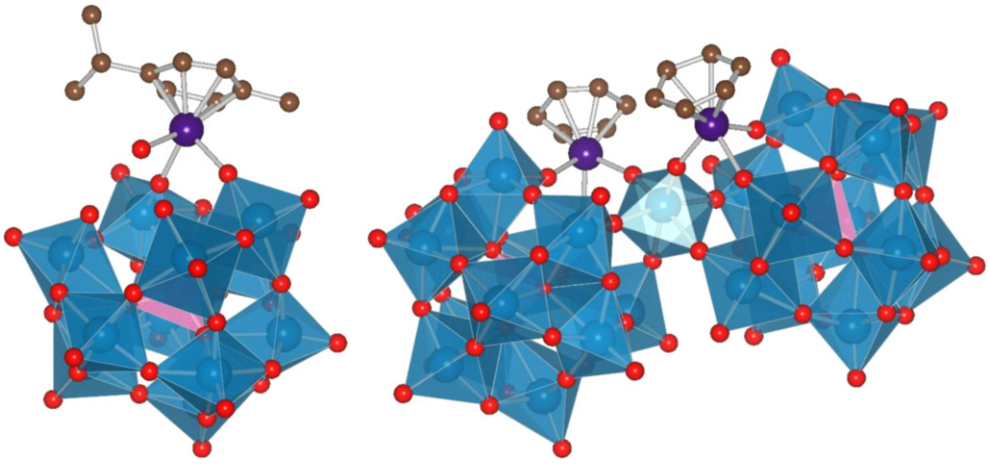

Fig. 11. Structures of: $[\{Ru^{II}(p\text{-cym})(H_2O)\}PW_{11}O_{39}]^{5-}$ (left) and $[\{Ru^{II}(C_6H_6)(PW_{11}O_{39})\}_2WO_2]^{8-}$ (right, both from Ref. [75]). P and other heteroatom tetrahedra = pink.

was moderately active in the racemization of 1-phenylethanol in chlorobenzene [49] (Fig. 11).

The nitrido derivative of the Keggin-type POM $[(Ru^{VI}N)PW_{11}O_{39}]^{4-}$ can be obtained: (a) as an alkaline salt from the reaction of $[PW_{11}O_{39}]^{7-}$ and $Cs_2[RuNCl_5]$ in water or (b) as the *tert*-butylammonium salt from $[PW_{11}O_{39}]^{7-}$ and $(Bu_4N)[RuNCl_4]$ in H_2O/MeCN. The polyanion serves as a pentadentate ligand for the $[Ru{\equiv}N]^{3+}$ moiety. This compound is active in nitrogen-transfer reactions. Addition of PPh_3 led to the isolation and the preliminary structure description of the phosphoranyminato derivative $[(Ru^{V}NPPh_3)PW_{11}O_{39}]^{3-}$ (see Fig. 12). Reaction can proceed further with another equivalent of phosphine, to give the *bis*(triphenylphosphine)iminium cation $(PPh_3{=}N{=}PPh_3)^+$ and $[(Ru^{III}H_2O)PW_{11}O_{39}]^{4-}$, thus completing the transfer [77]. In the course of investigations two other closely related species were isolated and characterized: $[(Ru^{III}N(OH)PPh_3)PW_{11}O_{39}]^{4-}$ and $[(Ru^{III}OPPh_3)PW_{11}O_{39}]^{4-}$ and ways of their interconversion envisaged [78]. The reactivity of various transition metal nitrido derivatives of the $[PW_{11}O_{39}]^{7-}$ anion was investigated by means of DFT calculations [79]. In addition, in its ground state (gaseous state) $[(Ru^{VI}N)PW_{11}O_{39}]^{4-}$ has a lower energy lying Ru-N antibonding orbitals (LUMO, LUMO+1) than the Os and Re analogues and thus is a stronger electrophile. Substitution by various heteroatoms influences relative energy of the LUMO but not the order nor the composition of the antibonding orbitals. Upon one-electron redox processes the [RuN] unit is a reduced center and the Ru–N distance increases. Solvation effects cause the absolute energies of orbitals to decrease but do not significantly change their order, composition or relative energies [80]. Triple bonding between Ru and N was also demonstrated together with a charge transfer from the nitrido ligand to the metal center, decreasing the nitrogen charge from −3 to almost 0 [81].

An hydrothermal synthesis from $[PW_{11}O_{39}]^{7-}$ and $[Ru_2(OAc)_4]Cl$ results in the dimeric complex $[O\{Ru^{IV}(OH)(PW_{11}O_{39})\}_2]^{10-}$. Two mono-lacunary Keggin units, oriented face-to-face, are connected via a $\{Ru(OH)–O–Ru(OH)\}^{4+}$ bridge (Fig. 13). The coordination number of both Ru centers is 6: with 2 terminal oxygen atoms from each cluster, one OH^- terminal ligand and one oxo linker. The Ru–O–Ru moiety is almost linear (175° angle) with d_{Ru-O} = 1.765(11) and 1.784(11) Å. Electrochemical studies in solution showed possibility of reduction of Ru^{IV}–O–Ru^{IV} to Ru^{III}–O–Ru^{III} and oxidation to Ru^{V}–O–Ru^{IV} [82].

The reaction of $Ru(Cp)(PPh_3)_2Cl$ with $H_3PW_{12}O_{40}$ in the presence of triethylamine in methanol yielded $(HEt_3N)[\{Ru^{II}(Cp)(PPh_3)_2\}]_2PW_{12}O_{40}]$ (Fig. 14). This air-stable, insoluble in most solvents compound, contains Ru complexes tethered to complete Keggin polyanion through bonds with its terminal oxygen atoms. It is an active catalyst in the solvent-free phenyl acetylene oligomerization. Moreover, in contrast to its precursor $Ru(Cp)(PPh_3)_2Cl$, it exhibits 70% selectivity towards (E)-enyne [83].

2.4.3.2. Silicon as the central atom in the Keggin unit (X = Si). The first method of producing $[Ru^{III}(H_2O)SiW_{11}O_{39}]^{5-}$ was described as a reaction between $RuCl_3$ and $[SiW_{11}O_{39}]^{8-}$ in water, at 90 °C

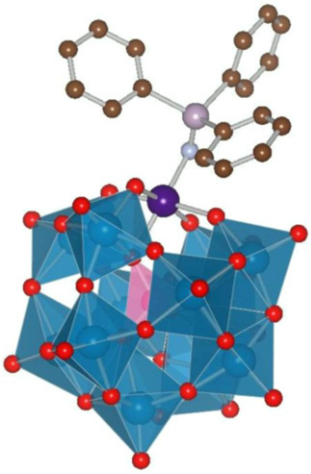

Fig. 12. Proposed structure for $[(Ru^{V}NPPh_3)PW_{11}O_{39}]^{3-}$ (Ref. [77]). N = greyish.

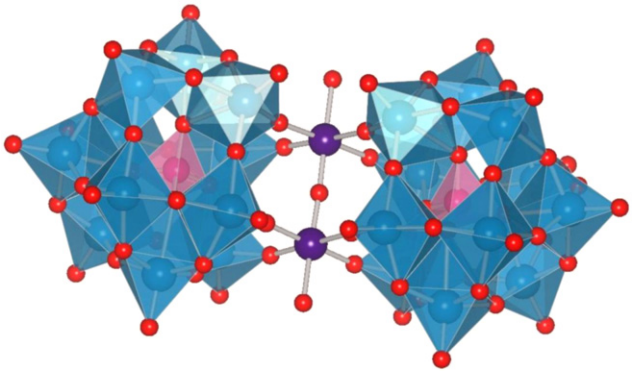

Fig. 13. Structure of $[O\{Ru^{IV}(OH)(PW_{11}O_{39})\}_2]^{10-}$ (Ref. [82]).

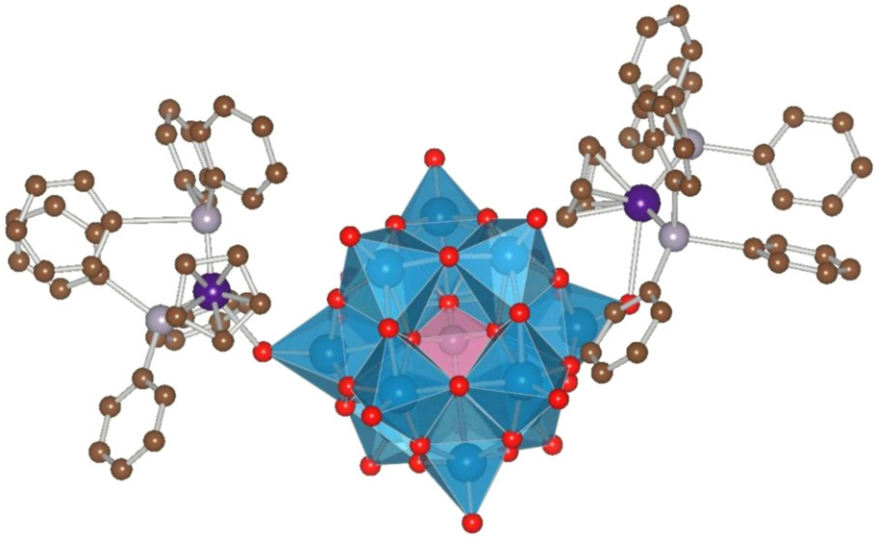

Fig. 14. Proposed structure for $[\{Ru^{II}(Cp)(PPh_3)_2\}_2PW_{12}O_{40}]^-$ (Ref. [83]).

[84,85] or in an organic solvent [86]. Subsequent studies showed that the product is a mixture of closely related compounds, differing probably by terminal ligands [59,87]. As an explanation served the fact, the commercially available $RuCl_3{\cdot}nH_2O$ contains various mono- and polymeric Ru(III) and Ru(IV) species [88]. Nevertheless, derivatives of the so-obtained $[Ru^{III}(H_2O)SiW_{11}O_{39}]^{5-}$ with other terminal ligands were reported, e.g. NO, N_2 [89].

Although not pure (or maybe just because of that), the tetrahexylammonium salt of the above compound(s?) made by this way was an efficient and robust catalyst in the liquid phase (1,2-dichloroethane) oxidation of hydrocarbons. The reaction outcome was strongly dependent on the oxidant used: *t*-butyl hydroperoxide, potassium persulfate, sodium periodate or iodosylbenzene, while H_2O_2 was simply decomposed to H_2O and O_2. The most selective oxidations proceeded with sodium periodate leading to more than 99% selectivity in oxidation of styrene and its derivatives to the corresponding benzaldehydes [84,85]. In the oxidation of cyclohexane with *t*-butyl hydroperoxide in benzene solutions, the products were only cyclohexanol and cyclohexanone. The Ru compound showed the highest turnovers and cyclohexanone yield in a series of complexes with various transition metals. The catalyst was stable in reaction conditions [90]. $[Ru^{III}(H_2O)SiW_{11}O_{39}]^{5-}$ was also an efficient catalyst in the cleavage oxidation of styrene to benzaldehyde and benzoic acid by $NaIO_4$ in biphasic 1,2-dichloroethane/H_2O systems [60]. Oxidation of alkanes and alcohols with O_2 proceeded also efficiently and with high turnover numbers, with no catalyst degradation [86]. This compound was employed as an efficient mediator in the indirect electrochemical cleavage of electron rich aryl olefins to the respective aldehydes [91] as well as in the electrochemical reduction of the nitrite ion in aqueous solutions [92].

An alternative synthetic way, by mixing $[SiW_{11}O_{39}]^{8-}$ and $[Ru(H_2O)_6](C_7H_7SO_3)_2$ in water under argon and followed by oxidation with O_2, was unsuccessful [59]. A new approach towards $[Ru^{III}(H_2O)SiW_{11}O_{39}]^{5-}$ has been explored by hydrothermal synthesis in deaerated water under inert atmosphere, from $K_8SiW_{11}O_{39}$ and $Ru(acac)_3$. Small concentrations of substrates yielded the desired product in a pure form. By employing the same procedure, the pure germanotungstate analogue could be obtained as well, while the phosphotungstate was contaminated. Electrochemical studies in solution showed the possibility of reducing $Ru^{III}(H_2O)$ to $Ru^{II}(H_2O)$ or oxidizing it to $Ru^{IV}(H_2O)$, $Ru^{IV}(OH)$ or $Ru^{IV}(=O)$ (depending on the pH) and further to $Ru^{V}(=O)$ [93,94]. $Cs_5[Ru^{III}(H_2O)SiW_{11}O_{39}]{\cdot}7H_2O$ prepared by this way showed a high activity in air oxidation of alkylaromatic compounds in water as solvent [93].

Recently, $[Ru^{III}(H_2O)SiW_{11}O_{39}]^{5-}$ was shown to catalyze photoreduction of CO_2 to CO in the presence of amines as reducing agents. Based on DFT calculations a side-on coordination mode of CO_2 to the metallic center was proposed as energetically favourable [95].

The DMSO derivative $[Ru^{III}(DMSO)SiW_{11}O_{39}]^{5-}$ was also prepared, as a result of the $H_2O \rightarrow$ DMSO ligand substitution in aqueous solution at 80 °C. During crystallographic analysis it was possible for the first time to distinguish clearly between electron densities of W and Ru atoms of the cluster and to prove unequivocally the Ru incorporation into the structure. Metal fills the lacuna of the polyanion, coordinating 5 oxygen atoms and the sulfur from DMSO (see Fig. 15, on the left). The similarity of the IR spectra of both silicotungstates served as an indirect evidence for the Ru incorporation in the lacuna of $[Ru^{III}(H_2O)SiW_{11}O_{39}]^{5-}$ [96]. In an earlier paper $[Ru^{II}(DMSO)_3(H_2O)\alpha\text{-}XW_{11}O_{39}]^{6-}$, X = Si, Ge compounds were described, showing regioselective bipodal attachment of an organometallic moiety to the polyanion (see Fig. 15, on the right). Silicotungstate was obtained from *cis*-$[Ru(DMSO)_4Cl_2]$ and $[\alpha\text{-A-}SiW_9O_{34}]^{6-}$ in acidic aqueous medium and the tight binding of DMSO ligands to Ru in the precursor was indicated as a key factor in its formation. Straightforward syntheses from $[SiW_{11}O_{39}]^{8-}$ were unsuccessful, thus suggesting the following sequence of events: (1) coordination of $[Ru(DMSO)_3(H_2O)]^{2+}$ to nonatungstate and (2) reorganization of the cluster. DMSO molecules and Keggin anion both serve as powerful stabilizing agents for the Ru(II) center, which is electrochemically almost inert in wide pH range 0–7, even in the presence of O_2 [97]. A wrong attribution of the type of the cluster has been pointed out for these two compounds (β_3 isomers rather than α) [73].

When the conditions of the initial hydrothermal experiment described above were slightly modified, different products could be isolated. For example, when the $K_8SiW_{11}O_{39}$ and $Ru(acac)_3$ concentrations were increased, IR and UV–vis spectra and cyclic voltammograms suggested the presence of a compound in a dimeric form for which the formula $[\{Ru^{III/IV}SiW_{11}O_{39}\}_2O]^{11-}$ was proposed (Fig. 16). This species is a mixed-valence complex, with two Keggin units joined by a Ru^{III}–O–Ru^{IV} bridge. In solution the Ru^{III}–O–Ru^{IV} bridge could be reversibly oxidized to Ru^{IV}–O–Ru^{IV} or reduced to Ru^{III}–O–Ru^{III}. A concomitant re-reduction leads to the disproportionation of the dimer into the

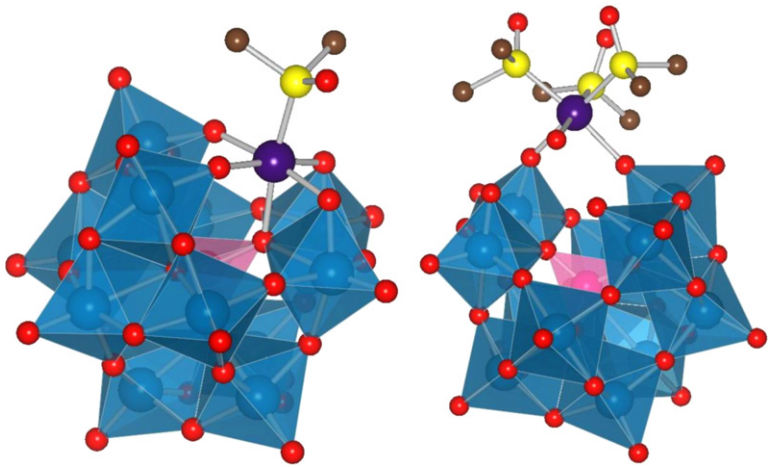

Fig. 15. Structures of $[Ru^{III}(DMSO)SiW_{11}O_{39}]^{5-}$ (left, Ref. [96]) and $[Ru^{II}(DMSO)_3(H_2O)SiW_{11}O_{39}]^{6-}$ (right, Ref. [97]).

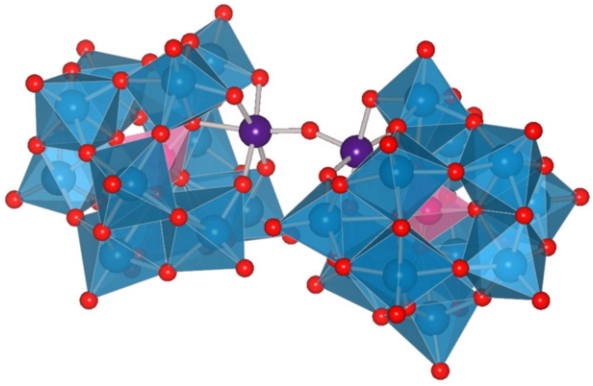

Fig. 16. Structure of $[\{Ru^{IV}SiW_{11}O_{39}\}_2O]^{10-}$ (Ref. [98]).

monomeric $[Ru^{II}(H_2O)SiW_{11}O_{39}]^{6-}$ [94]. This structural model was later confirmed by single crystal diffraction studies of the oxidized complex. The Ru^{IV}–O–Ru^{IV} bridge is short (average bond distance of 1.816 Å, suggesting multiple Ru–O bonding) and bent, with a Ru–O–Ru angle equal to 154°. An alternative synthesis from $[Ru^{III}(H_2O)SiW_{11}O_{39}]^{5-}$ was proposed and the effects of pH, temperature, atmosphere and reaction time investigated, leading to a discussion on the mechanism of the dimerization process [98]. When the reaction time was increased from 24 h to 5 days, $[Ru^{II}(CO)SiW_{11}O_{39}]^{6-}$ crystallized (Fig. 17). The carbon monoxide results from decomposition of acetylacetonate ion in hydrothermal conditions and acts as a terminal ligand, in perfect analogy to what was observed for H_2O or DMSO. The $Ru^{II}(CO)$ moiety could be oxidized to $Ru^{III}(CO)$, which showed an unexpected stability in acidic solutions [99].

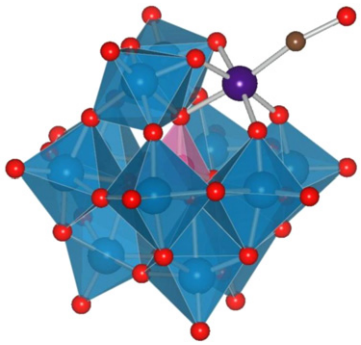

Fig. 17. Suggested structure for $[Ru^{II}(CO)SiW_{11}O_{39}]^{6-}$ (Ref. [99]).

Ru-functionalized tri- and di-lacunary silicotungstates (and their isostructural germanotungstate analogues) are also known, for example $[(Ru^{II}C_6H_6)_2\alpha\text{-A-}XW_9O_{34}]^{6-}$, X = Si, Ge [100] and $[(Ru^{II}C_6H_6)\{Ru^{II}(C_6H_6)(H_2O)\}\gamma\text{-}XW_{10}O_{36}]^{4-}$, X = Si, Ge [101]. These polyoxometalates are obtained by simple one-pot syntheses from $[Ru(C_6H_6)Cl_2]_2$ and the corresponding polyanion precursors $[\alpha\text{-A-}XW_9O_{34}]^{6-}$ or $[\gamma\text{-}XW_{10}O_{36}]^{4-}$ in aqueous solutions at pH = 6.0 and 2.5, respectively. In a similar manner, these two types of polyanions support two organometallic moieties (apparently, this is the upper limit as syntheses with excess of Ru did not yield more Ru-rich POM species) (Fig. 18). Only one organometallic moiety is in the lacunary position – probably due to the steric hindrance. The other one, bound to three bridging O_{W2} oxygens is found either on the bottom of the cluster (for tri-lacunary polyanions) or on its side (for di-lacunary ones). There are some notable differences, however, between the two types of complexes: Ru from the lacuna of $[\alpha\text{-A-}XW_9O_{34}]^{6-}$ forms 2 bonds with terminal O_W atoms and one with bridging O_{W_2X}, while in the case of $[\gamma\text{-}XW_{10}O_{36}]^{4-}$ in addition to 2 bonds with terminal O_W atoms, there is no connection to heteroatom and Ru ligates H_2O.

In a recent paper, the synthesis of nitrido derivatives of silico- and germanotungstate anions was reported. Single crystals of mixed organic-inorganic salts of $[\gamma\text{-}XW_{10}O_{36}\{(RuN)_2(\mu\text{-}O)_2\}]^{6-}$, where X = Si, Ge; could be isolated after the reaction of $K_8XW_{10}O_{36}$ with $Cs[RuNCl_5]$ in H_2O at room temperature. Two vicinal Ru centers fill lacuna of the polyanion with nitride ligands in *cis* geometry. They are tripodally anchored on two terminal oxygen atoms of the lacuna and bridging O_{SiW}. In addition there are two oxo bridges between them [102].

A lot of theoretical calculations were made on ruthenium-containing polyoxometalates, due to their various properties:

- For the α and β-Keggin species $[LXW_{11}O_{39}]^{n-}$ (X = Si(IV), P(V); L = $[Ru^{II}(DMSO)_3(H_2O)]^{2+}$, $[Ru^{II}(C_6H_6)(H_2O)]^{2+}$) the effect of the grafting of organometallic moieties on lacunary clusters was evaluated as well as the influence of the central ion. Structural differences between synthesized complexes could be explained by this way [103].
- For the γ-Keggin species $[Ru^{III}_2(OH)_2XM_{10}O_{36}]^{n-}$ (X = Al(III), Si(IV), P(V), S(VI); M = Mo(VI), W(VI) [104]) and $[Z_2(OH)_2SiW_{10}O_{36}]^{4-}$ (Z = Mo(III), Ru(III), Rh(III)) the geometries, electronic structures and energetics were elucidated

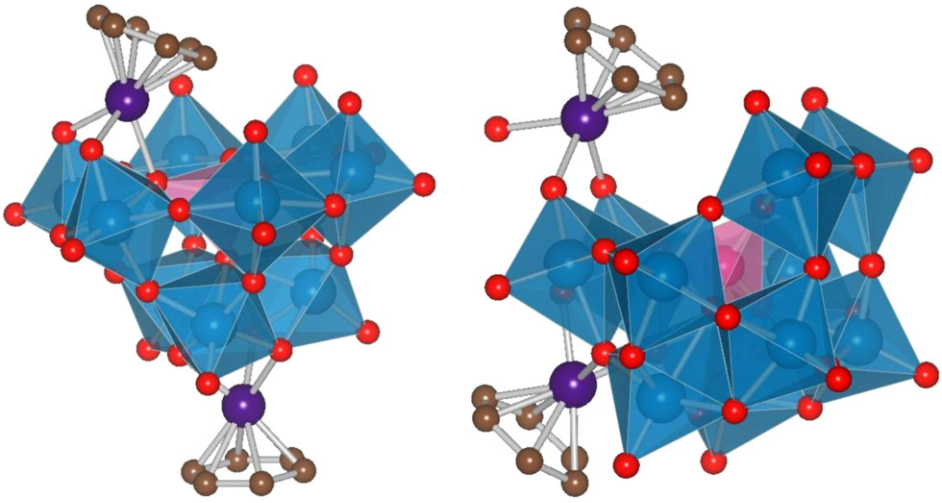

Fig. 18. Structures of: $[(Ru^{II}C_6H_6)_2\alpha\text{-A-}SiW_9O_{34}]^{6-}$ (left, Ref. [100]) and $[(Ru^{II}C_6H_6)\{Ru^{II}(C_6H_6)(H_2O\}\text{-}SiW_{10}O_{36}]^{4-}$ (right, Ref. [101]).

[105]. An important role of the heteroatom on the ground state and the reactivity was underlined, especially for polyoxotungstates. The theoretically predicted compound $[Ru^{III}_2(OH)_2(H_2O)_2SiW_{10}O_{36}]^{4-}$ was synthesized from $(\gamma\text{-}SiW_{10}O_{36})^{4-}$ and $RuCl_3$ and characterized. In a concomitant study, its performance in oxygen and water activation was investigated [106].

2.4.4. Ruthenium complexes sandwiched by two Keggin units

Simultaneously, three independent groups reported the synthesis of a new polyoxometalate sandwiching an adamantane-like tetraruthenium core: $[Ru^{IV}_4(\mu\text{-}O)_4(\mu\text{-}OH)_4Cl_4(\gamma\text{-}SiW_{10}O_{36})_2]^{12-}$ [107] and $[Ru^{IV}_4(\mu\text{-}O)_4(\mu\text{-}OH)_2(H_2O)_4(\gamma\text{-}SiW_{10}O_{36})_2]^{10-}$ [108,109]. The cluster is made from two stacked di-lacunary units, one of them being rotated towards the other by 90° (Fig. 19, on the left). Two adjacent Ru centers of the core are ligated to two oxygen atoms of the POM unit, without contacting the central Si tetrahedron. The synthetic procedures for the preparation of this compound are based on the *in situ* generation of tetraruthenium(IV) core out of (a) $[Ru^{III}(H_2O)Cl_5]^{2-}$ [107]; (b) $[Ru^{IV}_2OCl_{10}]^{4-}$ [108] or (c) $RuCl_3$ [109], followed by a self-assembly with $[\gamma\text{-}SiW_{10}O_{36}]^{8-}$ polyanions in acidic aqueous solutions. This compound turned out to be a highly efficient water splitting catalyst. Its performance in water oxidation to O_2 was tested with an excess of Ce(IV) at pH = 0.6 [108] and in the reaction:

$$4\,[Ru(2,2'\text{-bipy})_3]^{3+} + 2H_2O \rightarrow 4\,[Ru(2,2'\text{-bipy})_3]^{2+} + O_2 + 4H^+$$

at pH = 7 [109]. In concomitant studies various techniques were employed to study its high-valent intermediates [110] and a very fast hole scavenging process from photogenerated Ru(III) species was demonstrated [111].

The phosphotungstate analogue $[Ru^{IV}_4(\mu\text{-}O)_5(\mu\text{-}OH)(H_2O)_4(\gamma\text{-}PW_{10}O_{36})_2]^{9-}$, showing a comparable activity in water oxidation, was prepared in a similar manner [112].

Two tri-lacunary subunits $[XW_9O_{34}]^{9-}$, where X = As(V), P(V); each supporting a $[Ru(C_6H_6)]^{2+}$ group, are linked via an uncommon

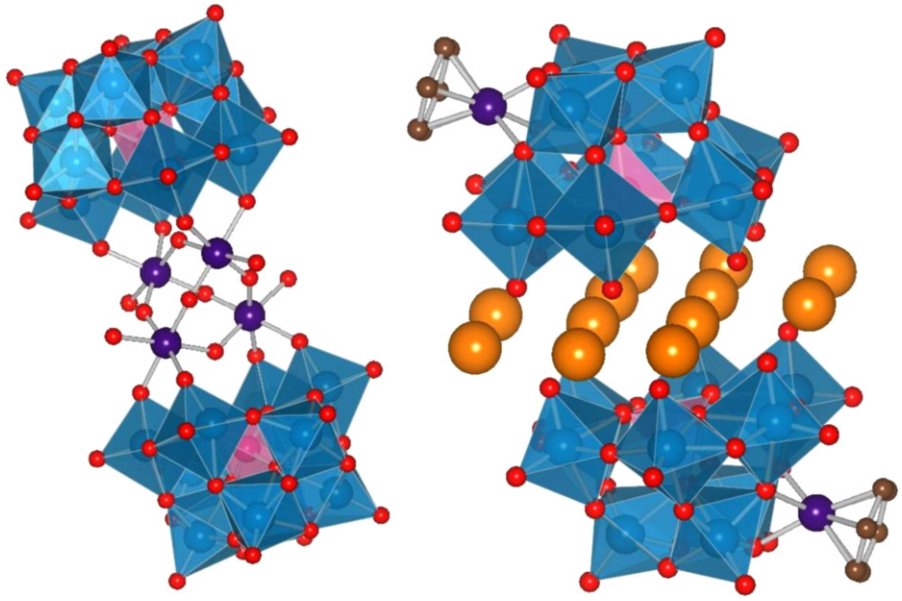

Fig. 19. Structures of $[Ru^{IV}_4(\mu\text{-}O)_4(\mu\text{-}OH)_2(H_2O)_4(\gamma\text{-}SiW_{10}O_{36})_2]^{10-}$ (left, Ref. [109]) and $[\{Na_6Ru(C_6H_6)AsW_9O_{34}\}_2]^{2-}$ (right, Ref. [113]). Na = orange. Water molecules omitted for clarity.

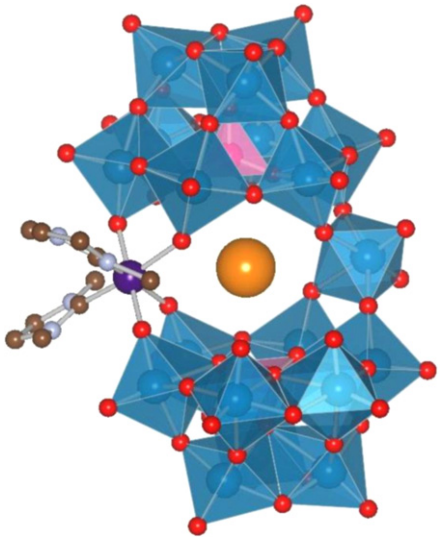

Fig. 20. Structure of $[(cis\text{-}Ru^{III}L_2)(cis\text{-}WO_2)(PW_9O_{34})_2]^{13-}$ with K^+ in the central cavity. H_2O molecules omitted for clarity (Ref. [114]). K = orange.

belt of sodium cations (Fig. 19, on the right). Such pseudo-sandwich compounds result from simple one-pot reactions between lacunary precursors and $[Ru(C_6H_6)Cl_2]_2$ in aqueous solutions [113].

2.4.4.1. Knoth type sandwiches: $[M_3(\alpha\text{-}A\text{-}XW_9O_{34})_2]$. $[(cis\text{-}Ru^{III}L_2)(cis\text{-}WO_2)(PW_9O_{34})_2]^{13-}$, where L = 1,3-dimethylimidazolidine-2-ylidene, is the first carbene derivative of a polyoxometalate. It is the product of the reaction between $[RuL_4Cl_2]$ and $[PW_{11}O_{39}]^{7-}$ in water. In the solution, carbenes released from the substrate are believed to induce the degradation of polyanions to various species. A consecutive exposure to air results in the oxidation of ruthenium. Finally the Ru^{III}-carbene fragments stimulate the exclusive formation of the tri-lacunary form of the polyoxometalate and the final compound could be precipitated. The polyanions in this sandwich structure are not directly one above the other, but slightly shifted (Fig. 20). That is why there is no expected third linker between them, in addition to the organometallic moiety and one WO_6 octahedron, like in classical Knoth type compositions. The Ru center coordinates two oxygen atoms of each subunit and two carbon atoms, with Ru–C bond lengths typical for double bonds (d_{Ru-C} = 2.00–2.05 Å). In the central cavity there is one K^+ and two H_2O molecules encapsulated [114].

2.4.4.2. Weakley type sandwiches: $[M_4(\alpha\text{-}B\text{-}XW_9O_{34})_2]$. $[WZnRu^{III}{}_2(OH)(H_2O)(ZnW_9O_{34})_2]^{11-}$ was presented as an outcome of Zn → Ru substitution carried out in boiling aqueous solution of $[WZn_3(H_2O)_2(ZnW_9O_{34})_2]^{12-}$ and $Ru(DMSO)_4Cl_2$, under Ar. Then, the reaction mixture was opened to air in order to oxidize Ru(II) to Ru(III). Based on a X-ray crystallography study this compound has been claimed to keep the sandwich structure of its precursor, where two B-ZnW_9O_{34} units are joined by a central belt, with an alternate arrangement of Ru, W, Zn and Ru atoms. The Ru centers were supposed to be octahedrally coordinated to 5 oxygen atoms of adjacent units with the sixth ligand either OH^- or H_2O [115]. Problems with isolation of this compound in a pure form were reported, however [55]. Later the methyltricaprylammonium salt of $[WZnRu^{III}{}_2(OH)(H_2O)(ZnW_9O_{34})_2]^{11-}$ was used in the hydroxylation of alkanes (adamantane, congressane) by molecular oxygen, at atmospheric pressure in 1,2-dichloroethane. The substrates were almost exclusively hydroxylated at tertiary carbon positions. A 10 h induction period before initiation was observed, that could be eliminated after reducing Ru(III) to Ru(II) with metallic Zn under Ar. In the epoxidation of alkenes with O_2, in similar reaction conditions, high selectivities were noted. A pre-incubation of the catalyst in O_2 had to be performed before the tests, because a simple mixing of substrate, catalyst and gas in the solvent gave no reaction [116,117]. A mechanism of inorganic dioxygenase type of molecular oxygen activation was proposed with Ru(II), Ru(III) and Ru(IV) intermediates based on all these observations [118]. In later studies, the Ru sandwich was inactive in the homogeneous liquid phase (in 1,2-dichloroethane) dioxygenation of DTBC (3,5-di-*tert*butylcatechol) [119]. Based on these results the claim about a dioxygenase nature of the catalyst was reinvestigated and compelling evidence was presented for a free-radical-chain process [120]. Current reexamination of the collected data strongly suggested that the claimed compound was the parent ion $[WZn_3(H_2O)_2(ZnW_9O_{34})_2]^{12-}$ with only traces of Ru present [121]. However several groups have worked on this ruthenium sandwich complex and it appears that it is possible, by varying slightly the experimental conditions, to obtain species with two ruthenium centers in the structure but these species are not isomerically pure. These mixtures display some dioxygenase activity while in the absence of ruthenium, as in the case of the Finke species, no activity is present. Only these data show that many things can be made in this chemistry.

In earlier catalytic studies the methyltricaprylammonium salt of this impure compound was tested in the catalytic oxidation of alkanes and alkenes with *t*-butyl hydroperoxide and H_2O_2 as oxidizing agents in biphasic water/1,2-dichloroethane systems. When using *t*-butyl hydroperoxide, the alkanes were oxidized efficiently and selectively while the alkenes gave a mixture of products. The Ru impurity containing complex proved better efficiency compared to Pd and Pt analogues. The situation was reversed in the oxidation of alkenes with H_2O_2 with a poor performance of the Ru compound. No catalytic activity of the parent pure-Zn sandwiches or of the Ru-substituted mono-Keggin compound was found in this system [115]. In contrast, the all-sodium salt did not show catalytic activity in oxidation of non-functionalized alkenes in 30% aqueous H_2O_2 used as a reaction medium (absence of organic solvent). On the other hand, out of a series of all-sodium salts of various transition-metal-substituted sandwiches, only the Ru analogue catalyzed the oxidation of alcohols. Moreover, allylic primary alcohols were predominantly epoxidized at the carbon–carbon double bond, but there was no difference in activity between polyoxometalates substituted with various transition metals. HPLC studies showed that under the reaction conditions (30% aqueous H_2O_2) all sandwich species are degraded. As a conclusion, the products of decomposition (undefined Ru-containing compound and peroxotungstate) were proposed as the catalytically active moieties in, respectively alcohol and alkenol oxidations. Alcohols and alkenols were also oxidized in 70% aqueous *t*-butyl hydroperoxide with somewhat higher activities than in H_2O_2, and for alkenols a different selectivity was observed. The catalyst was stable in *t*-butyl hydroperoxide, therefore intermediates other than peroxotungstate must be involved. A slight activity was also detected in the olefin oxidation by potassium peroxymonosulfate at neutral pH, followed by slow decomposition of the compound [122]. High conversion, chemo- (epoxides over ketones) and diastereoselectivity (*threo* isomers over *erythro* for alcohols with 1,3-allylic strain, the other way round for alcohols with 1,2-allylic strain) were observed in the catalytic epoxidation of chiral allylic alcohols with H_2O_2 in biphasic water/1,2-dichloroethane. Again, the transition metal (Ru, Pd, Pt and others) substituting sandwich had only a little effect on the reaction outcome, disproving its direct involvement in the mechanism. A peroxo tungsten complex was suggested as the active species, with a metal-alcoholate bonding between tungsten and the allylic alcohol [123,124]. When in the same process

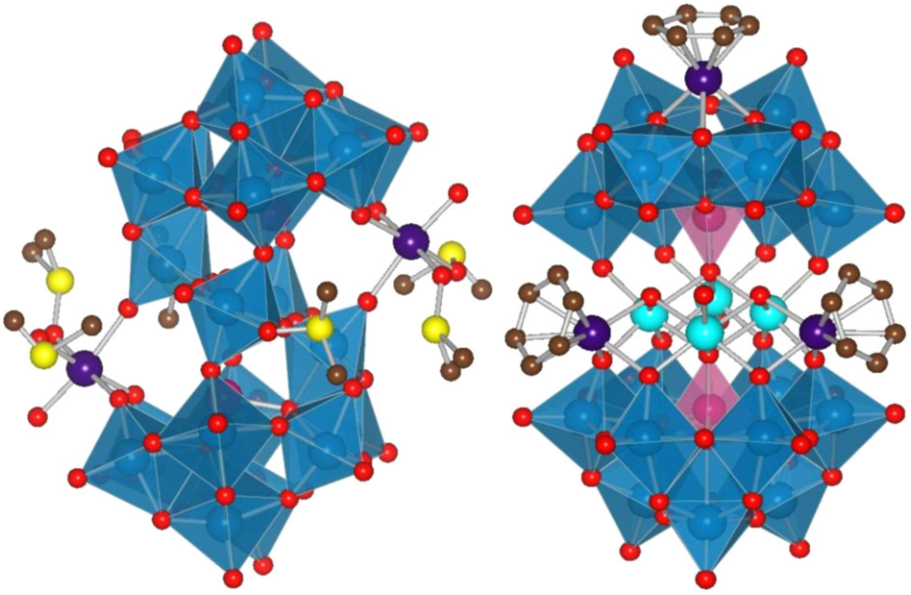

Fig. 21. Structures of: $[\{[(Ru^{III}(DMSO)_2(H_2O)][WO(DMSO)](SbW_9O_{33})\}_2]^{4-}$ (left, Ref. [129]) and $[\{Ru(C_6H_6)\}_3[Zn_4(OH)_2(H_2O)_2](AsW_9O_{34})(AsW_8O_{31})]^{6-}$ (right, Ref. [130]). Zn = light blue.

H_2O_2 was replaced by chiral organic hydroperoxides as an oxygen source, POMs substituted with various metals (Ru, Pd, Pt and others) reacted only at elevated temperature (50 °C) and showed different conversions but comparable diastereoselectivities. This indicates that the type of metal in the central ring of a sandwich plays important role in the hydroperoxide activation. Anyhow, the Ru-containing compound performed worse than the best catalyst in the series: $[ZnW(VO)_2(ZnW_9O_{34})_2]^{12-}$ [125].

$[Zn_2Ru^{III}{}_2(H_2O)_2(ZnW_9O_{34})_2]^{12-}$ was claimed to be active in the electrochemical generation of O_2 but structural analysis indicated rather a mixture of sandwich complexes with various central belt compositions [126].

2.4.4.3. Krebs type sandwiches: $[M_4(\beta\text{-}B\text{-}XW_9O_{33})_2]$ with lone pair containing heteroatoms, e.g. X = As(III), Sb(III), Bi(III), etc.. $[\{(Ru^{II}p\text{-cym})(WO_2)(SbW_9O_{33})\}_2]^{10-}$ is formed from $[\{[WO_2(OH)](WO_2)(SbW_9\ O_{33})\}_2]^{12-}$ by replacing two outer $[WO_2(OH)]^+$ groups with $[Ru(p\text{-cym})]^{2+}$. The Ru atoms are coordinated to three oxygen atoms of two $[\beta\text{-}B\text{-}SbW_9O_{33}]^{9-}$ units. This compound is a result of a self-assembly from $[Ru(p\text{-cym})Cl_2]_2$, Na_2WO_4 and Sb_2O_3 in acidic aqueous solution [127]. It was inactive in the racemization of 1-phenylethanol in chlorobenzene [49]. Another synthetic scheme involves the reorganization of the parent cluster in the presence of $[Ru(arene)Cl_2]_2$ in buffer solution at pH = 6.0. Four isostructural species were obtained by this way: $[\{(Ru^{II}arene)(WO_2)(XW_9O_{33})\}_2]^{10-}$; arene = benzene, *p*-cym; X = Sb(III), Bi(III). They were tested in solvent-free air oxidation of *n*-hexadecane and *p*-xylene. An increase of activity was observed in comparison to the parent polyanions and was attributed to the W → Ru substitution. In both cases a free radical mechanism was proposed. It was also shown that the POMs retained their structures during the reaction [128].

Another Krebs-type sandwich: $[\{[(Ru^{III}(DMSO)_2(H_2O)][WO(DMSO)](SbW_9O_{33})\}_2]^{4-}$ supports two Ru(III) centers, once again tripodally anchored on two neighbouring β-B-polytungstate units (Fig. 21, on the left). Two DMSO molecules in a less common O-mode and one H_2O complete the octahedral coordination sphere of each ruthenium. This compound was obtained from Ru(2,2′-bipy)$_3$Cl$_2$ and $K_6Na_4[Sb_2W_{20}Mn_2(H_2O)_6O_{70}]$ in mixed DMSO/H_2O medium. Interestingly, syntheses employing analogues of Mn-tungstoantimonate with other transition metals gave different products [129].

Synthesis from $[AsW_9O_{34}]^{9-}$, $Zn(OAc)_2$ and $[Ru(C_6H_6)Cl_2]_2$ in aqueous solution gave an interesting example of a asymmetric sandwich cluster: $[\{Ru(C_6H_6)\}_3[Zn_4(OH)_2(H_2O)_2](AsW_9O_{34})(AsW_8O_{31})]^{6-}$ (Fig. 21, on the right). Two out of the three organometallic groups are located in the central belt made by Zn atoms, coordinating to 3 bridging oxygens each, while the last group – also in tripodal coordination mode – decorates the $[AsW_8O_{31}]^{9-}$ unit [130].

2.4.5. Wells-Dawson structure $[X_2W_{18}O_{62}]^{n-}$

2.4.5.1. Ruthenium complexes with a complete Wells-Dawson structure. The grafting reaction of a Ru complex on the Dawson-type anion $[P_2Nb_3W_{15}O_{62}]^{9-}$ [131] was carried out in acetonitrile in N_2 atmosphere. $[(Ru^{II}C_6H_6)P_2Nb_3W_{15}O_{62}]^{7-}$, light- and air-stable, was obtained. The organometallic moiety is regiospecifically attached at the central position of the Nb_3O_9 group, via three bonds with bridging oxygen atoms [132,133]. The mixed $(Bu_4N)^+/Na^+$ salt was used in the catalytic oxygenation of cyclohexene with O_2. The main products were 2-cyclohexenone and 2-cyclohexen-l-ol. It was less active than $(Bu_4N)_5Na_3[Ir(COD)P_2Nb_3W_{15}O_{62}]$ [134].

Significantly, the same organometallic group $[RuC_6H_6]^{2+}$ could be grafted on $[1,2,3\alpha\text{-}P_2V_3W_{15}O_{62}]^{9-}$ via two different ways: (a) over one of the three vanadium octahedra, with bonds to two bridging and one terminal oxygen (off-center isomer, see Fig. 22, on the left) or (b) over the central site between vanadium octahedra, with bonds to three bridging oxygens (on-center isomer, see Fig. 22, on the right). The nature of the obtained product is dependent on the reaction conditions: synthesis from $(Bu_4N)_9[1,2,3\alpha\text{-}P_2V_3W_{15}O_{62}]$ and $[Ru(C_6H_6)Cl_2]_2$ in CH_2Cl_2 at room temperature gives an excess of (a), while in MeCN under reflux mainly (b) is obtained. The on-center isomer (b) is more stable, according to temperature-varied ^{31}P NMR [135].

2.4.5.2. Mono-lacunary Wells-Dawson structure. The Ru-containing compound $[Ru^{III}(H_2O)P_2W_{17}O_{61}]^{7-}$ based on mono-lacunary Daw-

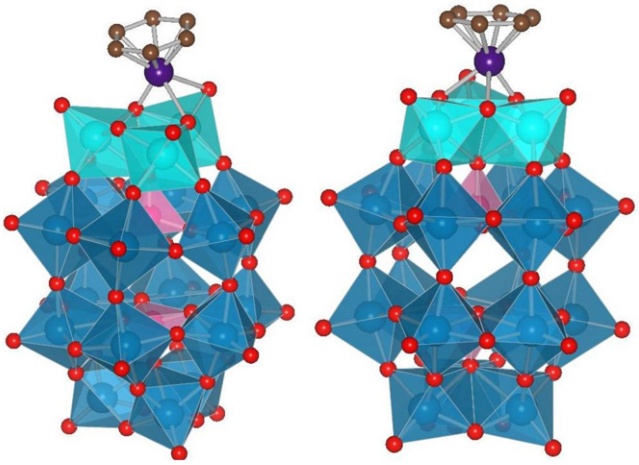

Fig. 22. Suggested isomers of $[(Ru^{II}C_6H_6)1,2,3\alpha\text{-}P_2V_3W_{15}O_{62}]^{7-}$ (Ref. [135]). V = light blue octahedra.

son cluster was obtained by mixing $[\alpha_2\text{-}P_2W_{17}O_{61}]^{10-}$ and $[Ru(H_2O)_6](C_7H_7SO_3)_2$ in water, under argon, followed by oxidation with O_2. Unfortunately this compound could not be isolated without minor impurities [59]. The reaction between $K_{10}P_2W_{17}O_{61}$ and $RuCl_3$, carried out in water with heating, yielded the dimeric species $[O\{Ru^{IV}L(P_2W_{17}O_{61})\}_2]^{16-}$, $L = OH^-$, Cl^-. This compound is stable in solution. The crystal structure revealed two polyanions with metallic centers situated above the lacunas, forming a short (2× 1.773(6) Å), linear Ru–O–Ru bridge (Fig. 23, on the left). The Ru atoms have an octahedral geometry with 2 oxygen atoms from each cluster, the central bridging oxygen and one additional OH^- or Cl^- ligand [87]. During the synthesis, after filtering off the brownish dimer, it was possible to precipitate another species from the mother liquor, using $(Bu_4N)Br$. By this way, the organic salt of $[Ru^{III}(H_2O)P_2W_{17}O_{61}]^{7-}$ has been obtained in pure form. Based on NMR spectra, the Ru atom was assumed to fill the lacuna of the cluster in an approximately octahedral coordination [136]. $[Ru^{III}(H_2O)P_2W_{17}O_{61}]^{7-}$ was an efficient catalyst in the cleavage oxidation of styrene to benzaldehyde and benzoic acid with $NaIO_4$ in biphasic 1,2-dichloroethane/H_2O systems [60].

Reaction of $K_{10}P_2W_{17}O_{61}$ in ice-cooled, acidic aqueous solution with *cis*-$[Ru(DMSO)_4Cl_2]$ yields another dimeric species, $[Ru^{II}(DMSO)_2(P_2W_{17}O_{61})_2]^{18-}$. In this product the central Ru atom links two polyanions and supports also two DMSO molecules (in S-mode), thus being in a quite unusual 10-fold coordination (Fig. 23, on the right). This compound is stable in the solid state but undergoes a slow decomposition in water. Consecutive oxidation of the dimer with Br_2 (only, O_2 and H_2O_2 do not work) leads to $[Ru^{III}(H_2O)P_2W_{17}O_{61}]^{7-}$ [55]. Arene derivatives $[Ru^{II}(arene)(H_2O)P_2W_{17}O_{61}]^{8-}$, arene = C_6H_6, *p*-cym, were obtained from water, $K_{10}P_2W_{17}O_{61}$ and the standard precursors $[Ru(arene)Cl_2]_2$. Quite unexpectedly, they were found water-soluble. In the structure, the Ru atoms are bound to two oxygens of the cluster and coordinate one additional water molecule [137]. The 4 Ru–POM compounds $[Ru^{II}(DMSO)_2(P_2W_{17}O_{61})_2]^{18-}$, $[Ru^{III}(H_2O)P_2W_{17}O_{61}]^{7-}$, $[Ru^{II}(arene)(H_2O)P_2W_{17}O_{61}]^{8-}$, arene = C_6H_6, *p*-cym, were tested in the oxidation of alcohols with O_2 in biphasic water/alcohol systems. $[Ru^{II}(p\text{-cym})(H_2O)P_2W_{17}O_{61}]^{8-}$ turned out to be the best in terms of activity and selectivity to carbonyl products. Oxygen radical and ruthenium-alcoholate species were suggested as possible intermediates [138].

$[H_2NaF_6W_{17}O_{56}]^{11-}$ is an example of lacunary polyfluorooxometalate cluster with the so-called quasi-Wells-Dawson structure. The central position is occupied by a Na^+ cation, surrounded by 6 F^- in a trigonal prism arrangement. There are two types of W atoms in octahedral coordination. 'Belt' tungstens are bound to one terminal and four bridging oxygens and one fluorine. 'Cap' W are bound to 4 bridging and 2 terminal oxygens [139]. This cluster could be easily substituted with Zn(II), and due to lability of this cation, further derivatized with other metal ions. $[Ru^{II}(H_2O)(H_2NaF_6W_{17}O_{55}])]^{11-}$ was obtained by this way. Ru^{2+} is assumed to be able to replace both belt and cap W atoms. This compound was inactive in the catalytic epoxidation of cyclooctene by H_2O_2 in biphasic 1,2-dichloroethane/H_2O systems. It exhibited, however, some activity in the dismutation of H_2O_2 to O_2 and H_2O [140].

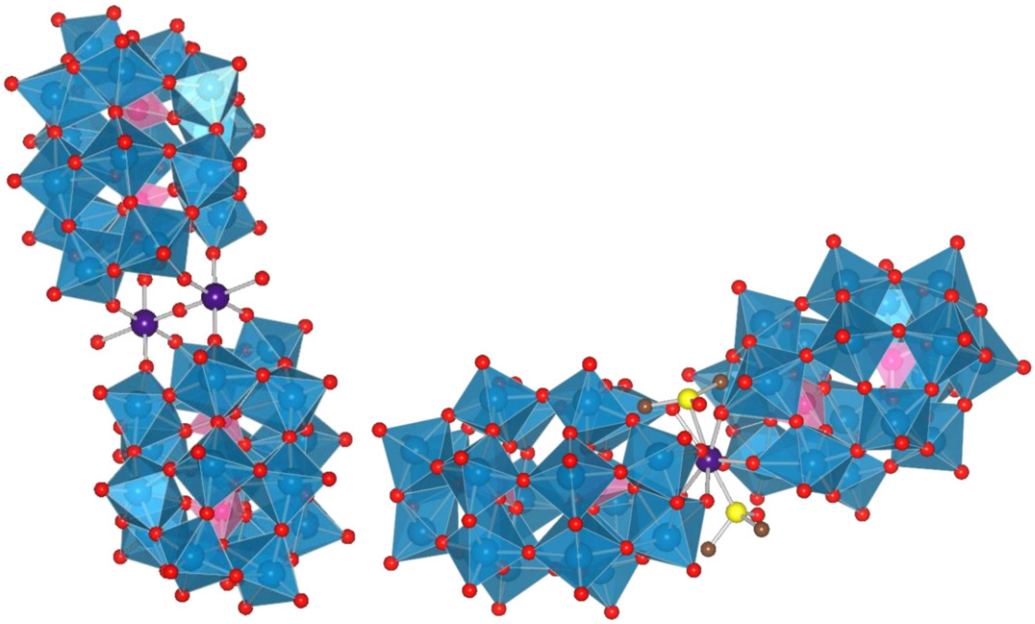

Fig. 23. Structures of: $[O\{Ru^{IV}(OH)(P_2W_{17}O_{61})\}_2]^{16-}$ (left, X-ray structure, Ref. [87]) and $[Ru^{II}(DMSO)_2(P_2W_{17}O_{61})_2]^{18-}$ (right, proposed structure, Ref. [55]).

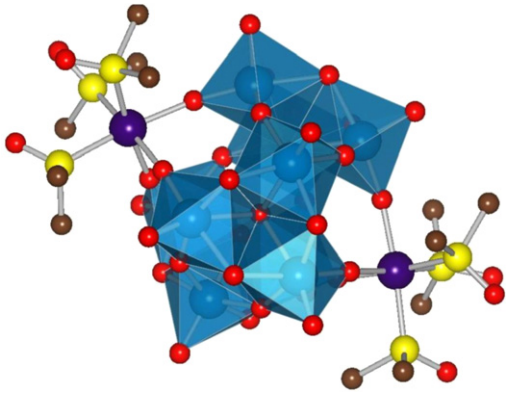

Fig. 24. Structure of $[\{Ru^{II}(DMSO)_3\}_2HW_9O_{33}]^{7-}$ (Ref. [141]).

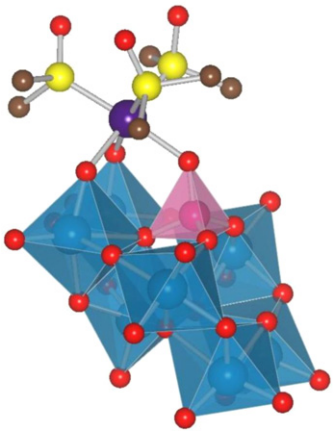

Fig. 26. Structure of $[Ru^{II}(DMSO)_3HPW_7O_{28}]^{6-}$ (Ref. [143]).

2.4.6. Other isopolytungstates

The Ru-functionalized cluster $[\{Ru^{II}(DMSO)_3\}_2HW_9O_{33}]^{7-}$ was obtained from Na_2WO_4 and *cis*-$Ru(DMSO)_4Cl_2$ in buffer solution at pH = 4.8. It is a novel nonatungstate unit, with three W_3O_{13} triads that form a molecular wheel (Fig. 24). Each Ru is bound to three bridging oxygen atoms and three DMSO molecules in a trigonal antiprismatic arrangement [141].

The 1D chain polymer $[Ru^{II}(H_2O)_2W_{12}O_{40}(OH)_2]^{8-}$ is a product of reaction between $Ru(MeCN)_4Cl_2$ and Na_2WO_4 in acidic aqueous solution (Fig. 25). The $[Ru(H_2O)_2]^{2+}$ units are linking paratungstate-B clusters. The Ru atom has an octahedral coordination formed by 4 oxygen atoms from two neighbouring polyanions and two water molecules [142].

2.4.7. Other heteropolytungstates

Three independent synthetic routes lead to the heptatungstate complex $[Ru^{II}(DMSO)_3HPW_7O_{28}]^{6-}$ (Fig. 26). *cis*-$[Ru(DMSO)_4Cl_2]$ could be reacted either with: (a) NaH_2PO_4 and Na_2WO_4 or (b) the all-sodium salt of $[HPW_9O_{34}]^{8-}$ or (c) the all-cesium salt of $[P_2W_5O_{23}]^{6-}$. This new type of polytungstate cluster is built from one W_3O_{13} triad and one half-ring of 4 WO_6 octahedra. The $[Ru(DMSO)_3]^{2+}$ group is attached on its top through bonds with 2 terminal O_W and one O_P atoms. In this complex Ru has a trigonal antiprismatic coordination. The synthesis of the corresponding arsenotungstate $[Ru^{II}(DMSO)_3HAsW_7O_{28}]^{6-}$ was also reported [143].

$[\{K(H_2O)\}_3[Ru^{II}(p\text{-cym})(H_2O)]_4P_8W_{49}O_{186}(H_2O)_2]^{27-}$ is a Ru-functionalized wheel-shaped macromolecule (Fig. 27). It is obtained in an acidic (pH = 6.0) aqueous solution of $[Ru(p\text{-cym})Cl_2]_2$ and the cyclic polyanion $[H_7P_8W_{48}O_{184}]^{33-}$. This cluster preserves the (somewhat distorted) structure of the precursor-4 fused P_2W_{12} units, with eight potential binding sites in the central cavity. Four of these sites are occupied by $[Ru(p\text{-cym})(H_2O)]^{2+}$ groups with Ru atoms coordinated to two oxygens from adjacent fragments. All four *p*-cymene molecules as well as two H_2O stick outside the cavity while the other two H_2O point inside it. The remaining four sites are shared between potassium cations and additional tungsten linkers $[cis\text{-}WO_2(H_2O)_2]^{2+}$, with 50% occupancy factor each. The inorganic allosteric effect upon Ru binding has also been discussed [144].

3. Polyoxometalates containing osmium

3.1. Polymolybdates

3.1.1. $[Mo_4O_{16}]^{8-}$

The osmium complex $[\{Os^{II}(\eta^6\text{-}p\text{-cym})\}_4Mo_4O_{16}]$ was synthesized and is the analogue of the previously described ruthenium complex. In the solid state it has a windmill-type structure and isomerizes in chlorobenzene. Its activity in racemization of 1-phenylethanol in chlorobenzene was lower than that of Ru compounds [49].

3.1.2. Other polymolybdates

The characterization and catalytic tests on $(NH_4)_4[Os^{II}(DMSO)_3Mo_7O_{24}]$ were described for the ruthenium analogue [56].

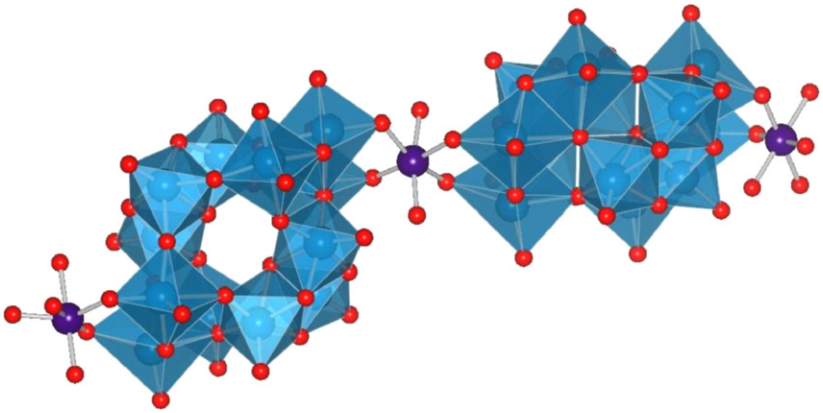

Fig. 25. Polymeric chain of $[Ru^{II}(H_2O)_2W_{12}O_{40}(OH)_2]^{8-}$ (Ref. [142]).

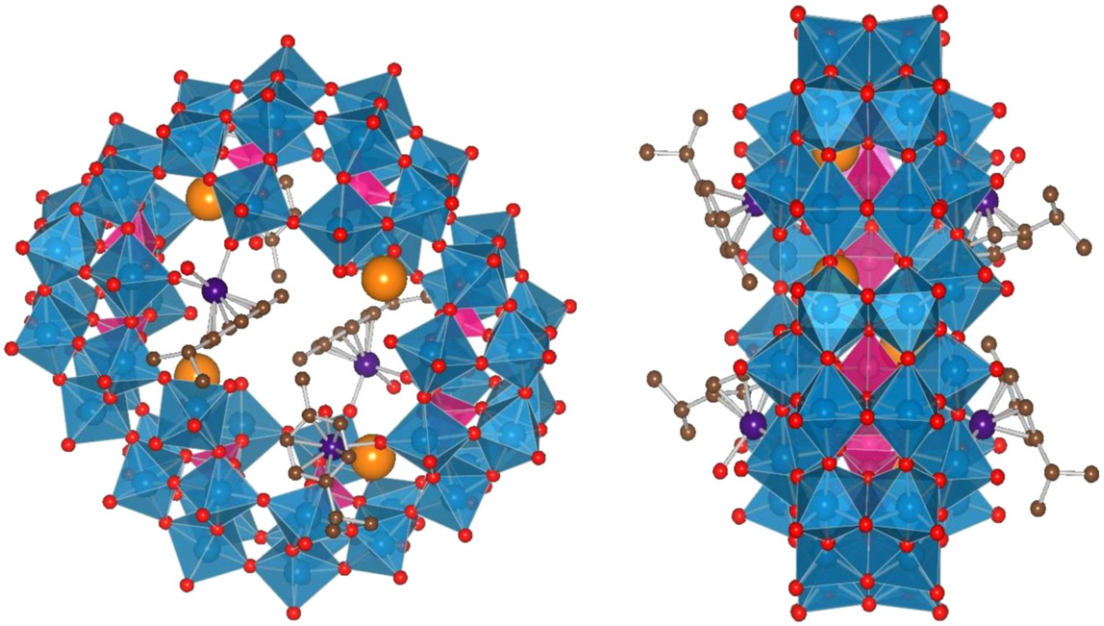

Fig. 27. Structure of $[\{K(H_2O)\}_3[Ru^{II}(p\text{-cym})(H_2O)]_4P_8W_{49}O_{186}(H_2O)_2]^{27-}$ (Ref. [144]). Front and side view.

3.2. Polytungstates

3.2.1. Keggin structure $[XW_{12}O_{40}]^{n-}$

The first Os-containing derivative of a Keggin-type POM was $[(Os^{VI}N)PW_{11}O_{39}]^{4-}$, which is analogous to the Ru species and is obtained by the following reaction in anhydrous MeCN in the presence of Et_3N:

$$(Bu_4N)[OsNCl_4] + (Bu_4N)_4[H_3PW_{11}O_{39}] \rightarrow (Bu_4N)_4[(OsN)PW_{11}O_{39}] + 3HCl + (Bu_4N)Cl$$

This compound is air-stable. The polyoxotungstate serves as a pentadentate ligand for the $[Os{\equiv}N]^{3+}$ moiety, via its oxygen atoms (see Fig. 28, on the left) [145]. DFT calculations on the fully oxidized form $[(Os^{VIII}N)PW_{11}O_{39}]^{2-}$ showed that the bonds in the Os-substituted cluster are shortened compared to $[PW_{12}O_{40}]^{3-}$. The presence of osmium modifies mainly the unoccupied orbitals, especially the LUMO, which is now localized on Os with only a small contribution from W (38.5% and 1.2%, respectively). Additionally, LUMO and HOMO–LUMO energy gap tend to have a lower energy. When the cluster is reduced, it is more likely for Os to accept the additional electron [146]. Calculations on ground, excited and reduction states of gaseous $[(Os^{VI}N)PW_{11}O_{39}]^{4-}$ were also performed. In the ground state the LUMO and LUMO+1 are formed predominantly from W d orbitals, whereas strong antibonding OsN orbitals are shifted to the higher LUMO+4 and LUMO+5. This complex is then a poorer electrophile than its Ru analogue. In the triplet and quintet excited states, the Os-N bond length is not strongly modified, due to the fact that the LUMO and LUMO+1 are not [OsN] antibonding orbitals. The [OsN] unit is not the reduction center, as additional electrons are localized on the POM ligand. Solvation effect causes the absolute energies of orbitals to decrease but does not significantly change their order, composition or relative energies [80].

The bidentate coordination mode of Os to the polytungstate unit, in analogy with the Ru congeners, is evidenced in the complexes $[\{Os^{II}(DMSO)_3(H_2O)\}\alpha\text{-}PW_{11}O_{39}]^{5-}$ and $[\{Os^{II}(\eta^6\text{-}p\text{-cym})(H_2O)\}\alpha\text{-}PW_{11}O_{39}]^{5-}$ [73].

3.2.2. Wells-Dawson structure $[X_2W_{18}O_{62}]^{n-}$

Two nitrido-functionalized mono-lacunary Dawson-type polytungstates, $[(Os^{VI}N)\alpha_1\text{-}P_2W_{17}O_{61}]^{7-}$ and $[(Os^{VI}N)\alpha_2\text{-}P_2W_{17}O_{61}]^{7-}$, were obtained using the same procedure than for the Keggin polyoxotungstate. These two complexes contain the $[Os{\equiv}N]^{3+}$ moiety, with the polyanion serving as a pentadentate ligand [147] (see Fig. 28, on the right).

3.2.3. Other polytungstates

Cis-$[Os(DMSO)_4Cl_2]$ reacts, in a buffer solution at pH = 6.0, either with: (a) As_2O_5 and Na_2WO_4 or (b) the all-sodium salt of $[HAsW_9O_{34}]^{8-}$ yielding in both cases $[Os^{II}(DMSO)_3HAsW_7O_{28}]^{6-}$, which has the same structure that its Ru analogue [148].

4. Polyoxometalates containing rhodium

4.1. Polyvanadates

4.1.1. $[V_4O_{12}]^{4-}$

$[(\eta^3\text{-}C_4H_7)_2Rh(MeCN)_2]PF_6$ and $(Bu_4N)VO_3$ were mixed in acetonitrile under N_2 flow yielding $(Bu_4N)_2[\{(\eta^3\text{-}C_4H_7)_2Rh^{III}\}_2(V_4O_{12})]$. The polyanion is formed by a V_4O_4 ring with each vanadium atom having two additional terminal oxygens. In this particular compound the ring has a twisted boat-chair conformation, with all vanadium atoms being co-planar (Fig. 29). The rhodium centers are coordinated to two terminal oxygens of adjacent vanadium atoms and two β-methallyl moieties (one *exo* and one *endo* towards the ring) in an octahedral arrangement. In the presence of CO gas or $P(OEt)_3$ in CH_2Cl_2 this compound undergoes a reductive coupling process and $(Bu_4N)_2[\{(\eta^4\text{-}C_8H_{14})Rh^{I}\}_2(V_4O_{12})]$ is obtained (C_8H_{14} = 2,5-dimethyl-1,5-hexadiene). This new compound is closely related structurally to its precursor. The POM is in a twisted chair conformation with 4 V and 2 O atoms co-planar while the two Rh species are bent towards the ring. They are in a square planar environment formed by two terminal oxygens and 2 allyl bonds [149]. The more thermodynamically stable is the *exo* form, with the sterically hindering methyl groups pointing outwards the cluster. It is exclusively present in the solid state but in solution a rotation of the organometallic groups on vanadium surface results in equilibrium between the two isomers, as observed in ^{51}V or

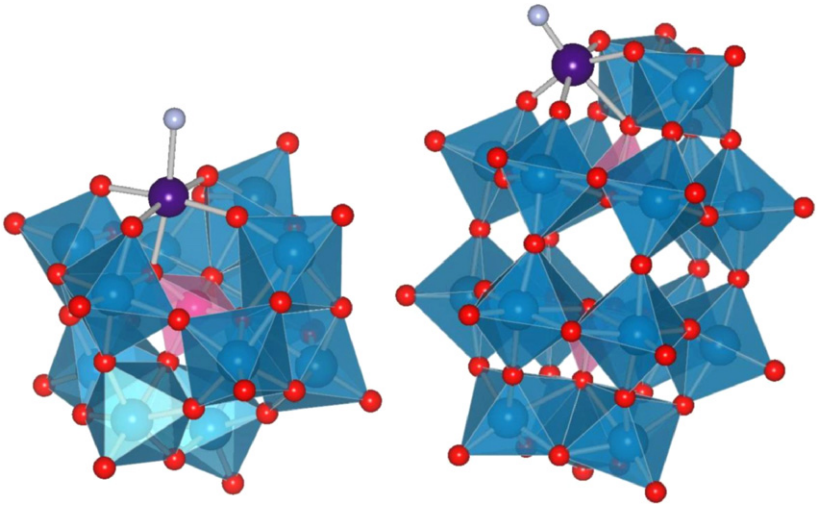

Fig. 28. Proposed structures for $[(OsN)PW_{11}O_{39}]^{4-}$ (left, Ref. [145]) and $[(OsN)\alpha_2\text{-}P_2W_{17}O_{61}]^{7-}$ (right, Ref. [147]).

^{1}H NMR spectra. For $[\{(\eta^4\text{-}C_6H_{10})Rh^I\}_2(V_4O_{12})]^{2-}$ (C_6H_{10} = 1,5-hexadiene) the situation is reversed, the *endo* isomer being the most stable [150].

Interestingly, the reaction of $[(\eta^3\text{-}C_4H_7)_2Rh^{III}(acac)]$ with $P(OEt)_3$ leads to a mixture of organic products instead of a coupling reaction, although both compounds have almost identical local environments of rhodium. The effect of grafting on the polyvanadate support on the activity and selectivity of the methallyl rhodium complexes is therefore pronounced, and is similar to the grafting on solid oxides like silica, alumina or titania [151].

Analogous procedures yield also salts of $[\{(COD)Rh^I\}_2(V_4O_{12})]^{2-}$ and $[\{(COD)Rh^I\}(V_4O_{12})]^{3-}$, when varying the Rh/V molar ratio. By means of ^{17}O NMR the intramolecular mobility of the organometallic fragments along the ring was shown, with a possible penta-coordinated Rh in a distorted trigonal bipyramid geometry as an intermediate [152].

4.1.2. *Lindqvist structure* $[V_6O_{19}]^{8-}$

The vanadate hexamer $[(Rh^{III}Cp^*)_4(V_6O_{19})]$ with Rh-organic species was first synthesized in an aqueous solution of $[RhCp^*Cl_2]_2$ and $NaVO_3$, and extracted with CH_2Cl_2 [153]. Later on, an organometal hydroxide route, employing aqueous solutions of $[RhCp^*(OH)_2]_2$ and V_2O_5, was proposed [154]. The compound is stable in non-aqueous solvents and neutral water, but at pH < 4 it gradually starts to lose organometallic species. Liberation of $[RhCp^*(H_2O)_3]^{2+}$ groups could be followed by substitution of $[IrCp^*(H_2O)_3]^{2+}$ ones, and allowed to produce a whole range of mixed rhodium–iridium clusters with the general formula: $[(Rh^{III}Cp^*)_{4-n}(Ir^{III}Cp^*)_n(V_6O_{19})]$ [153,155]. This compound was tested in the oxidation of cyclohexene with *t*-butyl hydroperoxide. The reaction, carried out in CH_2Cl_2 under N_2 in 70 °C, was not selective, yielding a mixture of allylic oxidation products [156].

Two vanadate clusters, $[\{(\eta^3\text{-}C_4H_7)_2Rh^{III}\}_2(V_4O_{12})]^{2-}$ and $[(Rh^{III}Cp^*)_4(V_6O_{19})]$, were grafted on silica. Consecutive studies showed that during the reaction the clusters retained their structure and that a partial elimination of organic ligands and a creation of bonds between rhodium and silanol groups took place (see Fig. 30). These catalysts were tested in the oxidation of propene to acetone with O_2. Compared to inert crystalline precursors, both grafted moieties showed a higher catalytic activity in this reaction [157,158]. $[(Rh^{III}Cp^*)_4(V_6O_{19})]$ deposited on silica was an active catalyst in the gas phase hydration of acetonitrile to acetamide and dehydrogenation of 2-propanol to acetone under mild conditions [159].

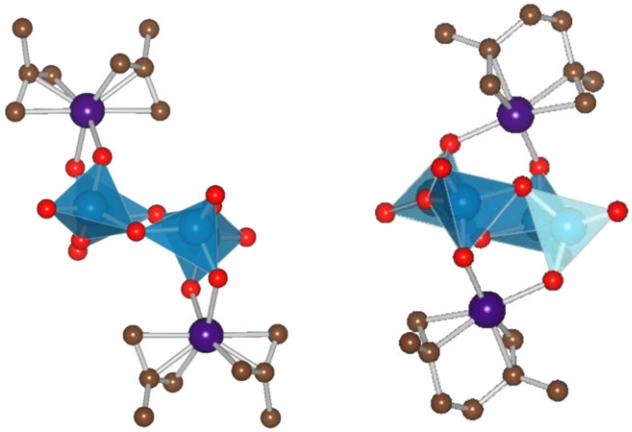

Fig. 29. Structures of: $[\{(\eta^3\text{-}C_4H_7)_2Rh^{III}\}_2(V_4O_{12})]^{2-}$ (left) and $[\{(\eta^4\text{-}C_8H_{14})Rh^I\}_2(V_4O_{12})]^{2-}$ (right, both from Ref. [149]). The latter is a product of reductive coupling of the former, in the presence of CO or $P(OEt)_3$.

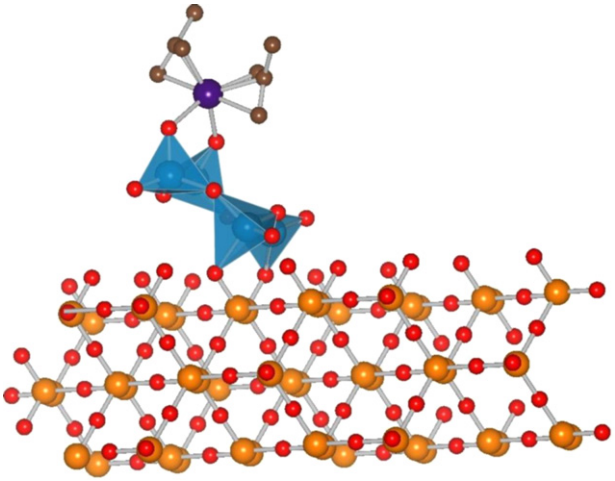

Fig. 30. $[\{(\eta^3\text{-}C_4H_7)_2Rh^{III}\}_2(V_4O_{12})]^{2-}$ grafted on silica (Ref. [157]). Si = orange.

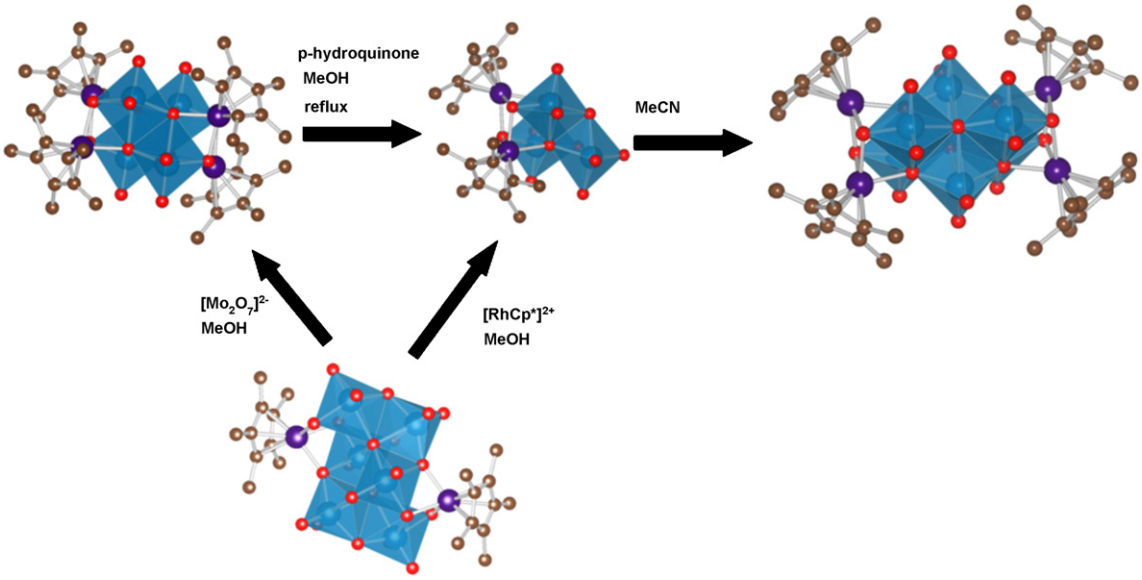

Fig. 31. Some transformations of polymolybdate clusters (Refs. [161,167]).

4.2. Polymolybdates

4.2.1. $[Mo_4O_{16}]^{8-}$ and/or its derivatives

An aqueous solution of Na_2MoO_4 and $[RhCp^*Cl_2]_2$ stirred for 3 h in 25 °C leads to the formation of $[(Rh^{III}Cp^*)_4Mo_4O_{16}]$. In the solid state this compound has a triple cubane structure. Due to the long distances there is no interaction between the metal atoms of the cluster [160]. Refluxing an equimolar solution of $[(Rh^{III}Cp^*)_4Mo_4O_{16}]$ and *p*-hydroquinone in MeOH for 3–4 h resulted in the conversion of this complex into $[(Rh^{III}Cp^*)_2Mo_3O_9(OMe)_4]$. This trishomocubane-type cluster has three bridging methoxy groups (the fourth one is terminal) capping vacant vertices. Upon dissolution in organic solvents (MeCN, CH_2Cl_2), two such fragments fuse together to yield the quadruple cubane $[(Rh^{III}Cp^*)_4Mo_6O_{22}]$ (see Fig. 31) [161]. In the presence of CH_3SH instead of *p*-hydroquinone, there is a strong dependence of the obtained products on the reaction conditions. At room temperature tetranuclear Mo_2Rh_2 clusters are formed [162,163]. Under reflux the organometallic and oxide fragments are separated and the salt of $[(Rh^{III}Cp^*)_2(\mu_2\text{-}SCH_3)_3]_4[Mo_8O_{26}]$ is produced [164]. Detailed investigation of the interconversion of this species was performed [165]. Rhodium derivatives produced in the reaction of $[(Rh^{III}Cp^*)_4Mo_4O_{16}]$ with 1,2-benzenedithiol do not contain any oxide fragments at all [166]. Another closely related species, $[(Rh^{III}Cp^*)_2Mo_6O_{20}(OMe)_2]^{2-}$, was obtained by reaction of $[RhCp^*Cl_2]_2$ and $(Bu_4N)_2Mo_2O_7$ in methanol. The cluster is formed by four MoO_6 and two $MoO_5(\mu\text{-}OMe)$ octahedra. The rhodium atoms coordinate two bridging oxygens and the oxygen of the methoxy group. Upon addition of $[RhCp^*]^{2+}$ or $Mo_2O_7^{2-}$ to its methanol solution, the aforementioned unit rearranges into $[(Rh^{III}Cp^*)_2Mo_3O_9(OMe)_4]$ and $[(Rh^{III}Cp^*)_4Mo_4O_{16}]$, respectively [167]. ESI-MS experiments showed that a key intermediate in the formation of $[(Rh^{III}Cp^*)_2Mo_6O_{20}(OMe)_2]^{2-}$, as well as in its methanolysis, is $[(Rh^{III}Cp^*)_2Mo_3O_8(OMe)_5]^-$ [168]. The transformation scheme of this "family" of polyoxoanions is presented in Fig. 31.

The complete $[(Rh^{III}Cp^*)_4Mo_4O_{16}]$ and incomplete $[(Rh^{III}Cp^*)_2Mo_3O_9(OMe)_4]$ clusters were grafted on silica and reduced with CO under photo-illumination. Only bridging Rh–O and Mo–O were selectively reduced. IR spectra taken afterwards showed two sets of carbonyl stretch bands, for CO molecules attached to Rh^{3+} and Mo^{4+}/Mo^{5+} atoms. The grafted compounds did not show any catalytic activity when tested in the metathesis of propene, even after CO/photoreduction. A consecutive complete evacuation of CO at 473 K did not cause the collapse of the cubane framework. In addition a high catalytic activity of oxygen-deficient Mo sites was noted (still, not as high as that of conventional Mo catalysts) and the reaction yielded equimolar mixture of ethene and 2-butenes. The incomplete cluster exhibited a 3-times higher activity than the complete one, due to much lower activation energy, as well as higher *trans*/*cis* ratios of 2-butenes [158,169].

4.2.2. Lindqvist structure $[Mo_6O_{19}]^{2-}$ and/or its derivatives

Reaction of $AgNO_3$ and $[Cp^*RhCl_2]_2$ in methanol generates *in situ* the solvated complex of rhodium $[RhCp^*(MeOH)_3]^{2+}$ that, combined with the nitrosyl derivate of the Lindqvist unit $[Mo_5O_{13}(OMe)_4(NO)]^{3-}$, yields $[Rh^{III}Cp^*(H_2O)\{Mo_5O_{13}(OMe)_4(NO)\}]^-$ as its *tert*-butylammonium or *tert*-methylammonium salts. Rhodium binds only to two axial oxygens of the cluster and completes its coordination sphere with a water molecule (Fig. 32). An excess of halide ions in the mother liquor during synthesis gives compounds of the type $[(Rh^{III}Cp^*)_2(\mu\text{-}X)\{Mo_5O_{13}(OMe)_4(NO)\}]$ (X = Cl or Br). Here, the bipodally grafted organometallic moieties are additionally linked through bridging halide ions [170,171].

4.2.3. Anderson structure $[Mo_6MO_{24}]^{n-}$

Reaction of $RhCl_3$ and $(NH_4)_6Mo_7O_{24}$ (molar ratio Rh:Mo = 1:6) in aqueous solution at pH = 4 gives $[H_6RhMo_6O_{24}]^{3-}$. The rhodium octahedron is located in the inversion center of the α-Anderson cluster [172]. By introducing stoichiometric amounts of $Al(NO_3)_3$ into reaction environment an attempt was made towards the obtention of a series of $[(Rh_x, Al_{1-x})Mo_6O_{24}]$ solid state solutions. However, due to the noticeable difference of the ionic radii of the rhodium and aluminium heteroatoms, the formation was limited to $x = 0.25$. A series of catalysts was then made by impregnation of γ-Al_2O_3 with pure $RhMo_6$, an equimolar mixture of $RhMo_6$ and $AlMo_6$ and $(Rh_{0.25}, Al_{0.75})Mo_6$. These three compounds were then tested in cyclohexene hydrogenation and thiophene hydrodesulfurization. All Rh-containing species showed better performance in the hydrogenation process than commercial CoMo and Rh catalysts and their activity was related to the Rh content. In hydrodesulfurization, on the other hand, there was no great difference between commercial systems and those prepared by this new way [173,174].

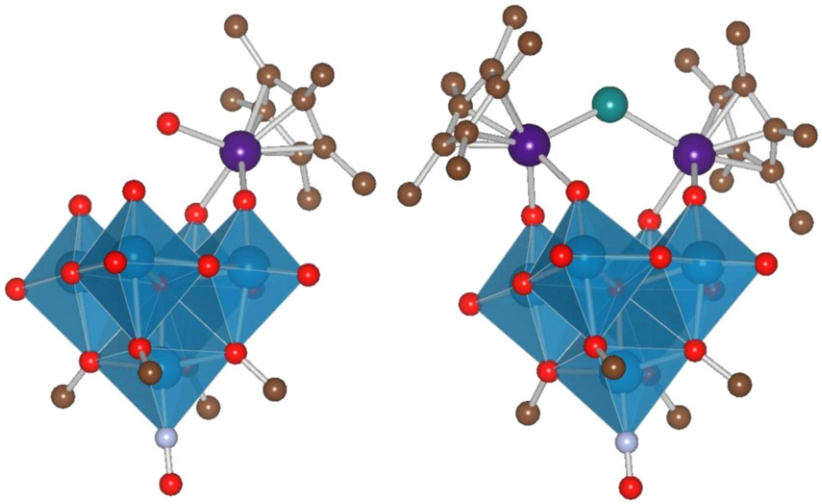

Fig. 32. Structures of $[Rh^{III}Cp^*(H_2O)\{Mo_5O_{13}(OMe)_4(NO)\}]^-$ (left) and $[(Rh^{III}Cp^*)_2(\mu\text{-}Br)\{Mo_5O_{13}(OMe)_4(NO)\}]$ (right, both from Ref. [170]). Br = green.

4.2.4. Wells-Dawson structure $[X_2Mo_{18}O_{62}]^{n-}$

An analogous procedure was used to prepare the Dawson cluster substituted with the Rh-acetate dimer (see details in Section 4.3.3). The goal was to obtain bifunctional electrocatalysts by deposition of alternating layers of Rh_2POM and polyamidoamine dendrimers on a glassy carbon electrode. The so-prepared systems were tested in the electrochemical reduction of nitrites and oxidation of arsenites [175].

4.2.5. Other polymolybdates

In contrast to all the previous examples, $[\{Rh^{III}Cp^*\}_8Mo^{V}{}_{12}O_{36}Mo^{VI}O_4]^{2+}$ is an example of a predominantly Mo(V) cluster. It is obtained in hydrothermal synthesis from MoO_3 and $[(RhCp^*)_2(OH)_3]Cl$. The Mo(V) atoms constitute the vertices of an octahedron with organometallic species capping the faces (Fig. 33). Each Rh atom is coordinated to three bridging oxygen atoms. A tetrahedral $Mo^{VI}O_4$ group is located inside the cation, with oxygen atoms weakly bonded to three adjacent Mo(V) [176].

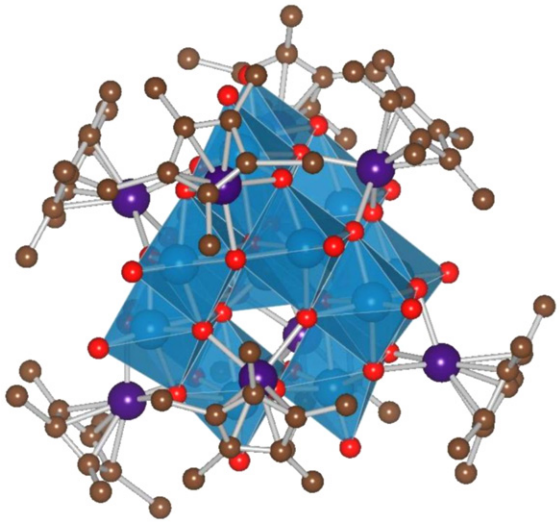

Fig. 33. Structure of $[\{Rh^{III}Cp^*\}_8Mo^{V}{}_{12}O_{36}Mo^{VI}O_4]^{2+}$ (Ref. [176]).

4.3. Polytungstates

4.3.1. $[W_4O_{16}]^{8-}$ and/or its derivatives

It is possible to produce selectively two isomers of the $[(Rh^{III}Cp^*)_4W_4O_{16}]$ cluster by varying the temperature of the reaction synthesis. When the reaction of $[Cp^*RhCl_2]_2$ with $(Bu_4N)_2WO_4$ in MeCN is carried out below 20 °C, the product has a triple-cubane structure, whereas above 60 °C the windmill form is isolated. No isomerization is observed in the solid state upon heating of the samples. On the other hand, in MeCN solution above 60 °C the triple-cubane compound isomerizes into the windmill one. The thermodynamic stability of both forms is dependent on the solvent used: while in MeCN the windmill form is the most stable, it is the triple cubane one in $CHCl_3$ and CH_2Cl_2 [177].

4.3.2. Lindqvist structure $[W_6O_{19}]^{2-}$ and/or its derivatives

A precipitate of dimeric $[\{(C_7H_8)Rh^{I}\}_5(cis\text{-}Nb_2W_4O_{19})_2]^{3-}$ is formed upon addition of Et_2O to an acetonitrile solution of $[(C_7H_8)Rh(MeCN)_2](PF_6)$ (where C_7H_8 = norbornadiene) and $(Bu_4N)_4[cis\text{-}Nb_2W_4O_{19}]$ in N_2 atmosphere. The two Lindqvist units are oriented face-to-face towards each other and linked through five $[Rh(C_7H_8)]^+$ moieties. The Rh atoms have a square planar geometry formed by two allylic bonds with the norbornadiene ligand and two oxygen atoms, one from each polyanion. Both terminal and bridging oxygen atoms of the POMs are used to bind the organometallic species, with the Nb terminal oxygens being preferred over W terminal ones [178]. When carbon monoxide is bubbled through a solution of the compound in CH_3NO_2, each C_7H_8 molecule is replaced by 2 CO, coordinating to Rh through their carbon atoms. The resulting complex $[\{(CO)_2Rh^{I}\}_5(cis\text{-}Nb_2W_4O_{19})_2]^{3-}$ retains its overall dimeric structure (Fig. 34, on the left). The square planar geometry around the Rh atoms is also preserved. Based on their connection mode to the oxygen atoms, different types of Rh complexes could be distinguished: (1) linked to bridging O_{Nb_2}, (2) to terminal O_{Nb} and (3) to bridging O_{NbW}. The same compound can also be obtained by reaction of $[(CO)_2RhCl]_2$ and $(Bu_4N)_4[cis\text{-}Nb_2W_4O_{19}]$ in CH_2Cl_2 under N_2. Noticeably, the same substrates mixed in $CHCl_3$ give $[\{(CO)_2Rh^{I}\}_3(cis\text{-}Nb_2W_4O_{19})_2]^{5-}$. Its structure derives from the above penta-rhodium moiety, by removal of two $[Rh(CO)_2]^+$ groups bound to O_{NbW} oxygen atoms (Fig. 34, on the right) [179].

$[(Rh^{III}Cp^*)cis\text{-}Nb_2W_4O_{19}]^{2-}$ is analogous to $[(Ru^{II}p\text{-}cym)cis\text{-}Nb_2W_4O_{19}]^{2-}$. However, the three possible diastereisomers of this compound (shown in Fig. 35) can be obtained depending on the

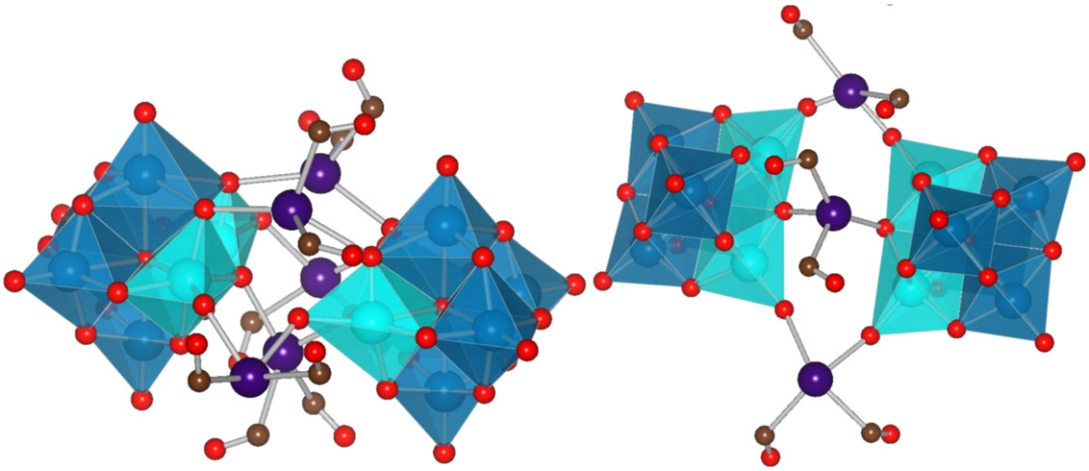

Fig. 34. Suggested structures of the dimers $[\{(CO)_2Rh^I\}_5(cis\text{-}Nb_2W_4O_{19})_2]^{3-}$ (left) and $[\{(CO)_2Rh^I\}_3(cis\text{-}Nb_2W_4O_{19})_2]^{5-}$ (right, both from Ref. [179]). Nb = light blue octahedra.

synthesis conditions: A mixture of $[Cp^*RhCl_2]_2$ with $(Bu_4N)_4[cis\text{-}Nb_2W_4O_{19}]$ in CH_2Cl_2 at room temperature gives isomers I and II. After elimination of the halide anions, $[(Cp^*)Rh(MeCN)_3]^{2+}$ and $[cis\text{-}Nb_2W_4O_{19}]^{4-}$ in $MeCN/CH_2Cl_2$ yield all three isomeric forms in a 1:1:1 ratio. Apparently, in this case, the negative surface charge is not localized exclusively around the Nb(V) centers but effectively spreads over the whole polyoxometalate. Again, all manipulations were routinely performed under N_2, but the product is air-stable [180].

4.3.3. Keggin structure $[XW_{12}O_{40}]^{n-}$

The reaction of metal complex $(C_7H_8)_2RhSnCl_3$ with $PW_{11}O_{39}^{7-}$ resulted in the formation of $[(C_7H_8)_2RhSnPW_{11}O_{39}]^{4-}$. According to the proposed structural model, the Sn atom fills the lacuna of the cluster and is linked to rhodium via a metal-metal bond [181]. It was also reported that Rh-substituted heteropolytungstates could be obtained by precipitation from hot, aqueous solutions of polyanions and simple inorganic rhodium salts, like chloride or nitrate, leading to species for which the formula $[\alpha\text{-}Rh^{III}(OH_{2-x})XW_{11}O_{39}]^{n-}$, X = B, Si, Ge, P; $x = 0$–2 was proposed [182]. However, these compounds were only characterized by infrared and NMR spectroscopies and no X-ray structure was reported.

New and more efficient procedures were developed later and various Rh-containing derivatives became accessible: $[Rh^{III}LPW_{11}O_{39}]^{n-}$, L = Cl^-, Br^-, I^-, H_2O, CN^-, CH_3COO^-, DMSO, py, or $[RhPW_{11}O_{39}]^{4-}$. In hydrothermal conditions the chloro- and bromo-compounds could be synthesized from simple substrates such as $H_3PW_{12}O_{40}$, $RhCl_3$ and LiCl/NaBr. The electrochemical reduction of $[RhClPW_{11}O_{39}]^{5-}$ leads to a dimeric $[(RhPW_{11}O_{39})_2]^{10-}$ complex (see Fig. 36) where the Keggin units are joined via a Rh-Rh metallic bond (Rh···Rh = 2.52(2) Å). This moiety could either undergo various reactions leading to ligand substitution: (i) directly for L = CN^-, DMSO, py; (ii) by chemical oxidation for L = Cl^-, Br^-, H_2O; (iii) electrochemically for L = Cl^-, CH_3COO^-, H_2O and (iv) photochemically for L = Br^-, I^-. Interestingly, the lines in the ^{183}W NMR spectra exhibited shifts that could be correlated with changes of the chemical softness of the terminal ligands on Rh [183]. Hydrothermal reaction of $PW_{11}O_{39}^{7-}/SiW_{11}O_{39}^{8-}$ with $RhCl_3$ in acetate buffer results in a rhodium-carbon bond formation and products with a formula: $[Rh^{III}(CH_2COOH)XW_{11}O_{39}]^{5-/6-}$, X = P, Si (see Fig. 36). The terminal functional group could be further derivatized, e.g. to amide [184].

Similarly, performing the synthesis with the rhodium acetate dimer $Rh_2(OAc)_4$ results in the grafting of a bimetallic moiety on the lacunary polyanion and formation of $[\{Rh^{II}{}_2(OAc)_2\}XW_{11}O_{39}]^{5-/6-}$, X = P, Si (see Fig. 36). In the solid state the axial Rh sites are occupied by DMSO solvent molecules. Preliminary investigations showed that $[\{Rh_2(OAc)_2\}PW_{11}O_{39}]^{5-}$ was less effective in cyclopropanation of styrene with ethyl diazoacetate than its dimeric precursor [185]. This compound was also tested in the electrochemical oxidation of L-methionine, L-cystine and As(III), in homogenous conditions, as well as a dopant in a xerogel-based carbon-composite electrode. It was stable and active in a wide pH range (between 2 and 10) [186]. In following studies, it was encapsulated in silica and used for the amperometric detection of peptides separated by HPLC [187].

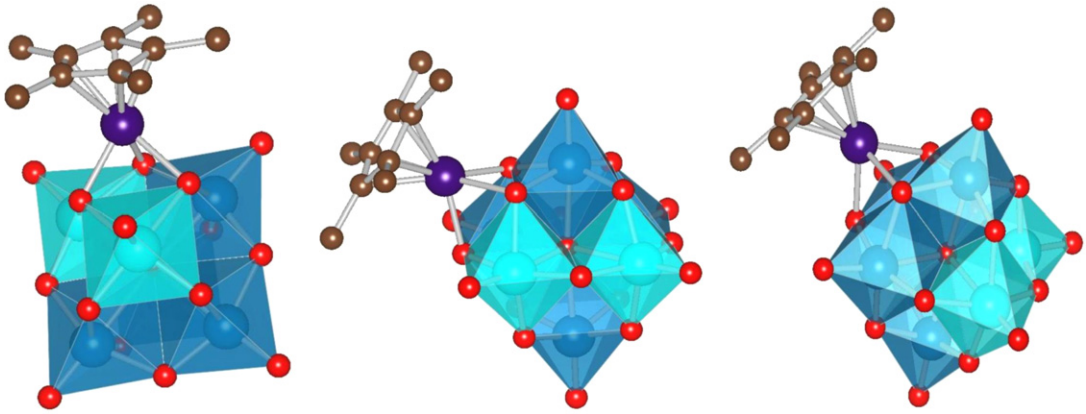

Fig. 35. Diastereoisomers of $[(Rh^{III}Cp^*)cis\text{-}Nb_2W_4O_{19}]^{2-}$: forms I, II and III, beginning from the left (Ref. [180]).

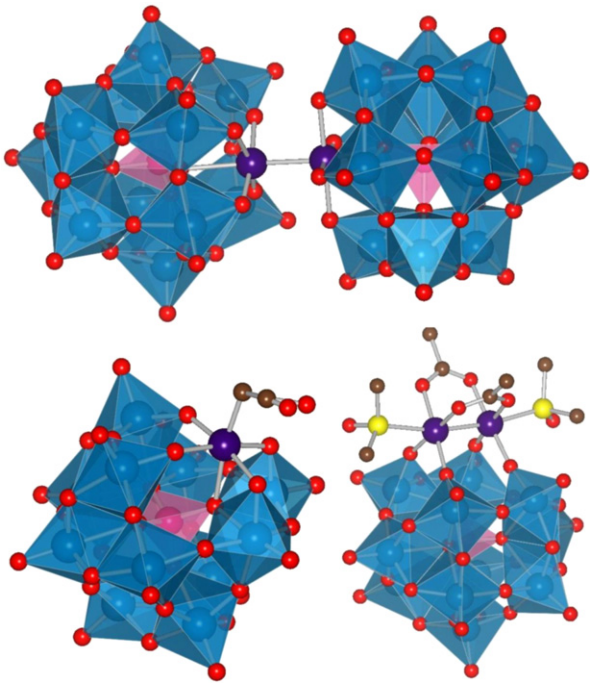

Fig. 36. Structures of: $[(RhPW_{11}O_{39})_2]^{10-}$, $[Rh(CH_2COOH)\ SiW_{11}O_{39}]^{6-}$ and $[\{Rh(OAc)(DMSO)\}_2PW_{11}O_{39}]^{5-}$ (top and below left and right, Refs. [183], [184] and [185], respectively).

The number of known dirhodium complexes grafted on POM was expanded with $[\{Rh_2(O_2CR)_2\}PW_{11}O_{39}]^{5-}$, R = *n*-Pr, CH_2Cl, CH_2OH, *ortho*- and *para*-C_6H_4OH, all these complexes being obtained in similar reactions. In the crystalline form the axial Rh sites are occupied by Cl^- anions. In each case, crystal structures showed presence of only one stereoisomer (out of 2 possible) – with the Rh–Rh bond perpendicular to a mirror plane of the polyanion. The axial chlorides were successfully substituted with methionine and cysteine [188]. The facile ligation of axial sites together with the high solubility in water of the alkali metal salts of these Rh_2–POM compounds makes them interesting materials for biological applications – especially in "heavy-atom" labelling of biomolecules [189,190].

When the grafting reaction is performed on a trisubstituted Nb-substituted polyanion in MeCN/DMSO, formation of the $[(Rh^{III}Cp^*)\beta\text{-}SiNb_3W_9O_{40}]^{5-}$ complex is noticed, where $[RhCp^*]^{2+}$ unit is most plausibly bound to the oxygen atoms of the NbW_2 site [191,192], while the V_3 site is preferred in the case of $[(Rh^{III}Cp^*)H_2(\alpha\text{-}PV_3W_9O_{40})]^{6-}$ (see Fig. 37). An additional interesting feature of the latter moiety is the presence of $[RhCp^*(DMSO)_3]^{2+}$ organometallic counterions in the structure, together with two surface H^+ originating from the protonated parent ion. This compound is stable in MeCN, in contrast to the corresponding V-containing Dawson clusters $[(Rh^{III}Cp^*)_2P_2V_3W_{15}O_{62}]^{5-}$ and $[(Rh^{III}Cp^*)P_2V_2W_{16}O_{62}]^{6-}$, see Section 4.3.5 [193].

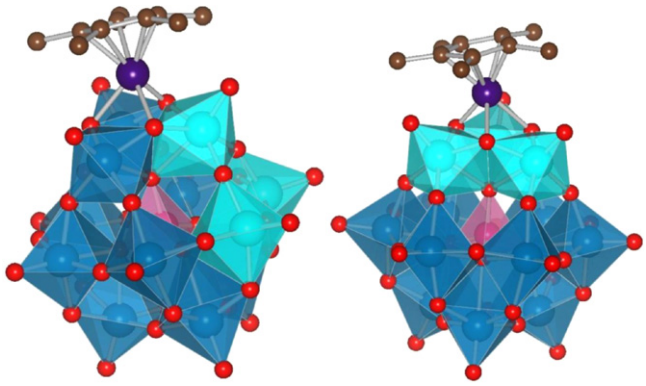

Fig. 37. Structures of: $[(Rh^{III}Cp^*)SiNb_3W_9O_{40}]^{5-}$ (left, Ref. [192]) and $[(Rh^{III}Cp^*)H_2PV_3W_9O_{40}]^{4-}$ (right, Ref. [193]). Nb,V = light blue.

Various heterogeneous catalytic systems containing supported polyoxoanions functionalized with Rh complexes were tested in hydrogenation reactions. A wide scope of supports, polyanions, organic ligands and substrates was screened, *inter alia*:

- *supports*: Montmorillonite K, carbon, γ-alumina, lanthana, etc.;
- *polyanions*: PW_{12}, PMo_{12}, SiW_{12}, $SiMo_{12}$;
- *ligands on Rh*: DiPamp, Prophos, Me-Duphos, BPPM, DPPB, BINAP, Skewphos;
- *substrates*: methyl 2-acetamidoacrylate, methyl 2-acetamidocinnamate, dimethyl itaconate, carvone.

The catalysts were prepared in ethanol, under inert atmosphere, by simple two step procedures: the support was firstly impregnated with the polyanion and then the metal complex was added. No studies were performed on the nature of the complex–polyanion interaction and the formation of defined species. However, the influence of these combinations on the reactions' activities and selectivities suggested a direct bonding rather than a cation-anion electrostatic attraction. Compared to homogeneous catalysts, these anchored systems were found equally active in low TON conditions and less active in high TON applications. Their advantage, however, lays in a possibility to be re-used several times without a loss of activity and selectivity and no metal leaching [194–196]. Another study compared performance of the Rh complexes with L-prolinamide and *N*-*tert*-butyl-L-prolinamide: (a) as homogeneous catalysts, (b) anchored on POM-functionalized NaY zeolite and (c) encapsulated in NaY zeolitic matrix ('ship-in-a-bottle' system) in hydrogenation of alkenes. Again, no conclusive proof was shown on the character of the Rh binding to polyanions. For all tested alkenes (hexene, cyclohexene and 1-methylcyclohexene) the heterogenized systems were more active than homogeneous ones, with anchored catalysts superior to encapsulated ones. In enantioselective hydrogenation of *trans*-2-methylpent-2-enoic acid the highest ee (enantiomeric excess) value was also reported for the anchored moiety [197].

The reaction of $K_8SiW_{11}O_{39}$ with $(OEt)_3SiCH_2CH_2PPh_2$ in H_2O/MeCN under Ar leads to the alkylsilane-functionalized POM (see also in Section 5.3.2). The terminal phosphine units are then used to coordinate rhodium(I) complex yielding the Wilkinson's type compound $[SiW_{11}O_{39}\{O(SiCH_2CH_2PPh_2)_2PPh_3Rh^{I}Cl\}]^{4-}$. This species was used in alkene hydrogenation reactions in both mono- and biphasic systems, showing higher efficiency on a molar basis than the classic $[Rh^{I}Cl(PPh_3)_3]$ catalyst. Furthermore, it could be easily separated from the product and re-used without loss of activity [198].

When $[Rh^{III}(H_2O)SiW_{11}O_{39}]^{5-}$ was used in the oxidation of cyclohexane with *t*-butyl hydroperoxide in benzene solutions, the products were cyclohexanol and cyclohexanone. Out of a series with various transition metals, the Rh compound was more active than Fe and Co but less than Ru one. Both Rh and Ru catalysts were stable in reaction conditions [90].

4.3.4. Rhodium complexes sandwiched by two Keggin units

A Rh-substituted Weakley-type sandwich was prepared in a standard manner, through Zn/Rh exchange reaction in boiling solution of the parent ion $[WZn_3(H_2O)_2(ZnW_9O_{34})_2]^{12-}$ and $RhCl_3$. Diffraction studies confirmed that this compound was isostructural with other late-transition-metal analogues. The methyltricapry-

lammonium salt of this compound was tested in the catalytic oxidation of alkenes with 30% H_2O_2 as oxidizing agent, in biphasic water/1,2-dichloroethane system. The overall reactivity was comparable to that of Pd and Pt analogues but higher than that of the Ru derivative. No decomposition of the catalyst was detected in the reaction environment. Additionally, the Rh POM was much more selective towards the oxidation of cyclohexene, comparably to the previously reported Mn-substituted specie. As the parent pure-Zn sandwiches were not active at all in oxidation processes, a peroxo unit formed at a tungsten atom was proposed as the catalytic center, with the transition metal being its activator [199]. In following studies the all-sodium salt did not show any catalytic activity in oxidation of various organic species (non-functionalized alkenes, alcohols) in 30% aqueous H_2O_2, 70% aqueous *t*-butyl hydroperoxide or peroxysulfate. Only allylic primary alcohols were predominantly epoxidized at carbon–carbon double bond and an undefined peroxotungstate, product of the sandwich decomposition, was suggested as the catalytically active moiety [122].

The same method was used to obtain the rhodium-containing Jeannin–Hervé $[Rh^{III}{}_2As^{III}{}_2W_{19}O_{67}(H_2O)_3]^{8-}$ and Krebs type $[Rh^{III}{}_2X^{III}{}_2W_{20}O_{70}(H_2O)_6]^{8-}$, X = Sb, Bi polyanions. Their activity in electroreduction of H_2O_2 was examined [200].

4.3.5. *Wells-Dawson structure $[X_2W_{18}O_{62}]^{n-}$*

Some Rh-substituted Dawson heteropolytungstates such as $[Rh^{III}(OH_{2-x})\alpha\text{-}X_2W_{17}O_{62}]^{n-}$, X = P, As; x = 0–2 were also mentioned in Ref. [182] but were not studied thoroughly. $[\{Rh^{II}{}_2(OAc)_2\}\alpha_2\text{-}P_2W_{17}O_{61}]^{8-}$ was only mentioned in [185].

The rhodium complexes were grafted mostly on the $[P_2Nb_3W_{15}O_{62}]^{9-}$ anion [131]. The reactions were carried out in acetonitrile in N_2 atmosphere. In a first step, the chloride ions were removed from the substrates like $[RhCp^*Cl_2]_2$ or $[Rh(COD)Cl]_2$ by precipitation with $AgBF_4$. Then, the *in situ* produced rhodium species were added to a solution of $[P_2Nb_3W_{15}O_{62}]^{9-}$. It was observed that mixed Na^+/Bu_4N^+ salts crystallized easier than all-Bu_4N^+ ones, and so in some cases single crystals became available for structural analyses. $[(Rh^{III}Cp^*)P_2Nb_3W_{15}O_{62}]^{7-}$ [132,133,201] and $[Rh^{I}(COD)P_2Nb_3W_{15}O_{62}]^{8-}$ [202] were obtained as salts with various counterions. The former, although synthesized under N_2, is air-stable. Its rhodium(III) complex is regiospecifically attached at the central position of the Nb_3O_9 surface, via three bonds with bridging oxygen atoms. The latter, however, shows two isomeric structures, on- and off-center, in which one Rh-support bond is created with a terminal oxygen atom (Fig. 38). Another example: $[Rh^{I}(CO)_2(P_2Nb_3W_{15}O_{62})]^{8-}$ was isolated at ∼−80 °C, after bubbling CO through a CH_2Cl_2 solution of $[Rh^{I}(COD)P_2Nb_3W_{15}O_{62}]^{8-}$. It is unstable at room temperature. After irradiation by a sun lamp under H_2 in ethanol, it leads to the formation of polyanion-stabilized $Rh^{\circ}{}_n$ nanoclusters, active in cyclohexene hydrogenation [203].

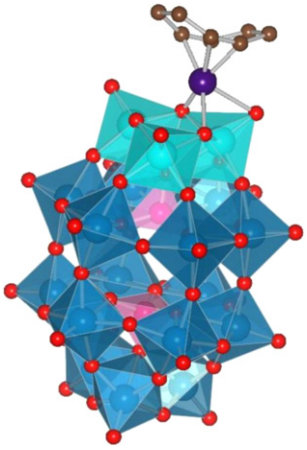

Fig. 38. Suggested off-center isomer of $[Rh^{I}(COD)P_2Nb_3W_{15}O_{62}]^{8-}$ (Ref. [202]).

$(Bu_4N)_5Na_3[Rh(COD)P_2Nb_3W_{15}O_{62}]$ was used in the catalytic oxygenation of cyclohexene with O_2. The main products were 2-cyclohexenone and 2-cyclohexen-l-ol. However, the Ir analogue was more active [134].

Vanadium-substituted heteropolytungstates were also investigated as supports for Rh complexes. The syntheses were different from those reported above in some crucial aspects. First of all, the target compounds were unstable in coordinating solvents (like MeCN), so ice-cooled CH_2Cl_2 was used. Reactions of $[Cp^*RhCl_2]_2$ with all-$(Bu_4N)^+$ salts of Dawson clusters were straightforward and did not require silver cations to eliminate halides. Pure products were obtained after consecutive cycles of precipitations with Et_2O and dissolutions in CH_2Cl_2. Two moieties were reported, $[(Rh^{III}Cp^*)_2P_2V_3W_{15}O_{62}]^{5-}$ [204] and $[(Rh^{III}Cp^*)P_2V_2W_{16}O_{62}]^{6-}$ [205]. The former is a rare example of a Wells-Dawson complex grafted with more than one organometallic complex. The rhodium atoms are tripodally anchored on vanadium octahedra. In the latter, the surface charge is apparently too low for more than one

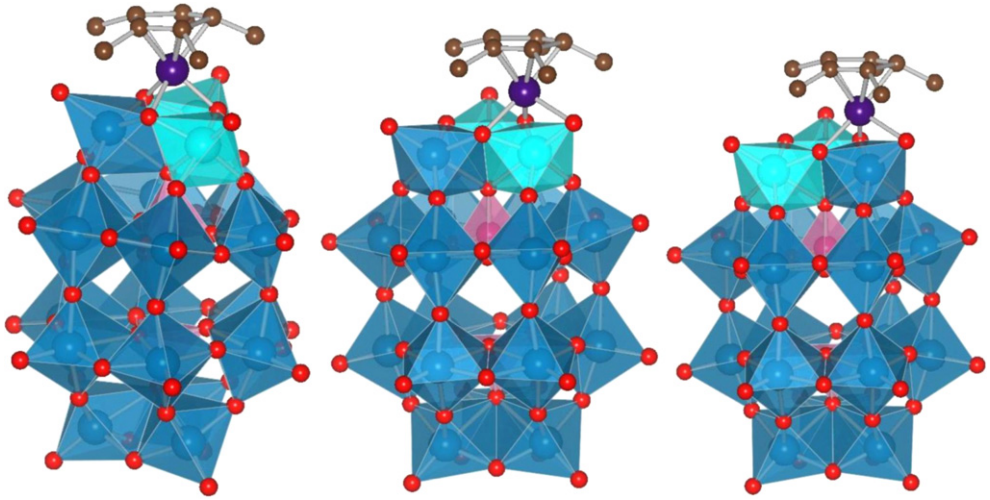

Fig. 39. Suggested diastereoisomers of $[(Rh^{III}Cp^*)P_2V_2W_{16}O_{62}]^{6-}$ (Ref. [205]). Forms: I, II and III from left to right.

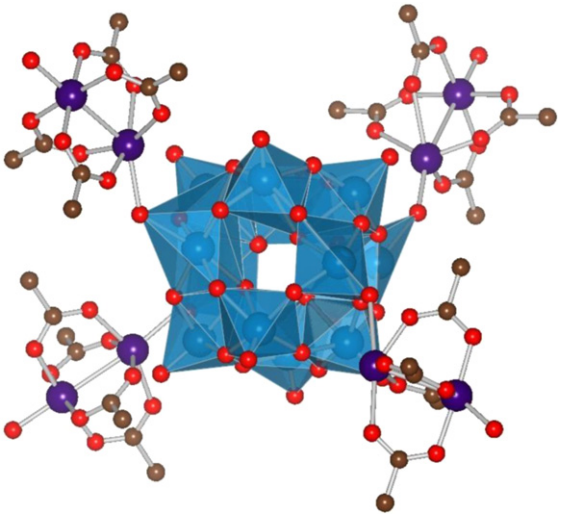

Fig. 40. Metatungstate unit with four linkers in the structure of $[Rh^{III}_4(OAc)_8(H_2W_{12}O_{40})]^{6-}$ (Ref. [142]).

$[RhCp^*]^{2+}$ group to be supported. Three diastereoisomers originate from possible modes of Rh coordination: (I) in the central position over the mini-surface, (II) over the vanadium or (III) tungsten octahedron. Multinuclear NMR studies confirmed that all of them are present in mother liquor in a 1:2:1 ratio and also when the product is precipitated in a poorly crystalline form. However, only one isomer (I or III in Fig. 39, which one exactly was not established by the authors) is isolated when single crystals are grown from CH_2Cl_2 at −20 °C.

4.3.6. Other polytungstates

$[Rh^{III}_4(OAc)_8(H_2W_{12}O_{40})]^{6-}$ is a 2D polymeric network composed of POMs linked via bimetallic units (Fig. 40). The metatungstate clusters have a Keggin-type structure but without a central tetrahedron of heteroatom. The neutral linker motif $[Rh_2(OAc)_4]$ is based on two rhodium atoms joined by a metallic bond (Rh···Rh = 2.383(4) Å). They are capped by four CH_3COO^- anions and complete their distorted octahedral coordination with terminal oxygen atoms of polyanions. The synthesis is carried out in acidic aqueous solution from Na_2WO_4, CH_3COONa and $RhCl_3$ [142].

5. Polyoxometalates containing iridium

5.1. Polyvanadates

Mixing $[Ir(COD)Cl]_2$ and $(Bu_4N)VO_3$ or $(Bu_4N)_3V_5O_{14}$ in acetonitrile under N_2 flow yields $(Bu_4N)_3[\{Ir(COD)\}(V_4O_{12})]$ and $(Bu_4N)_2[\{Ir(COD)\}_2(V_4O_{12})]$. These compounds are analogues of the Rh species described above [206].

The Ir-grafted vanadate hexamer $[(Ir^{III}Cp^*)_4V_6O_{19}]$, congener of the above described Ru and Rh species, was synthesized in a similar manner, from an aqueous solution of $[IrCp^*Cl_2]_2$ and $NaVO_3$, followed by extraction with CH_2Cl_2. All these compounds are isostructural. The complex is air-stable [153,155].

5.2. Polymolybdates

$[(Ir^{III}Cp^*)_4Mo_4O_{16}]$ is the iridium analogue of the rhodium molybdate cluster with triple cubane structure in the solid state, described in Section 3. These two compounds are isomorphous [160].

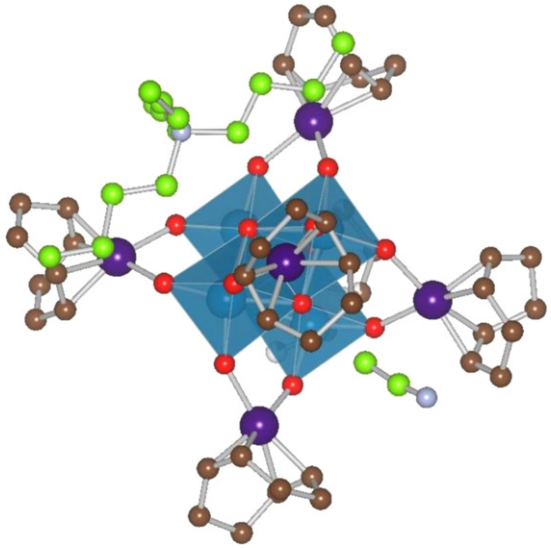

Fig. 41. MeCN and $(Bu_4N)^+$ in the cavities of $[\{Ir^I(COD)\}_6W_4O_{16}]^{2-}$. Their carbon atoms are in green for better visualization (Ref. [207]).

5.3. Polytungstates

5.3.1. $[W_4O_{16}]^{8-}$

The reaction of $[Ir(COD)Cl]_2$ and $(Bu_4N)_2WO_4$ in MeCN under anhydrous conditions leads to the formation of $(Bu_4N)_2[\{Ir^I(COD)\}_6W_4O_{16}]$. The distorted cubic core of the tetramer is capped over its faces by 6 $[Ir(COD)]^+$ groups. The square-planar geometry around the Ir center is completed by two terminal oxygens of the cluster. Each three adjacent organometallic groups form a cavity of flexible size, above the oxygen corner of the W_4O_4 cube. Two of the four cavities are narrow and deep whereas the other two are more open and shallow. Inside deep cavities 2 MeCN molecules are present, forming a host–guest type system. Surprisingly, they were methyl-oriented towards the core of the cube ("methyl-first" mode) and weakly interacting with iridium and bridging and terminal oxygens ($C_{CH_3}\cdots Ir = 3.60(3)$–$4.02(3)$ Å, $C_{CH_3}\cdots O_{WIr} = 3.10(3)$–$4.46(4)$ Å, $C_{CH_3}\cdots O_{W_3} = 3.08(4)$–$4.02(3)$ Å). The second type of cavities is approached, but not occupied, by $(Bu_4N)^+$ cations, bulkier than MeCN (Fig. 41) [207].

5.3.2. Lindqvist structure $[W_6O_{19}]^{2-}$ and/or its derivatives

$[Ir^I(COD)(Cp^*TiW_5O_{18})]^{2-}$ is obtained from $(Bu_4N)_3[Cp^*TiW_5O_{18}]$ and $[Ir^I(COD)(MeCN)]PF_6$ in THF under N_2. Crystal structure investigations showed that the Ir center is in a square pyramidal geometry coordinating olefinic bonds of COD and 2 doubly bridging oxygens of polyanion (Fig. 42, on the left) [208].

$[Nb_2W_4O_{19}]^{4-}$ reacts in dichloromethane with $[Ir(COD)(MeCN)_2]^+$ under nitrogen flow, leading to the formation of a dimeric complex [209]:

$$2\,[Nb_2W_4O_{19}]^{4-} + 5\,[Ir(COD)(MeCN)_2]^+ \rightarrow [\{Ir(COD)\}_5(Nb_2W_4O_{19})_2]^{3-} + 10MeCN.$$

This structure can be depicted as two Lindqvist clusters linked in a face-to-face mode via five four-coordinated $[Ir^I(COD)]^+$ units. Three iridium atoms are connected to bridging oxygens of the polyoxometalates while the other two are connected via terminal oxygen atoms. This compound rearranges in the presence of $[Nb_2W_4O_{19}]^{4-}$ ions and acetic acid, leading to a new dimer, with only two $[Ir^I(COD)]^+$ units (Fig. 42, on the right). The iridium atoms are in a square-planar coordination made by two terminal oxygens of the

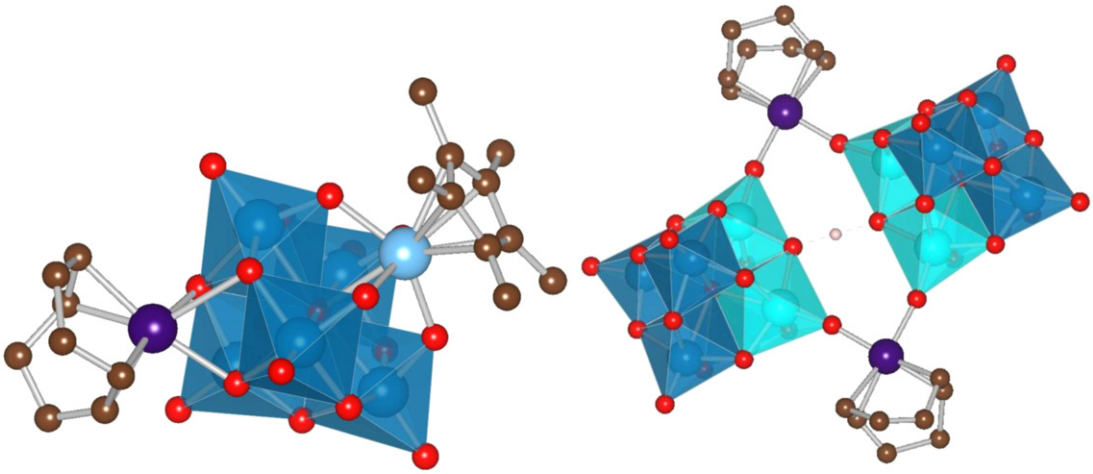

Fig. 42. Structures of: $[Ir^{I}(COD)(Cp^{*}TiW_5O_{18})]^{2-}$ (left, Ref. [208]) and $[\{Ir(COD)\}_2H(Nb_2W_4O_{19})_2]^{5-}$ (right, Ref. [209]). Ti = light blue, H = light pink.

Lindqvist units and two olefinic bonds of cyclooctadiene. A bridging proton inserted symmetrically between the clusters further strengthens the new compound: $[\{Ir^{I}(COD)\}_2H(Nb_2W_4O_{19})_2]^{5-}$.

When CO is bubbled through the solution of $(Bu_4N)_5[\{Ir(COD)\}_2H(Nb_2W_4O_{19})_2]$ in MeCN, each COD is replaced by two CO molecules, that coordinate to Ir linearly, through their C atoms (Fig. 43). However, the overall dimeric structure with hydrogen bridging and Ir centers exhibiting square-planar coordination remains unchanged [179].

5.3.3. *Keggin structure* $[XW_{12}O_{40}]^{n-}$

Reaction of the iridium metal complex containing trichlorostannane ligand $(PPh_3)_2Ir(CO)(H)_2SnCl_3$ with the $SiW_{11}O_{39}^{8-}$ polyanion resulted in the formation of the $[(PPh_3)_2Ir(CO)(H)_2SnSiW_{11}O_{39}]^{5-}$ polyanion. According to the proposed structural model, Sn fills the lacuna of the cluster and is bonded to iridium via a metal–metal bond [181].

A B-Keggin-type-supported iridium–COD complex can be obtained in a way similar to procedures described above. In the glovebox, $[Ir(COD)(MeCN)_2]^{+}$ is prepared *in situ*, from $AgBF_4$ and $[Ir(COD)Cl]_2$ in MeCN. In a next step, it is reacted with $(Bu_4N)_7[SiNb_3W_9O_{40}]$. As the all-$Bu_4N$ salt is difficult to isolate in good yields without significant amounts of $(Bu_4N)BF_4$ impurities, a mixed-cation method was applied. The final product, $(Bu_4N)_4Na_2[Ir^{I}(COD)B\text{-}SiNb_3W_9O_{40}]$ consists of a Keggin heteropolyoxometalate with one $[Ir(COD)]^{+}$ unit grafted on it. Two plausible ways of Ir–O bonding were proposed: via two bridging O_{NbW} and one bridging O_{W_2}, or via two bridging O_{NbW} and one terminal O_{Nb} (see Fig. 44) [210].

A series of iridium-substituted heteropolytungstates $[Ir^{IV}(H_2O)XW_{11}O_{39}]^{n-}$, X = B, Si, Ge or P, was prepared from the corresponding lacunary precursors and H_2IrCl_6 in hot water [211]. All these compounds showed high catalytic activities in the electrochemical reduction of nitrite. Mechanism's highlights involve reduction of Ir(IV) to Ir(III) which in turn reduces NO_2^{-} to NO. Another Ir(III) center exchanges its labile water molecule with NO and a nitrosyl adduct is reversibly produced. The non-substituted Keggin parent ions are not active in this process [212].

5.3.4. *Wells-Dawson structure* $[X_2W_{18}O_{62}]^{n-}$

The synthesis of a Ir–COD complex bound to a Wells-Dawson polyanion bears a great resemblance to the already mentioned procedures. The starting material is in this case the all-$(Bu_4N)^{+}$ salt of $[P_2Nb_3W_{15}O_{62}]^{9-}$ [131]. Structural studies on $[Ir^{I}(COD)P_2Nb_3W_{15}O_{62}]^{8-}$ were performed mainly by means of various NMR techniques due to the lack of single crystals suitable for diffraction experiments. Fortunately, the structure solution of $Na_9[P_2Nb_3W_{15}O_{62}]$ was available for drawing analogies [213]. ^{31}P NMR showed that the product is obtained as a single regioisomer, even though multiple support sites are available. Iridium was 5-

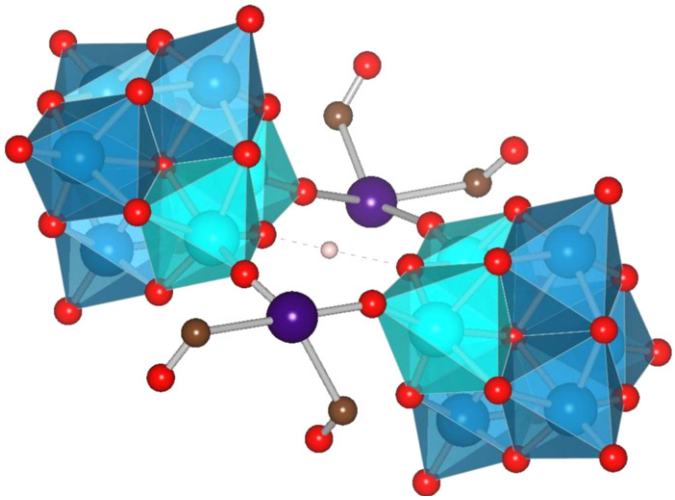

Fig. 43. Suggested structure of $[\{Ir^{I}(CO)_2\}_2H(Nb_2W_4O_{19})_2]^{5-}$ (Ref. [179]).

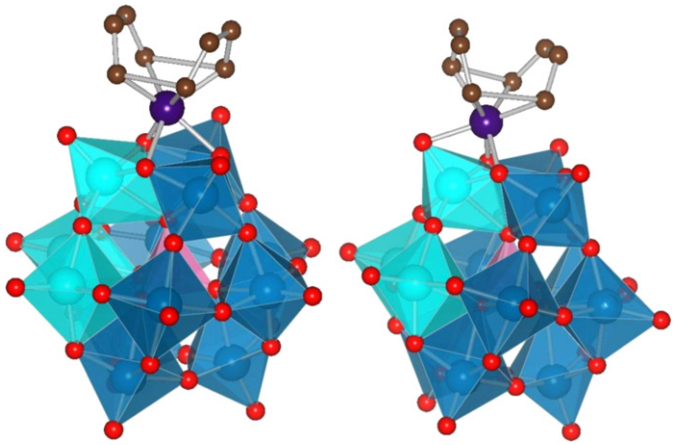

Fig. 44. Two possible modes of Ir bonding to Keggin unit in $[Ir(COD)SiNb_3W_9O_{40}]$ (Ref. [210]).

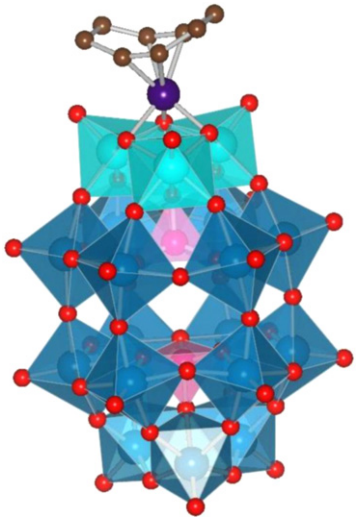

Fig. 45. The most probable binding mode of $[Ir(COD)]^+$ to the $[P_2Nb_3W_{15}O_{62}]^{9-}$ anion (Ref. [215]).

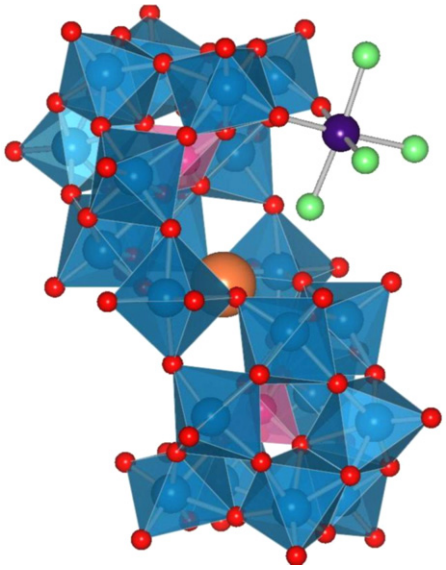

Fig. 46. Structure of $[\{Ir^{III}Cl_4\}K(WO_2)_2(A\text{-}PW_9O_{34})_2]^{14-}$ (Ref. [223]). Cl = green, K = orange.

coordinated (local C_s symmetry environment imposed on the C_{3v} ion) and linked to the Nb_3O_9 surface with three Ir–O bonds (see Fig. 45) [214]. A direct evidence of bonding to at least one bridging oxygen, situated at the top of the anion, came from ^{17}O NMR, where a downfield shift of O_{Nb_2} was reported in comparison to its parent ion. The most probable suggested structure was with three $Ir–O_{Nb_2}$ bonds (like in $[Ir(COD)P_3O_9]^{2-}$: 2 short and a longer one, all dynamically changing their lengths and becoming equivalent on the ^{17}O NMR time scale). Although less likely to appear, three fluxional structures with an Ir bridging mode to two O_{Nb_2} and one terminal O_{Nb} could not be completely excluded [202,215]. Investigations with positive and negative ion fast atom bombardment mass spectrometry (FAB-MS) revealed main fragmentation pathways of the complex through cationization ($Bu_4N^+/H^+/Na^+$) and WO_3 and O_2/H_2O loss [216].

The $(Bu_4N)_5Na_3[Ir^I(COD)P_2Nb_3W_{15}O_{62}]$ polyoxometalate was tested as a catalyst in the hydrogenation of cyclohexene with H_2. The reported TOF was about 3 times lower than for the most dispersed oxide-supported Ir available, i.e. ultra (ca. 80%) dispersed 1% Ir/η-Al_2O_3. In the initial step, upon uptake of H_2, a release of cyclooctane (COA) was observed (ratio of $3H_2$:1COA). As there was no visible trace of colloidal $Ir^{(0)}$ in the solution, which should be related to a decomposition of the organometallic-polyanion moiety, a catalytic intermediate with a formula like $[\{Ir(H)_2(solvent)P_2Nb_3W_{15}O_{62}\}^{8-}]_x$ was suggested [217]. Only later it turned out that under reductive conditions this compound is degraded after all. Ir nanoclusters of 20–30 Å, stabilized by POMs, are produced by interaction with H_2 and they are responsible for the catalytic activity [218]. On the other hand, $(Bu_4N)_5Na_3[Ir(COD)P_2Nb_3W_{15}O_{62}]$ is stable in oxidation processes. When used in catalytic oxygenation of cyclohexene with O_2, the main products were 2-cyclohexenone and 2-cyclohexen-l-ol. The presence of the polyanion ligand enhanced the reaction rate 100-fold, in comparison to [Ir(COD)Cl]. The rate constants for oxidation were solvent-dependent, the highest one being for CH_2Cl_2 and the lowest for DMSO [134]. Following studies showed that the reaction mechanism is the classical Haber–Weiss free-radical-chain autooxidation [219] and that the catalytic specie involved is the polyoxoanion-supported $[(Bu_4N)_6Na_3(HO)_3Ir^{III}(P_2W_{15}Nb_3O_{62})]_x$ ($x = 1, 2$) [220]. In the co-oxidative epoxidation of cyclohexene to cyclohexene oxide, with O_2 and using isobutyraldehyde as a reductant, the $(Bu_4N)_5Na_3[Ir(COD)P_2Nb_3W_{15}O_{62}]$-catalyzed process exhibited as high conversion as any metal-catalyzed one. However, in terms of selectivity ratio SR, both catalyzed processes turned out to be inferior (SR = 10–15) to the initiated uncatalyzed one (SR = 28–40) while showing nearly the same conversion and epoxide yield [221].

As in the Lindqvist-derivative, the cyclooctadiene ligand can be easily replaced by two CO molecules upon bubbling the solution of $[Ir(COD)P_2Nb_3W_{15}O_{62}]^{8-}$ with CO in MeCN or CH_2Cl_2. The IR spectrum of $[Ir^I(CO)_2(P_2Nb_3W_{15}O_{62})]^{8-}$ shows two carbonyl bands at 2046 and 1966 cm^{-1}, characteristic of *gem*-dicarbonyl species. Two isomers, one with the C_{3v} symmetry and one with a lower symmetry, can co-exist in solution. The formation of the non-C_{3v} species is induced by the addition of a second cation (e.g. Na^+) and heating [203].

The preparation of the Ir(IV)-substituted mono-lacunary Wells-Dawson polyanion $[Ir^{IV}(H_2O)P_2W_{17}O_{61}]^{6-}$ has been reported. On the basis of the NMR spectra iridium was assumed to fill the lacuna of the cluster with an approximately octahedral coordination [136]. This complex was used for the electrochemical reduction of nitrite ions in aqueous solution [222].

5.3.5. Other polytungstates

In order to obtain the Ir-substituted cluster $[\{Ir^{III}Cl_4\}K(WO_2)_2(A\text{-}PW_9O_{34})_2]^{14-}$, nonatungstate units were first generated *in situ* in aqueous solution by reacting $K_{10}[\alpha_2\text{-}P_2W_{17}O_{61}]$ and K_2WO_4 at pH = 6.8. In a second step $IrCl_3$ was added to the reaction mixture. In the structure, two A-PW_9O_{34} clusters in *anti* configuration are joined by two $[WO_2]^{2+}$ linkers (Fig. 46). The central cavity is occupied by a potassium cation. Only one octahedral iridium per cluster, coordinating two terminal oxygens and four chlorines, was observed, although two symmetric easily accessible sites are available. This compound showed quite the same activity than its $IrCl_3$ precursor in water oxidation [223].

6. Polyoxometalates containing palladium

6.1. Polyvanadates

The vanadate-supported organopalladium complex $[\{(\eta^3\text{-}C_4H_7)Pd^{II}\}_2V_4O_{12}]^{2-}$ was obtained by reaction of $[Pd(\eta^3\text{-}C_4H_7)Cl]_2$ with $(Bu_4N)VO_3$ in acetonitrile. The structure contains two β-methallyl-Pd complexes on the opposite sides of the tetravanadate ring, related through an inversion center. The palladium is in a

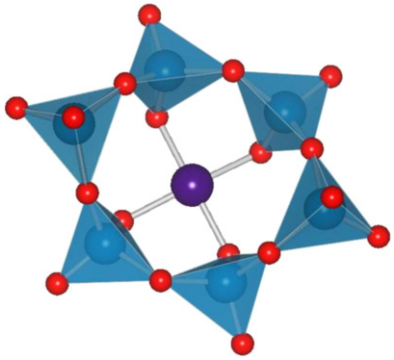

Fig. 47. Structure of the cyclic hexavanadate with Pd complex $[Pd^{II}V_6O_{18}]^{4-}$ (Ref. [225]).

square planar geometry made by two C and two terminal O atoms [224].

Reaction of $[Pd(C_6H_5CN)_2Cl_2]$ and $(Et_4N)VO_3$ in acetonitrile yields $[Pd^{II}V_6O_{18}]^{4-}$. In this compound palladium, in a square planar geometry, is incorporated in the center of the oxovanadate ring by coordination to four oxygen atoms (Fig. 47). The ring has a boat conformation. When labile benzonitrile ligands are replaced with COD in the substrate, the Pd-free mixed valence decavanadate $[V_{10}O_{26}]^{4-}$ is formed [225].

6.2. Polymolybdates

The synthesis and characterization of an Anderson-like polyoxometalate with palladium in the central position has been recently reported [226]. Two $PdMo_6O_{24}$ units are bridged by a proton, leading to a $[Pd_2Mo_{12}O_{48}H]^{15-}$ dimeric anion. The compound is not very stable and it decomposes when its X-ray photoelectron spectrum is recorded.

Interactions of Pd(II) with $H_3PMo_{12}O_{40}$ in acidic aqueous solutions were investigated. However it was found that palladium was not incorporated in the structure of unsaturated heteropolyanions created *in situ*, such as $PMo_{11}O_{39}^{7-}$ and $PMo_9O_{34}^{9-}$. The $\{PdPMo_9\}$ species that has been precipitated as cesium salt is rather an aqua or hydroxo palladium complex adsorbed on the polyanion surface [227].

6.3. Polytungstates

6.3.1. Lindqvist structure $[W_6O_{19}]^{2-}$ and/or its derivatives

Reaction of Na_2WO_4 and $K_2[PdCl_4]$ in water leads to the formation of chocolate-brown crystals of $[Pd^{II}{}_2W_{10}O_{36}]^{8-}$. In the structure, two $[W_5O_{18}]^{6-}$ Lindqvist units deprived of WO groups are oriented towards each other with their open spaces. Two Pd atoms in a square planar geometry are linking these two units by coordinating to oxygen atoms of each group (Fig. 48) [228].

6.3.2. Keggin structure

6.3.2.1. Phosphorus as the central atom in the Keggin unit (X = P). Pd/POM complexes were precipitated as Bu_4N^+ salts from aqueous solutions of $Pd(H_2O)_4^{2+}$ and $PW_{11}O_{39}^{7-}$ at pH = 2 and 4. Three types of species were observed, the complexes $\{PdPW_{11}O_{39}\}$ and $\{PW_{11}O_{39}Pd–O–PdPW_{11}O_{39}\}$ and oligomeric palladium hydroxide stabilized by polyoxometalate, the latter two compounds being formed preferentially at higher pH. A square planar coordination of Pd was suggested for all complexes. The benzene oxidation to phenol in biphasic benzene/water system with O_2/H_2 gas mixture was catalyzed with 98% selectivity by these systems. The highest yield was observed for a Pd/POM ratio of 2 and decreased when the pH was changed from 2 to 4. The main catalytic activity was attributed to dissolved complexes of reduced Pd(0) with POMs [229]. Further tests were carried out on SiO_2 impregnated with these complexes, with or without subsequent H_2 treatment. Hydrogenation at low temperature led to reduction of some Pd(II) to Pd(0) but the structure of the polyanions was preserved. Catalytic reactions included liquid phase (in MeCN) oxidation of benzene and cyclohexane with O_2/H_2. The products were: phenol and cyclohexanol/cyclohexanone mixture, respectively. A pre-reduction of the samples improved their catalytic activity [230].

A catalyst precursor with the elemental composition $K_5Pd(H_2O)PW_{11}O_{39}$ was deposited by wet impregnation on γ-alumina and active carbon and tested in the hydrogenation of arenes. Noticeably, this system had a completely different behaviour than the commercial Pd/C, i.e. it showed a preference towards the reduction of aromatic rings to saturated cycles, even in the presence of distal ketone groups that remained intact. Pd(0) clusters stabilized by $PW_{11}O_{39}^{7-}$ polyoxometalates were proposed as the 'true' catalytic species. The activity and selectivity were not affected by the type of support. These Pd clusters were more efficient than Ru and Rh ones [231]. Another way to these POM-stabilized Pd nanoclusters is through reaction of $K_5Pd(H_2O)PW_{11}O_{39}$ with acetophenone under H_2. The resulting catalysts were tested in various coupling reactions of bromoarenes in aqueous media [232].

6.3.2.2. Silicon as the central atom in the Keggin unit (X = Si). Reaction of the $(PPh_3)Pd(C_3H_5)SnCl_3$ metal complex containing the trichlorostannane ligand with $SiW_{11}O_{39}^{8-}$ polyanion, followed by spontaneous disproportionation of the product resulted in the obtention of $[(C_3H_5)Pd(SnSiW_{11}O_{39})_2]^{11-}$ [181].

Detailed studies on $K_6[Pd^{II}SiW_{11}O_{39}]$ deposited on γ-Al_2O_3 [233] and amorphous SiO_2–Al_2O_3 [234] upon redox treatments at elevated temperatures showed strong interactions of polyanions with supports and increased thermal stability of these obtained systems by comparison to bulk samples.

A series of palladium-substituted heteropolytungstates $[Pd^{II}(H_2O)XW_{11}O_{39}]^{n-}$, X = B, Si, Ge or P, was prepared from lacunary precursors and $PdCl_2$ in hot water [211]. The $[Pd^{II}SiW_{11}O^{39}]^{6-}$ complex absorbed on a surface of a glassy carbon electrode was used in the electrochemical reduction of H_2O_2 [235] and nitrite [236] in aqueous solutions.

The procedure towards the obtention of a Pd–salen–POM hybrid (similar to Rh compound synthesis) involves the incorporation of a functionalized alkylsilane into the lacuna of the polyoxometalate, the formation of the salen ligand and the metalation. UV–VIS, NMR and EPR examinations showed the presence of an oxidized metallosalen center best described as a hybrid of a metal–salen cation

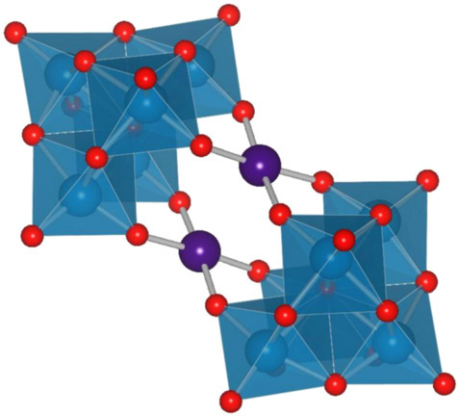

Fig. 48. Structure of $[Pd^{II}{}_2(W_5O_{18})_2]^{8-}$ (Ref. [228]).

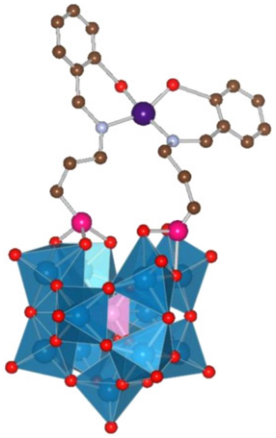

Fig. 49. Suggested structure of the Pd–salen–polyanion compound (Ref. [237]). Si = pink balls and tetrahedron.

radical and an oxidized Pd(III)–salen species (Fig. 49). The whole compound could be seen as a charge transfer complex, formed across long, three-carbon alkyl spacer, where the polyoxometalate is an electron acceptor. As there was no direct evidence of a POM reduction, the negative charge was suggested to be delocalized over the whole complex [237].

6.3.3. Palladium complexes sandwiched by two Keggin units

In order to stabilize the first example of a Pd terminal oxo complex the electron-accepting ligand framework of a phosphotungstate was used. $[Pd^{II}_3(PW_9O_{34})_2]^{12-}$ was kinetically precipitated from a mixture of $PdSO_4$ and $[PW_9O_{34}]^{9-}$ at pH = 4.9. In acidic media it undergoes a Pd loss and a consecutive oxidation by O_2 to finally yield $[Pd^{IV}(=O)(OH)WO(OH_2)(PW_9O_{34})_2]^{13-}$. Two polyanions fused by a $[WO(H_2O)]^{4+}$ group form a clam-like structure and use 4 oxygen atoms to support the $[PdO(OH)]^+$ moiety with very short multiple Pd–O bond (1.60(2) Å) *trans* to a longer Pd–OH bond (1.99(2) Å) (Fig. 50). The oxo ligand is hidden in the cluster cavity. Pd exhibits an octahedral geometry [238,239]. However the synthesis of this compound has not been reproduced by other groups [240].

6.3.3.1. Knoth type sandwiches: $[M_3(\alpha\text{-A-}XW_9O_{34})_2]$. Mixing aqueous solutions of $Na_8HPW_9O_{34}$ and $Pd(NO_3)_2$ at room temperature produced a compound for which the formula $[Pd_3(PW_9O_{34})_2]^{12-}$ was postulated, based on elemental analysis. No thorough studies were performed on it – only a drawing analogy with its cobalt

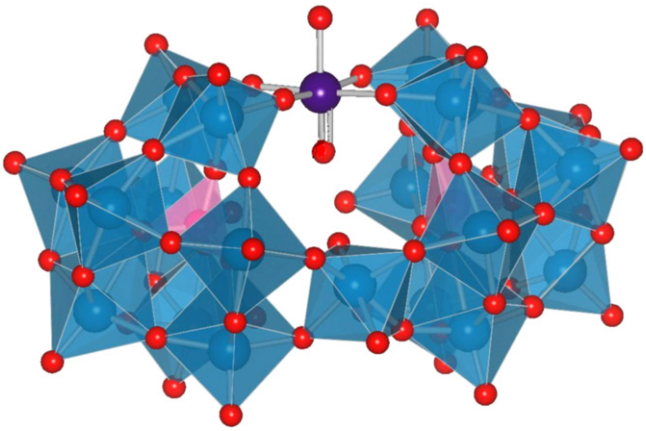

Fig. 50. Clam-like structure of $[Pd^{IV}O(OH)WO(OH_2)(PW_9O_{34})_2]^{13-}$ (Ref. [238]).

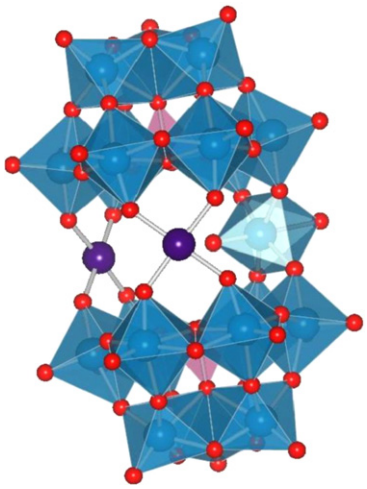

Fig. 51. Structure of $[Pd_2\{WO(H_2O)\}(\alpha\text{-A-}PW_9O_{34})_2]^{10-}$ (Ref. [245]).

congener was given [241], a structure containing two α-A-type polyoxometalate units linked through a belt of three Pd ions. Upon acidification with HCl, a stepwise demetalation and Pd → W substitution was observed, but the $\{Pd_2W(PW_9O_{34})_2\}$ intermediate was not isolated [242].

Reaction of $Na_8HPW_9O_{34}$ with $[Pd(H_2O)_4]^{2+}$ in acidic solution yields $[Pd^{II}_3(\alpha\text{-A-}PW_9O_{34})_2]^{12-}$. An excess of Pd is present as oligomeric hydroxide fragments. Addition of sulphates of Fe(III) and Cu(II) gives the bimetallic compounds Pd_2FeL_2, $PdFe_2L_2$ and Pd_2CuL_2 where $L = PW_9O_{34}^{9-}$. The V^{5+} and Pd^{2+} cations do not form mixed complexes. The solutions were examined by means of multinuclear NMR and UV–VIS spectroscopy and the corresponding precipitates of cesium salts also by IR and differential dissolution method [243]. The catalytic performance of these compounds in solution was investigated in oxygen reduction to water and benzene oxidation to phenol in biphasic benzene/water system with O_2/H_2 gas mixture. Both reactions are dependent on the presence of Pd(0) species. The most effective were bimetallic Pd(II)–Fe(III) complexes [244]. Samples of SiO_2 impregnated with $[Pd_3(PW_9O_{34})_2]^{12-}$ and mixed Pd(II)–Fe(III) complexes, with or without subsequent H_2 treatment, were used for liquid phase (in MeCN) oxidation of benzene and cyclohexane with O_2/H_2. The products were phenol and cyclohexanol with cyclohexanone, respectively. The monometallic moiety was a poor catalyst, even after reduction. The bimetallic species were highly active but only after hydrogen treatment [230].

Recently, a detailed structural examination of a series of Pd-substituted sandwiches with the formula $[Pd_x\{WO(H_2O)\}_{3-x}(\alpha\text{-A-}PW_9O_{34})_2]^{(6+2x)-}$, $x = 1$–3, was carried out. These complexes were obtained from reactions of aqueous solutions of $Pd(NO_3)_2$ and $[P_2W_{20}O_{70}(H_2O)_2]^{10-}$, $[P_2W_{19}O_{69}(H_2O)]^{14-}$ and $[PW_9O_{34}]^{9-}$, respectively. Single crystal diffraction results were in agreement with the main structural features of the already mentioned model: two Keggin units joined by a Pd/W central belt. ^{183}W NMR showed that the $[WO(H_2O)]^{4+}$ groups of the monosubstituted derivative are not equivalent, possibly the aquo ligand of one group is localized in the cavity, while H_2O of the other sticks out. The disubstituted compound exists in solution in equilibrium with its possible isomer. The water molecule from the $[WO(H_2O)]^{4+}$ group points outside the lacuna (Fig. 51). The central belt is completed with three potassium cations. The trisubstituted complex could be obtained only when using the potassium (and not the sodium) salt of the POM as a substrate [245].

Reaction of $Pd(CH_3COO)_2$ and $K_{10}[\alpha\text{-A-}SiW_9O_{34}]$ in CH_3COONa buffer (pH = 4.8) in the presence of CsCl yielded the sandwich silicotungstate $[Cs_2KPd_2^{II}WO(H_2O)(SiW_9O_{34})_2]^{9-}$. An attempted

synthesis from the sodium salt of polyanion was not successful, once again indicating the important role of potassium counterions in the structure stabilization. Structural studies showed that two Keggin-type clusters were linked via two square-planar Pd atoms, coordinating oxygens from different W_3O_{13} triads of each unit and via a $[WO(H_2O)]^{4+}$ group, with the water molecule pointing inside central cavity. Central belt is completed by two cesium and one potassium cations [246].

6.3.3.2. Weakley type sandwiches: $[M_4(\alpha\text{-}B\text{-}XW_9O_{34})_2]$. When $K_2[PdCl_4]$ was added to an aqueous solution of parent ion $[WZn_3(H_2O)_2(ZnW_9O_{34})_2]^{12-}$, the labile zinc atoms were exchanged with Pd(II), yielding $[WPd^{II}{}_2Zn(H_2O)_m(ZnW_9O_{34})_2]^{12-}$ where *m* was presumed to be 0, but its value is yet undetermined. No detailed structural studies were done on it [247]. Catalytic tests involving this compound were described in detail in the chapter about Ru. In short, high activity and moderate selectivity (comparable with Pt and Rh, better than for the Ru analogue) were reported in the oxidation of alkenes to epoxides with H_2O_2 in biphasic water/1,2-dichloroethane systems by its methyltricaprylammonium salt. In contrast to typical Pd(II) complexes behaviour, no ketonization was observed. The monosubstituted Pd–POM and the sandwich compound showed similar reactivity, even though the nature of the catalytically active species was different: $[PO_4\{WO(O_2)_2\}_4]^{3-}$ in the former case and the sandwich itself in the latter, but with a reaction centered on tungsten rather than on the noble metal atom – an example of Pd neighbouring effect. When using *t*-butyl hydroperoxide, alkanes were oxidized efficiently and selectively but the Ru congener proved superior efficiency. A metal oxo intermediate was suggested as catalytically active in this reaction [115]. The performance in epoxidation of chiral allylic alcohols with H_2O_2 was good but the transition metal substituting the sandwich was not involved in the mechanism [124]. When in the same process H_2O_2 was replaced by chiral organic hydroperoxides as an oxygen source, the activity was poor [125]. Similarly to the Rh analogue, the all-sodium salt was not active in the oxidation of various organic species (non-functionalized alkenes, alcohols) in 30% aqueous H_2O_2, 70% aqueous *t*-butyl hydroperoxide nor in peroxysulfate. Only allylic primary alcohols were predominantly epoxidized at the carbon–carbon double bond and an undefined peroxotungstate was suggested as the catalytically-active moiety [122].

On the other hand, reaction of $PdCl_2(DMSO)_2$ with the hexadecyltrimethylammonium salt of a parent ion, performed in CH_2Cl_2 gave a compound with Pd center presumed to ligate the sandwich polyoxometalate on one of its terminal positions. This conclusion could not be proved, however, due to the lack of monocrystals. Nevertheless, this compound was an active catalyst in aerobic oxidation of alcohols in trifluorotoluene, showing high selectivity to aldehydes and an interesting reactivity preference towards primary aliphatic alcohols over secondary ones [248].

6.3.3.3. Jeannin–Hervé type sandwiches: $[M_3(\alpha\text{-}XW_9O_{33})_2]$ with lone pair containing heteroatoms, e.g. X = As(III), Sb(III), etc.. $[Cs_2Na(H_2O)_{10}Pd^{II}{}_3(SbW_9O_{33})_2]^{9-}$ was the first Pd-substituted polyoxoanion to be characterized by means of single-crystal diffraction. It was obtained from a mixture of $Pd(CH_3COO)_2$ and $Na_9[\alpha\text{-}SbW_9O_{33}]$ in aqueous acidic medium (pH = 4.8) in the presence of CsCl and KCl. The structure (Fig. 52, on the left) consists of two tungstoantimonate clusters linked via three square-planar Pd atoms, coordinating two oxygens from the same W_3O_{13} triad of each unit. The central belt is completed with two cesium and one sodium cations [249].

Later the synthesis of the tungstoarsenate analogue $[Cs_2Na(H_2O)_8Pd^{II}{}_3(AsW_9O_{33})_2]^{9-}$ was described, but this time $PdCl_2$ was used as a metal source, as reactions with $Pd(CH_3COO)_2$ gave $[Na_2(H_2O)_2Pd^{II}WO(H_2O)(\alpha\text{-}B\text{-}AsW_9O_{33})_2]^{10-}$. Again, planar Pd linkers coordinated to oxo groups from the same triad were observed. Interestingly, 3d metal derivatives (e.g. Co(II), Zn(II), etc.) of sandwich tungstoarsenates tend to have linkers coordinated to oxygen ligands from different triads. Supposedly, the binding mode is dependent on the geometry preferred by the linker: square-planar to square pyramidal, respectively. The compound was used to deposit Pd(0) thin films on a glassy carbon electrode surface which proved to be efficient in electrochemical reduction of dioxygen [250]. As mentioned above, $[Na_2(H_2O)_2Pd^{II}WO(H_2O)(\alpha\text{-}B\text{-}AsW_9O_{33})_2]^{10-}$ was first obtained as an undesired product of the reaction of $Pd(CH_3COO)_2$ and $Na_9[\alpha\text{-}AsW_9O_{33}]$. Then, a synthetic procedure involving the all-potassium salt of dilacunary precursor $[As_2W_{19}O_{67}(H_2O)]^{14-}$ was developed. Two clusters are linked via one square-planar Pd, coordinating oxygens from different W_3O_{13} triads of each unit and a $[WO(H_2O)]^{4+}$ group, with the water molecule external to the cavity (Fig. 52, on the right). Apparently the lone pair of As(III) is a steric hindrance for a long $W–OH_2$ bond. The central belt is completed with two sodium cations, one of them occupying the third addenda site. This unprecedented feature could serve as an explanation for the low stability of this compound in solution [250].

Reactions of $PdSO_4$ with 3d metal sulfates (with one exception for V(V) for which $NaVO_3$ was used), and $[As_2W_{19}O_{67}(H_2O)]^{14-}$ at pH = 6 gave a series of bimetallic species. All these compounds were examined by UV–VIS and IR spectroscopy and their corresponding cesium salts were also studied by the differential dissolution method. For a molar ratio Pd:M:POM = 1:1:1, the presence of compounds with the general formula $[MPd^{II}As_2W_{19}O_{67}(H_2O)_2]^{10-/9-}$ where M = Fe(III), Co(II) and Cu(II), was observed. In the same conditions syntheses with Ti(IV) and V(V) resulted in the formation of $[As_2W_{19}O_{67}(OH_x)_2\ PdO]^{10-2x/8-2x}$ with Pd not incorporated in the polyanion but rather deposited on its surface in the form of hydroxide species. A double excess of Pd over POM yielded the monometallic $[Pd^{II}{}_2As_2W_{19}O_{67}(H_2O)_2]^{10-}$ compound [251].

6.3.3.4. Krebs type sandwiches: $[M_4(\beta\text{-}B\text{-}XW_9O_{33})_2]$ with lone pair containing heteroatoms, e.g. X = As(III), Sb(III), Bi(III), etc.. The Krebs-type sandwich decorated with Pd(II) complex $[Pd_3(H_2O)_9Bi_2W_{22}O_{76}]^{8-}$ was reported as a result of a synthesis from $PdCl_2$ and $[Bi_2W_{22}O_{74}(OH)_2]^{12-}$ or $[BiW_9O_{33}]^{9-}$ in aqueous buffer solution at pH = 4.8. The cluster surface supports square planar metal complexes via bonds with its terminal oxygen atoms. Three Pd are delocalized over six positions and complete their coordination spheres with three water molecules. The synthesis of the X = Sb(III) analogue was unsuccessful [252].

6.3.4. Wells-Dawson structure $[X_2W_{18}O_{62}]^{n-}$

The synthesis of the Pd(II)-substituted mono-lacunary Wells-Dawson polyanion $[Pd^{II}(H_2O)P_2W_{17}O_{61}]^{8-}$ has been reported. Based on NMR spectroscopy Pd was assumed to fill the lacuna of the cluster in an approximately octahedral coordination [136].

7. Polyoxometalates containing platinum

7.1. Polyvanadates

Reaction of $Na_2[Pt(OH)_6]$ and $NaVO_3$ in an aqueous solution (pH = 4.3) yields $Na_5[H_2Pt^{IV}V_9O_{28}]\cdot 21H_2O$, the first example of a Pt-substituted decavanadate. The incorporation of Pt is fully regioselective in one of the central addenda sites, with preferential binding to 6 bridging oxygen atoms (Fig. 53). The Pt coordination is octahedral, with Pt–O bond lengths ranging from 1.980(3) to 2.027(3) Å. Two protons attached to the compound help to develop a dimeric structure in the solid state, via H bonds. A successful

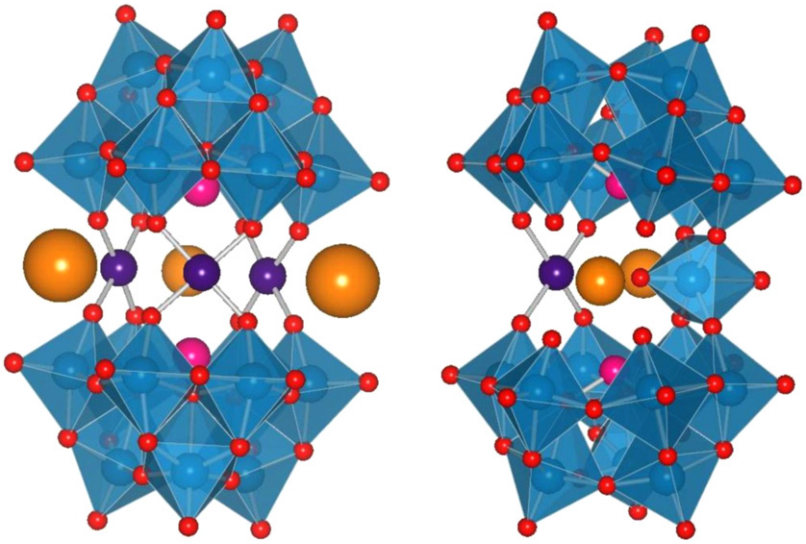

Fig. 52. Structures of $[Cs_2Na(H_2O)_{10}Pd^{II}{}_3(SbW_9O_{33})_2]^{9-}$ (left, Ref. [249]) and $[Na_2(H_2O)_2Pd^{II}WO(H_2O)(\alpha\text{-B-}AsW_9O_{33})_2]^{10-}$ (right, Ref. [250]). Water molecules are omitted for clarity. Cs, Na = orange.

use of ^{195}Pt NMR to investigate the compound has been reported [253], as noted elsewhere – due to the highly symmetrical coordination environment of Pt [254]. The proposed assignment of the NMR spectrum was later confirmed by means of relativistic DFT calculations [255–257].

7.2. Polymolybdates

A series of Pt(IV)-containing Anderson-type clusters with various degrees of protonation was reported in the course of years. They were isolated from aqueous solutions of $[Pt(OH)_6]^{2-}$ and $[Mo_7O_{24}]^{6-}$ or $[MoO_4]^{2-}$ salts by adjusting the pH values. Introduction of lanthanide ions (La^{3+}, Nd^{3+}), that have a very large oxide affinity, made possible isolation of diprotonated salts at pH ~2 (instead of anticipated pH ~8, where polyoxomolybdates become unstable). Furthermore, two isomers of the cluster: "planar" α and "bent" β (Fig. 54) were observed to transform into each other when the pH of the mother liquor was changed. Apparently gradual protonation of the polyanion plays an important role in the isomerization. In the solid state, the clusters connect via an extensive network of hydrogen bonds, either directly to form dimers, or through crystallization water molecules and by coordination to counterions. Recently, a homologous series of hydrogen-bonded Pt molybdates was extended when organic salts of trimers and one tetramer were crystallized from MeCN/toluene or MeCN/Et_2O solutions [258]. The structures are summarized in Table 1 (see Section 7.3.1).

$[PtMo_6O_{24}]^{8-}$-catalyzed processes are not mentioned in the literature. The cluster was used, however, as a precursor for bimetallic $[PtMo_6]$ catalysts. In one report, silica and alumina were impregnated with an aqueous solution of the Pt-substituted polyanion and reduced with hydrogen [259]. In the other one, impregnation of magnesia was followed by calcination in oxygen atmosphere [260]. Only in the case of silica, the precursor's framework was retained upon impregnation.

7.3. Polytungstates

7.3.1. Anderson structure $[W_6MO_{24}]^{n-}$

As for molybdenum, a series of polytungstates with varying number of protonated oxygen atoms is also known and has been compiled in Table 1. No β isomer was isolated, however, whatever the pH of the synthesis.

7.3.2. Keggin structure

7.3.2.1. Phosphorus as the central atom in the Keggin unit (X = P). Deposition of Bu_4N^+ salts of Pt/POM complexes from aqueous solutions of $PtCl_4{}^{2-}$ and $PW_{11}O_{39}{}^{7-}$ at pH = 4 resulted in one type of complex with an averaged composition Pt/POM = 2. No di- or oligomeric species have been detected, due to the too slow rate of their formation. Its catalytic activity in the benzene oxidation to

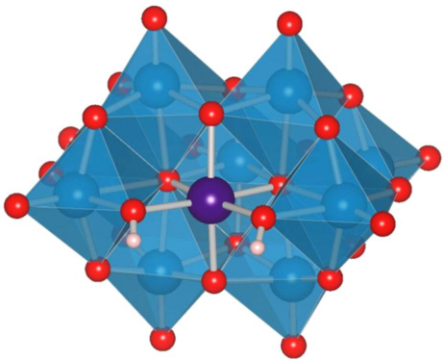

Fig. 53. Structure of $[H_2PtV_9O_{28}]^{5-}$ (Ref. [253]).

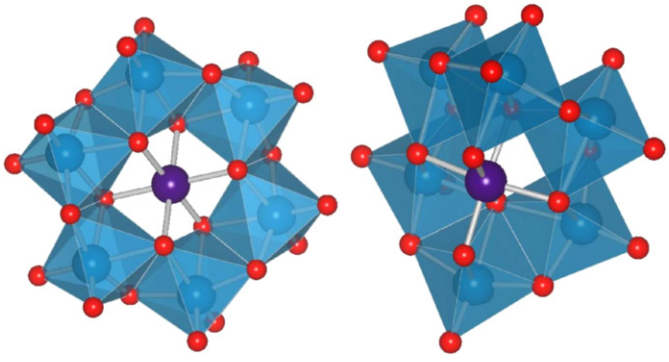

Fig. 54. α (left) and β (right) isomers of the Anderson $[PtMo_6O_{24}]^{8-}$ cluster (Ref. [261,264]).

Table 1
Polymolybdates and polytungstates Anderson type clusters containing Pt.

Cation(s)	Isomer	Polyanion	Presence of dimers	pH	Ref.
La_2	α	$H_2PtMo_6O_{24}$	No	2.0	[261]
Nd_2	α	$H_2PtMo_6O_{24}$	No	3.2	[262]
$(NH_4)_{4.5}$	α	$H_{3.5}PtMo_6O_{24}$	Yes	6.4	[263]
K_4	β	$H_4PtMo_6O_{24}$	No	5.4	[264]
$(NH_4)_4$	β	$H_4PtMo_6O_{24}$	No	5.4	[265]
$K_{3.5}$	α	$H_{4.5}PtMo_6O_{24}$	Yes	2.5, 2.85	[265–267]
K_2	α	$H_6PtMo_6O_{24}$	No	1.6, 0.7	[268,269]
KNa	α	$H_6PtMo_6O_{24}$	No	0.5	[270]
$(Bu_4N)_7(Et_3NH)$	α	$H_{16}[PtMo_6O_{24}]_3$	Trimer	–	[258]
$(Bu_4N)_9$	α	$H_{23}[PtMo_6O_{24}]_4$	Tetramer	–	[258]
$(C_3H_6N_3)^+$	α	PtW_6O_{24}	No	–	[271]
K_6Na_2	α	PtW_6O_{24}	No	7.5	[272]
Na_8	α	PtW_6O_{24}	No	7.2	[273]
Na_6	α	$H_2PtW_6O_{24}$	No	5.5	[274]
$Na_{5.5}$	α	$H_{2.5}PtW_6O_{24}$	Yes	4.7	[275]
Na_5	α	$H_3PtW_6O_{24}$	No	6.2	[276]
K_5	α	$H_3PtW_6O_{24}$	Yes	4.5	[277]
$K_{2.5}$	α	$H_{5.5}PtW_6O_{24}$	Yes	3.5	[278]

phenol in biphasic benzene/water system with O_2/H_2 gas mixture was one order of magnitude lower than for the Pd species obtained in similar conditions [229].

7.3.2.2. Silicon as the central atom in the Keggin unit (X = Si). Reaction of a platinum metal complex containing the trichlorostannane ligand with the $SiW_{11}O_{39}^{8-}$ polyanion resulted in the formation of $[(p\text{-}FC_6H_4)Pt\{P(C_2H_5)_3\}SnSiW_{11}O_{39}]^{5-}$ [181].

Keggin-type anions that stoichiometrically incorporated Pt atoms in 1:1 ratio were obtained from reaction of $PtCl_6^{2-}$ and $SiW_{11}O_{39}^{8-}$ in acetone under N_2. They were then deposited on a graphite electrode and used as an anode catalyst for electrochemical methanol oxidation [279].

Comparison of the behaviour of bulk and γ-Al_2O_3-deposited $K_4[Pt^{IV}SiW_{11}O_{39}]$ showed a strong interaction with the support and an enhanced thermal stability of the supported system in redox cycles [280].

The double Pt-substituted silicotungstate $(CH_6N_3)_8[\alpha\text{-}SiPt_2W_{10}O_{40}]\cdot 6H_2O$ was synthesized from aqueous solution of $Pt(OH)_6^{2-}$, $SiW_{11}O_{39}^{8-}$ and $CH_5N_3\cdot HCl$ [281]. It was suggested later that the assignment was incorrect and that the presented data fit better with the guanidinium salt of $SiW_{11}O_{39}^{8-}$ [254].

Reaction of $Pt(COD)I_2$ with $LiCH_3$ in diethyl ether under argon gave the complex $[Pt(COD)(CH_3)_2]$ that was consecutively grafted on dehydroxylated $H_4SiW_{12}O_{40}$ deposited on silica. Upon the process, the presence of gaseous methane was detected, evidencing the cleavage of one Pt–Me bonds. The final composition of the product could be expressed as $[Pt(COD)(CH_3)]/SiW_{12}O_{40}/SiO_2$ (Fig. 55). A successful COD-to-diimine ligand exchange reaction was performed on the grafted moiety [282]. Reactions of various analogous systems were also studied: the complexes $[Pt(Bipym)(CH_3)_2]$ and $[Pt(DMSO)_2(CH_3)_2]$ were also grafted on silica-supported $SiW_{12}O_{40}$, followed by release of stoichiometric amounts of CH_4. In the case of asymmetric $[Pt(COD)(CH_3)Cl]$, detection of HCl and CH_4 showed that both Pt–Cl and Pt–C bonds could be cleaved, with a preference towards breaking of the former (70:30 ratio). Interestingly, reactions with the unsupported polyanion resulted in ionic moieties with a formula like $[PtL(CH_3)]_4(SiW_{12}O_{40})$, L = COD, Bipym. The covalently anchored complexes were inactive in methane oxidation with oxygen, although silica-supported polyanions alone are able to completely oxidize CH_4 to CO_2. Only in the presence of *oleum* and without O_2, $[Pt(Bipym)(CH_3)]/SiW_{12}O_{40}/SiO_2$ converted methane into CH_3OSO_3H [283].

7.3.3. Platinum complexes sandwiched by two Keggin units

The Pt terminal oxo complex was obtained in a bit different manner than the Pd-containing one and their structures differ slightly as well. First, $[Pt^{II}(PW_9O_{34})_2]^{16-}$ was precipitated with KCl from an aqueous solution of $PtCl_4^{2-}$ and $PW_9O_{34}^{9-}$. After redissolution in water and 3-day exposure to air, crystals of $[Pt^{IV}(O)(OH_2)(PW_9O_{34})_2]^{16-}$ were collected. Four planar oxygen atoms of two independent Keggin polyanions are supporting the octahedral Pt. In addition the metal center coordinates one oxo ligand through a very short multiple bond (1.720(18) Å) and in a *trans* position a water molecule (2.29(4) Å). The oxo moiety is situated outwards the inter-cluster space [284]. However, questions were raised about the conclusiveness of shown evidence for structure determination [240].

When $K_2[PtCl_4]$ was added to a solution of the sandwich-type polyoxometalate $[WZn_3(H_2O)_2(ZnW_9O_{34})_2]^{12-}$ with α-B-Keggin units, the labile zinc atoms were exchanged with Pt(II), to yield $[WPt^{II}{}_2Zn(H_2O)_m(ZnW_9O_{34})_2]^{12-}$ where *m* was presumed to be 0 but its value is yet undetermined. No detailed studies were

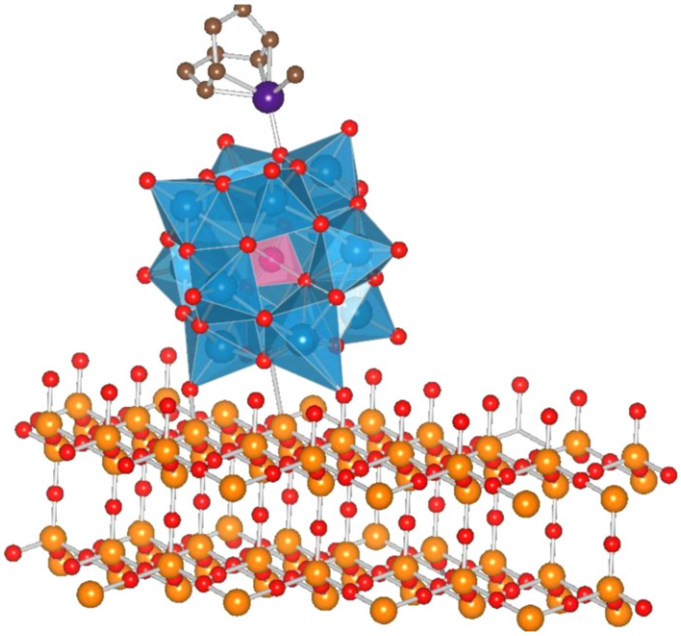

Fig. 55. $[\{Pt(COD)(CH_3)\}SiW_{12}O_{40}]$ grafted on silica (Ref. [282]).

made – only the ^{195}Pt NMR signal was mentioned to be broadened and difficult to observe [247]. Catalytic tests involving this compound were described in detail in the chapter about Ru. In short, a high activity and a moderate selectivity (comparable with those of Pd and Rh, better than for the Ru analogue) were observed in the oxidation of alkenes to epoxides with H_2O_2 in biphasic water/1,2-dichloroethane systems by its methyltricaprylammonium salt. When using *t*-butyl hydroperoxide the alkanes were oxidized efficiently and selectively but the Ru congener gave superior results. A metal oxo intermediate was suggested as catalytically active in this reaction [115]. The performance in catalytic epoxidation of chiral allylic alcohols with H_2O_2 was good but the transition metal substituting sandwich was not involved in the mechanism [124]. When in the same process H_2O_2 was replaced by chiral organic hydroperoxides as oxygen source, the activity of the compound was poor [125]. The all-sodium salt did not show catalytic activity in oxidation of various organic species (non-functionalized alkenes, alcohols) neither in 30% aqueous H_2O_2, 70% aqueous *t*-butyl hydroperoxide nor peroxysulfate. Only allylic primary alcohols were predominantly epoxidized at carbon–carbon double bond and an undefined peroxotungstate was suggested as catalytically-active moiety [122].

7.3.4. Wells-Dawson structure $[X_2W_{18}O_{62}]^{n-}$

In the $(Bu_4N)_7[\{Pt^{II}(COD)\}P_2V_3W_{15}O_{62}]\cdot 2Bu_4NBF_4$ complex the Pt atom has a square-pyramidal geometry and coordinates the olefinic bonds of COD and three oxygen atoms of one vanadium(V) site. This compound shows a good catalytic activity in the oxidation of cyclohexanol with 30% hydrogen peroxide. The main product is cyclohexanone with 100% selectivity. V^{4+}–V^{5+} redox processes are thought to play the major role in the mechanism [285].

$[Pt^{II}(H_2O)P_2W_{17}O_{61}]^{8-}$ was a poor catalyst in the cleavage oxidation of styrene to benzaldehyde and benzoic acid with $NaIO_4$ in biphasic 1,2-dichloroethane/H_2O systems [60].

8. Polyoxometalates containing silver

The versatility of Ag(I) in creating supramolecular architectures – its ability to form from 2 up to 8 bonds with various donor atoms in a wide range of observed coordination geometries – results in a considerable interest of chemists in this element. This chapter about Ag is therefore devoted predominantly to the description of progress in the field of combined coordination chemistry of Ag and POMs, strictly speaking – ways to put them together, either exclusively or together with other metallorganic building blocks. Examples of reaction catalyzed by such moieties are still rare, and as such will be given less attention. At the very beginning, it is worth underlining the tunability of presented structures, i.e. their topology can be easily influenced by only slight modifications of reaction conditions – especially by introducing highly-coordinating solvents and coupling their effects with the presence of cations of various sizes and rigidities. This proves the functionality of Ag and its usefulness in supramolecular chemistry.

8.1. Polyvanadates

In neutral $[Ag_{40}(t\text{-BuC}{\equiv}C)_{22}(CF_3COO)_{12}(V_{10}O_{28})]$ the polyoxovanadate made from 10 edge-sharing octahedra is embedded in a cage of 40 silver atoms held together by means of multiple argentophilic interactions, Ag–O_{POM} bonding (Ag–$O_{terminal}$ bond lengths in the range of: 2.452(7)–2.928(7) Å) and further stabilized by organic ligands coordinated to its outer surface. This compound is a result of the reaction between (*t*-BuC≡C)Ag, CF_3COOH and $(Et_4N)_3H_3V_{10}O_{28}$ in MeOH and is soluble in organic solvents [286].

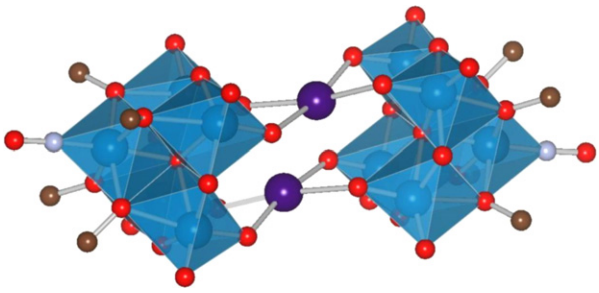

Fig. 56. Structure of $[Ag_2\{Mo_5O_{13}(OMe)_4(NO)\}_2]^{4-}$ (Ref. [288]).

Reactions of $(Bu_4N)_3H_3V_{10}O_{28}$ and $AgNO_3$ in DMSO/MeCN at different $\{V_{10}\}$/Ag ratios yield the 1D chain polymer $[Ag_3(DMSO)_6][Ag(DMSO)_3]H_2V_{10}O_{28}$ and the 2D polymer $[Ag_3(DMSO)_6][Ag(DMSO)_2]H_2V_{10}O_{28}$. In both compounds polyvanadates are linked via tri-centered $[Ag_3(DMSO)_6]^{3+}$ bridges, but while in the former additional $[Ag(DMSO)_3]^+$ group decorates the cluster, in the latter $[Ag(DMSO)_2]^+$ serves as a linker between parallel chains. Both species in crystalline form are reduced with hydrazine in H_2O/DMSO to produce nanowires of Ag nanoparticles embedded in amorphous vanadium oxide matrix Ag@VO_x [287].

8.2. Polymolybdates

Table 2 gives an up-to-date overview of architectures involving Ag ions coordinated to iso- or heteropolymolybdate clusters, as described in the literature. The number of silver centers taken from the chemical formula of a given compound was divided into types based on their coordination number, geometry, type of donor atoms and their origin (whether polyoxometalate POM and/or other ligands L). The crystallographic independence of Ag sites was not taken into account. Ag-donor bond lengths (sometimes averaged "av.") and structure-stabilizing argentophilic interactions were included in the table as well. The classification follows firstly the type of polyanion, then the increasing dimensionality of the so-created Ag–POM modules (once again – not of complete crystal structures), discriminating situations when on one hand there exists a connection between one silver cation and more than one polyoxometalate cluster and, on the other hand, silver coordinates to only one polyanion and structure is held by means of its interactions with additional ligands. In the same sequence compounds are described in the text. In our literature perusal we focused on analyzing possible modes of silver bridging of POMs, leaving somewhat aside Ag centers when incorporated in discreet inorganic–organic cations or cationic chains, especially in the case of compounds where all these types of silver behaviour were revealed simultaneously.

8.2.1. Lindqvist structure $[Mo_6O_{19}]^{2-}$ and/or its derivatives

Complexes of the complete $[Mo_6O_{19}]^{2-}$ or lacunary $[Mo_5O_{18}]^{6-}$ Lindqvist unit with silver have not yet been described. However, the well-known derivative of this type $[Mo_5O_{13}(OMe)_4(NO)]^{3-}$ reacts with silver nitrate in methanol, yielding $(Bu_4N)_4[Ag_2\{Mo_5O_{13}(OMe)_4(NO)\}_2]$. Its structure consists of discreet centrosymmetrical anions, with 2 $[Mo_5O_{13}(OMe)_4(NO)]^{3-}$ "monomers" linked through $[Ag–Ag]^{2+}$ bridge, with short Ag···Ag distance of 2.873(2) Å. (Fig. 56). This value is significantly lower than the sum of the 2 van der Waals radii of Ag ($r_{vdW\text{-}Ag}$ = 1.72 Å) and as a consequence a strong bonding interaction is expected [288].

Table 2
Silver–polymolybdates architectures. In the second column type and multiplicity of silver centers are given, followed by coordination number, geometry, type and origin of donor atoms in the third, e.g. "$1\times O_{POM\text{-}long}$" indicates coordination of a silver center to one oxygen originating from a polyoxometalate, with a bond classified as long (ca. 2.7–3.0 Å) and therefore weak. Priming results from more than one POM or L coordinated to a given center. Bond lengths in the fourth column and metallic Ag–Ag interactions in the fifth are given in Å. In the sixth column topology of Ag–POM moiety versus whole structure's dimensionality are shown.

Chemical formula	Type (multiplicity) of Ag centers	Coordination number; geometry/donor atoms$_{(\text{their -origin})}$	Bond length Ag–X (Å)	Ag···Ag distance (Å)	Topology: Ag–POM moiety/overall	Ref.
$(Bu_4N)_4[Ag_2\{Mo_5O_{13}(OMe)_4(NO)\}_2]$	1 (×2)	4; square planar/2×O_{POM} 2×$O_{POM'}$	Ag–O: 2.342–2.477	2.873(2)	0D/0D	[288]
$[(H_2O)_5Na_2(C_6NO_2H_4)(C_6NO_2H_5)_3Ag_2]$ $[Ag_2IMo_6O_{24}(H_2O)_4]\cdot 6.25H_2O$	1 (×2)	4; square planar/2×O_{POM} 2×$O_{POM'}$	Ag–O: 2.568(15)–2.583(14)	Ag 1···Ag 1 2.9312(14)	1D/3D	[289]
	2 (×2)	3; T-shaped/1×$O_{POM\text{-}long}$ 1×N_L 1×$N_{L'}$	Ag–$O_{POM\text{-}long}$: 2.869; 2.874 Ag–N: 2.130(17)–2.158(16)			
$[(H_2O)_4Na_2(C_6NO_2H_5)_6Ag_3][IMo_6O_{24}]\cdot 6H_2O$	1 (×2)	4/1×O_{POM} 1×$O_{POM'}$ 1×N_L 1×$N_{L'}$	Ag–O: 2.586(5)–2.631(5) Ag–N: 2.178(6)–2.191(6)	Ag 1···Ag2 3.242	1D/3D	[289]
	2 (×1)	2; linear/1×N_L 1×$N_{L'}$	Ag–N: 2.153(6)			
$(C_6NO_2H_6)_2[(C_6NO_2H_5)_2Ag][Cr(OH)_6Mo_6O_{18}]\cdot 4H_2O$	1 (×1)	4/1×O_{POM} 1×$O_{POM'}$ 1×O_L 1×$O_{L'}$	av. Ag–O: 2.422		1D/2D	[289]
$Ag_3[MnMo_6O_{18}\{(OCH_2)_3CNH_2\}_2(DMSO)_5]\cdot 3DMSO$	1 (×1)	5/2×O_{POM} 1×O_L 1×$O_{L'}$ 1×$O_{L''}$	Ag–O_{POM}: 2.425–2.488		1D/1D	[290]
	2 (×1)	4/1×O_{POM} 1×O_L 1×$O_{L'}$ 1×$O_{L''}$	Ag–O_{POM}: 2.552 Ag–O_L: 2.298–2.479			
	3 (×1)	2; linear/1×N_{POM} 1×$N_{POM'}$	Ag–N: 2.175(6)			
$Ag_3[MnMo_6O_{18}\{(OCH_2)_3CNH_2\}_2$ $(DMSO)_6(MeCN)_2]\cdot DMSO$	1 (×1)	5/2×O_{POM} 1×O_L 1×$O_{L'}$ 1×$O_{L''}$	Ag–O_{POM}: 2.414–2.680		1D/1D	[290]
	2 (×1)	5/1×N_{POM} 1×O_L 1×$O_{L'}$ 1×$O_{L''}$ 1×$O_{L'''}$	Ag–N_{POM}: 2.258			
	3 (×1)	4/1×N_{POM} 1×O_L 1×N_{MeCN} 1×$N_{MeCN'}$	Ag–N_{POM}: 2.239			
$[Ni(H_2O)_6][Ag_2Ni(OH)_6Mo_6O_{18}]\cdot 8H_2O$	1 (×2)	5; pyramid/2×O_{POM} 2×$O_{POM'}$ 1×$O_{POM''}$	Ag–$O_{POM\text{-}terminal}$: 2.341–2.607 Ag–$O_{POM\text{-}bridging}$: 2.385		2D/3D	[291]
$[Ag_3(H_2O)_4][Cr(OH)_6Mo_6O_{18}]\cdot 3H_2O$	1 (×2)	6/2×O_{POM} 1×$O_{POM'}$ 1×$O_{POM''}$ 1×O_{H_2O}	Ag–$O_{POM\text{-}terminal}$: 2.377(7)–2.592(8) Ag–$O_{POM\text{-}bridging}$: 2.418(7)–2.430(7)		3D/3D	[292]
	2 (×1)	5; pyramid/2×O_{POM} 1×$O_{POM'}$ 1×O_{H_2O} 1×$O_{H_2O'}$	Ag–$O_{POM\text{-}terminal}$: 2.465(8)–2.624(5) Ag–$O_{POM\text{-}bridging}$: 2.563(6)			
$(PPh_4)_2[Ag_2(DMSO)_4(Mo_8O_{26})]$	1 (×2)	6/4×O_{POM} 1×O_L 1×$O_{L'}$	Ag–O: 2.355(2)–2.624(2)		0D/0D	[293]
$(Bu_4N)_2[Ag_2(Mo_8O_{26})]$	1 (×2)	4; square planar/2×O_{POM} 2×$O_{POM'}$	Ag–O: 2.2704(17)–2.4143(15) (Ref. [293]), 2.282–2.424 (Ref. [294])	2.8531(4) (Ref. [293]) 2.8702(17) (Ref. [294])	1D/3D	[293] [294]
$(PPh_4)_2[Ag_2(DMF)_2(Mo_8O_{26})]\cdot 2DMF$	1 (×2)	7/2×O_{POM} 2×$O_{POM'}$ 2×$O_{POM\text{-}long}$ 1×O_L	Ag–O_{POM}: 2.4–2.5 Ag–$O_{POM\text{-}long}$: 2.85	3.1299	1D/1D	[295]
$(H_2NMe_2)_2[Ag_2(DMF)_2(Mo_8O_{26})]\cdot 2DMF$	1 (×2)	7/2×O_{POM} 2×$O_{POM'}$ 2×$O_{POM\text{-}long}$ 1×O_L	Ag–O_{POM}: 2.4–2.5 Ag–$O_{POM\text{-}long}$: 2.85	3.0201	1D/1D	[295]
$[Ag(C_7H_{12}O_2N)(MeCN)]_2[Ag_2(MeCN)_2$ $(Mo_8O_{26})]\cdot 2MeCN$	1 (×2)	7/4×O_{POM} 2×$O_{POM'\text{-long}}$ 1×N_{MeCN}	Ag–$O_{POM\text{-}long}$: 2.8–2.9	Ag 1···Ag 1 3.181	1D/1D	[295]
	2 (×2)	3; trigonal/1 × $O_{C_7H_{12}O_2N}$ 1 × $N_{C_7H_{12}O_2N}$ 1×N_{MeCN}				
$(PPh_4)_2[Ag_2(MeCN)_2(Mo_8O_{26})]\cdot 2MeCN$	1 (×2)	6/4×O_{POM} 1×$O_{POM'\text{-long}}$ 1×N_{MeCN}	Ag–O_{POM}: 2.3–2.7 Ag–$O_{POM\text{-}long}$: 2.8	3.647	1D/1D	[295]
$[(Ag(DMF))_2(Ag(DMF)_2)_2(Mo_8O_{26})]$	1 (×2)	7/2×O_{POM} 2×$O_{POM'}$ 2×$O_{POM\text{-}long}$ 1×O_L	Ag–O_{POM}: 2.4–2.6 Ag–$O_{POM\text{-}long}$: 2.7–2.9	Ag 1···Ag 1 3.0549(5)	2D/2D	[295]
	2 (×2)	4; square planar/1×O_{POM} 1×O_L 1×$O_{L'}$ 1×$O_{L''}$				
$[Ag_4(4atrz)_2Cl][Ag(Mo_8O_{26})]$	1 (×1)	4; square planar/2×O_{POM} 2×$O_{POM'}$	Ag–O_{POM}: 2.355(6)–2.451(6)		1D/3D	[296]
	2 (×2)	2; linear/1×N_L 1×$N_{L'}$	Ag–N: 2.164(6), 2.225(6)			
	3 (×2)	2; linear/1×N_L 1×Cl	Ag–N: 2.163(6) Ag–Cl: 2.435(2)			
$[Ag_5(trz)_4]_2[Ag_2(Mo_8O_{26})]$	1 (×2)	4; tetrahedral/2×O_{POM} 1×$O_{POM'}$ 1×N_L	Ag–O_{POM}: 2.356(10)–2.510(9) Ag–N: 2.165(11)		1D/3D	[296]
	2 (×5)	2; linear/1×N_L 1×$N_{L'}$	Ag–N: 2.085(12)–2.117(12)			

Table 2 (*Continued*)

Chemical formula	Type (multiplicity) of Ag centers	Coordination number; geometry/donor atoms$_{(\text{their-origin})}$	Bond length Ag–X (Å)	Ag···Ag distance (Å)	Topology: Ag–POM moiety/overall	Ref.
$[Ag_2(3atrz)_2][Ag_2(3atrz)_2(Mo_8O_{26})]$	1 (×2)	4; tetrahedral/2×O_{POM} 1×N_L 1×$N_{L'}$	Ag–O_{POM}: 2.411(3)–2.578(4) Ag–N: 2.181(4)–2.210(5)		2D/3D	[296]
	2 (×2)	2; linear/1×N_L 1×$N_{L'}$	Ag–N: 2.205(4)–2.120(4)			
$[\{Ag_4(tpyprz)_2(H_2O)\}(Mo_8O_{26})]$	1 (×2)	4/1×O_{POM} 2×N_L 1×$N_{L'}$	Ag–O_{POM}: 2.471(2) Ag–N: 2.224(3)–2.720(2)	Ag 1···Ag 1 3.0093(5)	2D/2D	[297]
	2 (×1)	4; tetrahedral/2×N_L 2×$N_{L'}$	Ag–N: 2.227(3)–2.423(2)			
	3 (×1)	3/1×N_L 1×$N_{L'}$ 1 × O_{H_2O}	Ag–N: 2.215(3)			
$(Bu_4N)_2[Ag_2(DMSO)_2(Mo_8O_{26})]$	1 (×1)	6/4×O_{POM} 1×O_L 1×$O_{L'}$	av. Ag–O_{POM}: 2.555(3) Ag–O_L: 2.366(3)–2.495(3)	Ag 1···Ag 1 3.8899(6)	2D/2D	[293]
	2 (×1)	4/2×O_{POM} 1×O_L 1×$S_{L'}$	av. Ag–O_{POM}: 2.375(3) Ag–O_L: 2.514(2) Ag–S_L: 2.462(3)	Ag 2···Ag 2 4.848(6)		
$[Ag_4(DMSO)_8(Mo_8O_{26})]$	1 (×2)	6/4×O_{POM} 1×O_L 1×$O_{L'}$	Ag–O: 2.296(3)–2.581(2)		2D/2D	[290]
	2 (×2)	6/2×O_{POM} 1×O_L 1×$O_{L'}$ 1×$S_{L''}$ 1×$S_{L'''}$	Ag–O: 2.343(2)–2.449(2)			
$(HDMF)[Ag_3(DMF)_4(Mo_8O_{26})]$	1 (×2)	5; pyramid/2×O_{POM} 2×$O_{POM'}$ 1×O_L	av. Ag–O_{POM}: 2.413(3) Ag–O_L: 2.442(3)	Ag 1···Ag 1 3.1475(6)	2D/2D	[293]
	2 (×1)	6; octahedral/2×O_{POM} 2×$O_{POM'}$ 1×O_L ×1$O_{L'}$				
$[Ag_{10\cdot4}(PV_2Mo_{10}O_{40})_2(NO_3)_{0\cdot4}]\cdot(MeCN)_{17.3}\cdot(H_2O)_{1.5}$	1 (×2)	4/2×O_{POM} 1×$O_{POM'}$ 1×N_L	av. Ag–O_{POM}: 2.40 (terminal); 2.49 (bridging) av. Ag–N_L: 2.24		0D/0D	[298]
	2 (×4)	4/2×O_{POM} 1×N_L 1×$N_{L'}$				
$\{Ag(phen)_2\}_2[\{Ag(phen)\}_2(\alpha\text{-}PMo_{12}O_{40})]$	1 (×1)	4; tetrahedral/1×O_{POM} 1×$O_{POM'}$ 2×N_L	Ag–O_{POM}: 2.597; 2.400 Ag–N_L: 2.231–2.449		1D/3D	[299]
	2 (×1)	4; tetrahedral/2×O_{POM} 2×N_L				
	3 (×1)	4; tetrahedral/2×N_L 2×$N_{L'}$				
$[Ag_3(2,4'\text{-}bipy)_3PMo_{12}O_{40}]$	1 (×1)	4; tetrahedral/1×O_{POM} 1×$O_{POM'}$ 1×N_L 1×$N_{L'}$	Ag–O_{POM}: 2.453(4)–2.500(4) Ag–N_L: 2.224(5)–2.240(5)		1D/1D	[300]
	2 (×2)	2; linear/1×N_L 1×$N_{L'}$	Ag–N_L: 2.120(5)–2.147(6)			
$Ag_2[Mo_{12}O_{46}(AsC_6H_4\text{-}4\text{-}NH_2)_2(AsC_6H_4\text{-}4\text{-}NH_3^+)_2]\cdot2H_2O\cdot8MeCN$	1 (×1)	4; tetrahedral/1×O_{POM} 1×$N_{POM'}$ 1×N_{MeCN} 1×$N_{MeCN'}$	Ag–O_{POM}: 2.65 Ag–N_{POM}: 2.26 av. Ag–N_{MeCN}: 2.32		1D/1D	[301]
	2 (×1)	4; tetrahedral/1×O_{POM} 1×N_{MeCN} 1×$N_{MeCN'}$ 1×$N_{MeCN''}$	Ag–O_{POM}: 2.57 av. Ag–N_{MeCN}: 2.24			
$[Ag_3(2,2'\text{-}bipy)_4(\alpha\text{-}PMo_{12}O_{40})]\cdot2H_2O$	1 (×2)	4; tetrahedral/1×O_{POM} 2×N_L 1×$N_{L'}$	Ag–O_{POM}: 2.516(8) Ag–N_L: 2.155(10)–2.328(11)	Ag 1···Ag 2 2.9270(12)	1D/3D	[302]
	2 (×1)	2; linear/1×N_L 1×$N_{L'}$				
$[\{Ag(2,2'\text{-}bipy)\}_2\{Ag_4(2,2'\text{-}bipy)_6\}\alpha\text{-}PVMo_{11}O_{40}]$	1 (×2)	4/2×O_{POM} 2×N_L	Ag–O_{POM}: 2.373(9)–2.462(9)	Ag 2···Ag 4 3.131(2)	1D + 1D/3D	[302]
	2 (×2)	3/1×O_{POM} 2×N_L				
$[\{Ag(2,2'\text{-}bipy)\}_2\alpha\text{-}PVMo_{11}O_{40}]$	3 (×2)	3/1×O_{POM} 1×N_L 1×$N_{L'}$	Ag–N_L: 2.204(14)–2.507(14)	Ag 4···Ag 4 2.936(3)		
	4 (×2)	4/2×N_L 2×$N_{L'}$				
$[Ag_4(Hfcz)_2(SiMo_{12}O_{40})]$	1 (×2)	3; T-shaped/1×O_{POM} 1×N_L 1×$N_{L'}$	Ag–O_{POM}: 2.540(6) Ag–N_L: 2.265(7); 2.319(7)		2D/3D	[303]
	2 (×2)	2; linear/1×N_L 1×$N_{L'}$	Ag–N_L: 2.202(6); 2.215(6)A			
$[Ag(MeCN)_4][Ag_3(MeCN)_8(SiMo_{12}O_{40})]$	1 (×1)	4/1×O_{POM} 1×$O_{POM'}$ 2×N_{MeCN}	av. Ag–$O_{POM\text{-terminal}}$: 2.47 av. Ag–N: 2.18	Ag 1···Ag 2 2.964(2)	2D/3D	[304]
	2 (×1)	4/1×O_{POM} 3×N_{MeCN}	Ag–$O_{POM\text{-terminal}}$: 2.391(9) av. Ag–N: 2.28			
	3 (×1)	4; trigonal pyramid/1×O_{POM} 3×N_{MeCN}	Ag–$O_{POM\text{-terminal}}$: 2.71 av. Ag–N: 2.16–2.28			
	4 (×1)	4;distorted tetrahedral/4×N_{MeCN}	Ag–N: 2.20–2.36			
$[Ag_6(PV_2Mo_{10}O_{40})](CH_3COO)\cdot8H_2O$	1 (×2)	8/4×O_{POM} 4×$O_{POM'}$	av. Ag–O_{POM}: 2.466–2.779		3D/3D	[305]
	2 (×2)	7/4×O_{POM} 1×$O_{POM'}$ 1×$O_{POM''}$ 1 × O_{H_2O}				
	3 (×2)	6/1×O_{POM} 1×$O_{POM'}$ 1×$O_{POM''}$ 1×$O_{POM'''}$ 1 × O_{H_2O} 1 × $O_{H_2O'}$				

bipy = bipyridine; 4atrz = 4-amino-1,2,4-triazole; trz = 1,2,4-triazole; 3atrz = 3-amino-1,2,4-triazole; tpyprz = tetra-2-pyridylpyrazine; Hfcz = fluconazole-[2-(2,4-difluorophenyl)-1,3-di(1*H*-1,2,4-triazol-1-yl)propan-2-ol] phen = 1,10-phenanthroline.

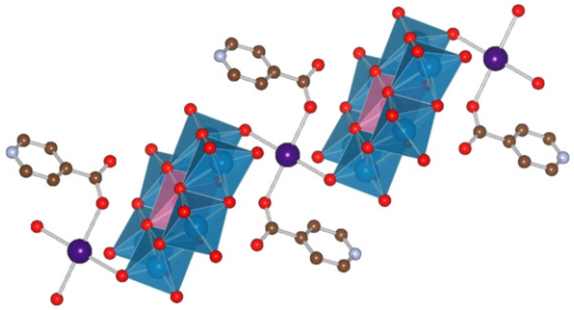

Fig. 57. 1D chain structure of $[\{(C_6NO_2H_5)_2Ag\}\{Cr(OH)_6Mo_6O_{18}\}]^{2-}$ (Ref. [289]).

8.2.2. Anderson structure $[Mo_6MO_{24}]^{n-}$

Reactions of Anderson-type clusters with $AgNO_3$ or Ag_2CO_3 and additional ligands take place in water, DMSO, MeCN or mixed media and require mild heating up to 50–60 °C. Three types of direct silver bridging of polyoxometalate clusters into 1D chain-like structures were described [289]. A new type of structural motif, is created *in situ* by reaction of the A-type Anderson cluster $[IMo_6O_{24}]^{5-}$ with $AgNO_3$ and pyridine-4-carboxylic acid. $[IMo_6O_{24}(H_2O)_4]^{5-}$ connects to the adjacent polyanion via a $[Ag–Ag]^{2+}$ bridge, with each silver in a square planar geometry. The Ag–Ag distance is short (ca. 2.9 Å) and an attractive interaction is present. When using a slightly different ligand, pyridine-3-carboxylic acid, in an otherwise identical synthetic procedure, there is a dramatic change in the structure of the product. This time "classical" Anderson clusters $[IMo_6O_{24}]^{5-}$ remain unchanged and are bound via unprecedented trinuclear silver moieties. The Ag atoms arrange in a linear manner, perpendicularly to the axis of the chain, with two pyridine ligands *trans*-coordinated to each of them. Next, two outer ones form 2 Ag–O bonds each, with adjacent POMs. Only one Ag center, squeezed between two polyoxoanions, keeps together chains in $(C_6NO_2H_6)_2[(C_6NO_2H_5)_2Ag][Cr(OH)_6Mo_6O_{18}]\cdot 4H_2O$. The coordination sphere of Ag is made by 2 oxygen atoms of Anderson clusters of B-type (i.e. with each Cr heteroatom forming an octahedral complex of six OH groups) and 2 carboxyl oxygens from pyridine-4-carboxylic acid molecules in *trans* arrangement (see Fig. 57).

Two compounds, (**1**) $Ag_3[MnMo_6O_{18}\{(OCH_2)_3CNH_2\}_2(DMSO)_5]\cdot 3DMSO$ and (**2**) $Ag_3[MnMo_6O_{18}\{(OCH_2)_3CNH_2\}_2(DMSO)_6(MeCN)_2]\cdot DMSO$ [290], illustrate in an elegant way how the overall structure could be influenced by incorporation of additional solvent molecules. In the absence of acetonitrile, the *tris*-derived Anderson clusters $[MnMo_6O_{18}\{(OCH_2)_3CNH_2\}_2]^{3-}$ use their tripodally anchored amine groups to form linear N–Ag–N bridges with each other. Then, two parallel strands join via $[Ag_2(DMSO)_2]^{2+}$ 4-membered rings established between terminal oxygen atoms of POMs, into a double-chain of (**1**). In (**2**), again $[Ag_2(DMSO)_2]^{2+}$ 4-membered rings are present, but this time one of their silver centers links to the amine group and not to the terminal oxygen. On the other hand, a linear bridging N–Ag–N motif is not observed. Instead, Ag which is attached to the other amine group, having coordinated 2 MeCN and 1 DMSO molecules, decorates the cluster.

Each polyoxomolybdate unit coordinates via its terminal and bridging oxygen atoms 6 Ag^+ cations in $[Ni(H_2O)_6][Ag_2Ni(OH)_6Mo_6O_{18}]\cdot 8H_2O$ [291]. The silver centers, in a square pyramidal coordination, link three neighbouring POMs to create infinite planes separated by $[Ni(H_2O)_6]^{2+}$ octahedra and water molecules (see Fig. 58).

The purely-inorganic 3D architecture of $[Ag_3(H_2O)_4][Cr(OH)_6Mo_6O_{18}]\cdot 3H_2O$ [292] is based only on Ag linkers. B-type Anderson clusters are joined into chains, chains into sheets and finally into an open framework, with channels filled with lattice water molecules. The silver atom is coordinated to terminal and bridging oxygen atoms of the polyanions.

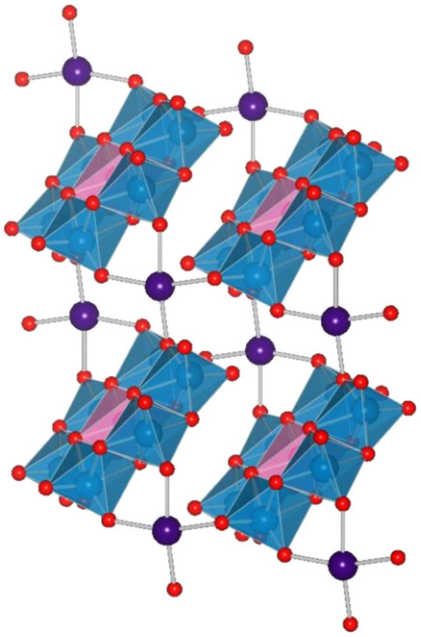

Fig. 58. 2D plane of $[Ag_2Ni(OH)_6Mo_6O_{18}]^{2-}$ (Ref. [291]).

8.2.3. $[Mo_8O_{26}]^{4-}$

The richest possibilities in constructing new architectures are offered by a combination of Ag centers and the $[\beta\text{-}Mo_8O_{26}]^{4-}$ unit, although other isomers of the polyoxomolybdate (ζ and γ) can also be found. It has been actually argued that the real precursor in the synthesis of these compounds is the $[Ag\{Mo_8O_{26}\}Ag]^{2-}$ synthon, rather than individual $\{Ag_2\}$ and $\{Mo_8\}$moieties [293].

The general synthetic strategy to obtain Ag–POM architectures involves reactions of simple Ag salts (predominantly nitrate, fluoride or acetate) with molybdates (e.g. $[(Bu_4N)_2(Mo_6O_{19})]$, Na_2MoO_4, MoO_3) in solvents such as water, methanol, DMF, DMSO, and MeCN at ambient conditions [290,293–295]. The other route is via cation and ligand exchange reactions [295]. The use of hydrothermal synthesis has also been reported [296,297].

By introducing rigid, bulky cations such as PPh_4^+ it is possible to isolate from the solution crystalline salts of the monomeric $[Ag_2(DMSO)_4(Mo_8O_{26})]^-$ units [293]. The silver atoms are bound to 4 terminal oxygens on both sides of the POM, with the coordination spheres completed by 2 oxygen atoms from 2 DMSO molecules (see Fig. 59).

The $PPh_4^+ \rightarrow Bu_4N^+$ cation exchange reaction induces the loss of DMSO ligands in $[Ag_2(DMSO)_4(Mo_8O_{26})]^-$ and polymeriza-

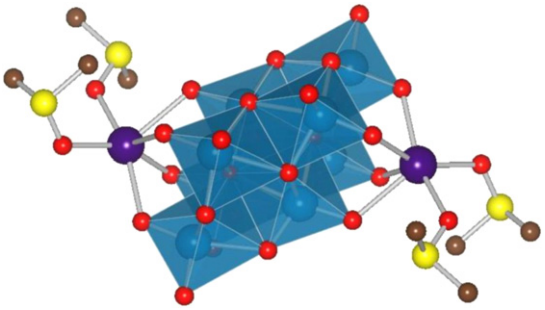

Fig. 59. Structure of the $[Ag_2(DMSO)_4(Mo_8O_{26})]^-$ monomeric unit (Ref. [293]).

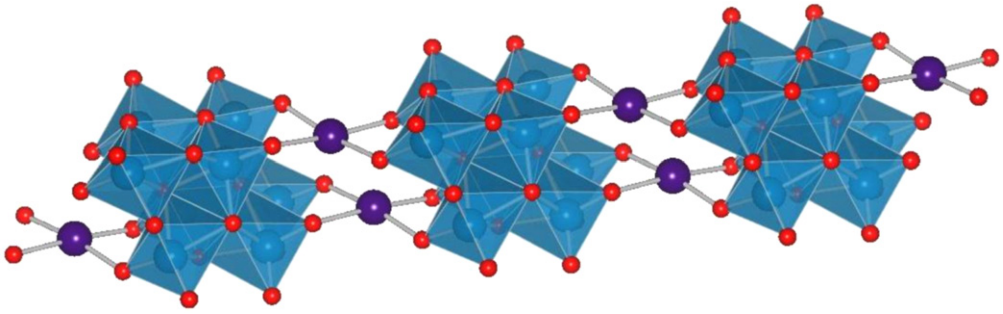

Fig. 60. Scheme of 1D chain of $\{Mo_8\}$units with $[Ag–Ag]^{2+}$ bridges (Ref. [294]).

tion [295]. In this simplest example of 1D structure, chains of $[Ag_2(Mo_8O_{26})]^{2-}$ anions propagate infinitely, their charge being counterbalanced by Bu_4N^+ wrapped around them. The silver centers, in a slightly distorted square planar coordination, connect to two different POMs (see Fig. 60). The Ag–Ag distance of ca. 2.86 Å suggests strong argentophilic attractive interaction in the $[Ag–Ag]^{2+}$ bridge, further stabilizing the structure. Another synthetic approach to $[Ag_2(Mo_8O_{26})]^{2-}$ involve an *in situ* rearrangement of the Lindqvist $[Mo_6O_{19}]^{2-}$ cluster [293,294]. This process was studied carefully by means of cryospray mass spectrometry (CSI-MS). Various monoanionic defragmentation series were identified, among which Ag-containing one with $[AgMo_2O_7]^-$ and $[AgMo_4O_{13}]^-$ units-building blocks of the $[Ag\{Mo_8O_{26}\}Ag]^{2-}$ synthon. The structure directing role of organic cations was also evidenced in this case [306].

The presence of highly coordinating solvents (e.g. DMF) results in the formation of $(PPh_4)_2[Ag_2(DMF)_2(Mo_8O_{26})]\cdot 2DMF$ and $(H_2NMe_2)_2[Ag_2(DMF)_2(Mo_8O_{26})]\cdot 2DMF$ with similar structural features. The Ag environment reorganizes slightly. One DMF molecule coordinates to each center with its oxygen atom, outwards of the axis of the chain, serving as an organic spacer. In the meantime two additional (per center) weak, long range Ag–O bonds (ca. 2.8 Å) with adjacent POMs are being developed. Even if the Ag–Ag distance is a little bit longer (ca. 3.0–3.2 Å), an attractive interaction still exists [295].

Sometimes, DMF molecules, instead of playing the role of spacers, actually help to develop 2D networks, inserting in between neighbouring chains, like in $[(Ag(DMF))_2(Ag(DMF)_2)_2(Mo_8O_{26})]$. Additional Ag ions, in a highly distorted square planar geometry and single-bounded to the POM, are needed to complete the bridging motif [295].

In a peculiar compound $(PPh_4)_2[Ag_2(MeCN)_2(Mo_8O_{26})]\cdot 2MeCN$, no Ag–Ag interaction is found, due to shift of the Ag positions. The tetracoordinated Ag ions cap POM units, instead of connecting them. The structure is supported solely on the basis of weak, long range Ag–O bonds (ca. 2.8 Å) with adjacent POMs (one per center) and should be treated more like a precursor than a real 1D polymer [293,295].

Different ways of linking polyoxomolybdate clusters into 1D chain were demonstrated in $[Ag_4(4atrz)_2Cl][Ag(Mo_8O_{26})]$ and $[Ag_5(trz)_4]_2[Ag_2(Mo_8O_{26})]$ [296]. In the former, only one Ag atom in a square planar geometry is sandwiched between neighbouring POMs, while in the latter 2 Ag in a distorted tetrahedral environment form 3 bonds with the POMs (in a 2 + 1 mode) and one bond with nitrogen from the perpendicularly running cationic chains.

$[Ag_2(3atrz)_2][Ag_2(3atrz)_2(Mo_8O_{26})]$ is an interesting example of $\{\gamma\text{-}Mo_8\}$ units condensed into 1D chains and then connected with the ones above and below by 6-membered rings of $[Ag_2(3atrz)_2]^{2+}$ units (do not mistake with cationic chains of the same formula also present in the structure) into 2D arrays. Each Ag center is in a distorted tetrahedral arrangement made by 2 terminal oxygens of the POM and 2 nitrogen atoms from two 3atrz molecules [296].

In $[\{Ag_4(tpyprz)_2(H_2O)\}(Mo_8O_{26})]$ [297], only one Ag center (out of three different types) is linked to the POM, whereas in $(nBu_4N)_2[Ag_2(DMSO)_2(\zeta\text{-}Mo_8O_{26})]$ [293] and $[Ag_4(DMSO)_8(Mo_8O_{26})]$ [290] which have two types of Ag centers, all of them are interacting with the POM. The connectivity to adjacent Ag–POM units in these three compounds is realized so to say "indirectly" via a complicated arrangement of ligands forming linear bridges and/or rings. The former structure could be actually perceived as Ag–organic 1D chains being linked by POM units. It is clearly visible here that the access to expanded architectures is not necessarily dependent on using more sophisticated ligands, such as tpyprz.

Finally, the 2D array in $(HDMF)[Ag_3(DMF)_4(Mo_8O_{26})]$ originates from a combination of strands, with POMs joined together by penta- and hexacoordinated silver centers [293].

8.2.4. *Keggin structure* $[XMo_{12}O_{40}]^{n-}$

The syntheses of Ag–Keggin compounds are relatively not complicated. They differ only in minor details from procedures already described for other polyoxomolybdates.

The structure of $[Ag_{10.4}(PV_2Mo_{10}O_{40})_2(NO_3)_{0.4}]\cdot 17.3(MeCN)\cdot 1.5(H_2O)$ consists of discreet dimers of Keggin units joined together by two silver ions in a tetrahedral coordination (see Fig. 61). Each silver connects to three oxygen atoms of two adjacent POMs in a 2 + 1 mode, the coordination sphere being filled up by MeCN molecules. There are also 2 decorating $[Ag(MeCN)_2]^+$ groups per each cluster and Ag^+ counterions not bound to POMs [298].

1D chains of $[\{Ag(phen)_2\}_2\{Ag(phen)\}_2(PMo_{12}O_{40})]$ are created when $[Ag(phen)]^+$ groups are inserted between neighbouring

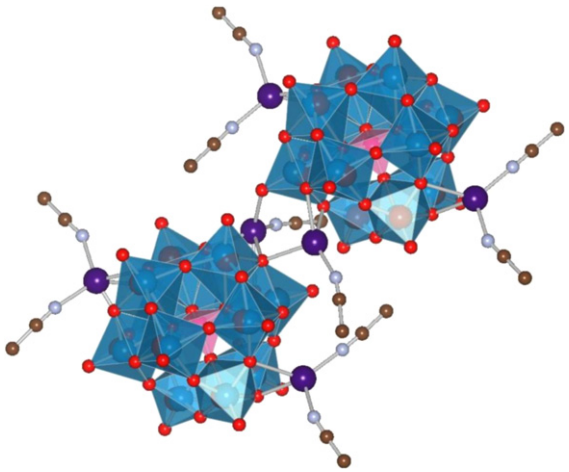

Fig. 61. Structure of the $Ag_{10.4}P_2V_4Mo_{20}O_{80}(NO_3)_{0.4}$ dimer (Ref. [298]).

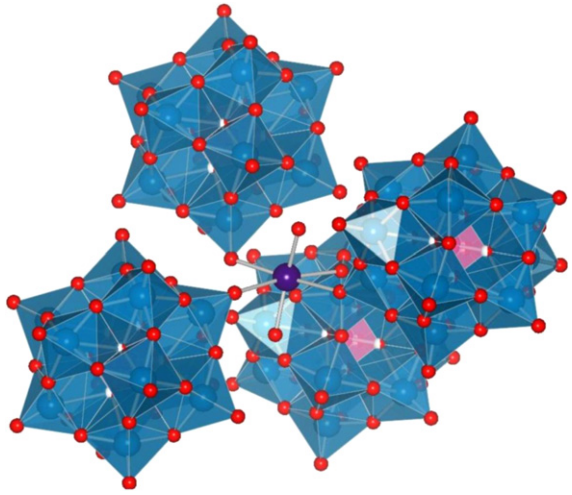

Fig. 62. One type of silver centers of $[Ag_6(PV_2Mo_{10}O_{40})](CH_3COO)\cdot 8H_2O$, coordinating four different Keggin units as well as 2 H_2O molecules in a *trans* conformation (Ref. [305]).

POMs and bridge them via Ag–O bonds. Noteworthily, the other $[Ag(phen)]^+$ group behaves in a non-bridging, decorating way. A third type of Ag center is found in the complex cations $[Ag(phen)_2]^+$ [299].

$Ag_2[Mo_{12}O_{46}(AsC_6H_4\text{-}4\text{-}NH_2)_2(AsC_6H_4\text{-}4\text{-}NH_3^+)_2]\cdot 2H_2O\cdot 8MeCN$ is an example of an architecture based on inverse Keggin cluster, i.e. with heteroatoms localized on the surface of the unit, not inside of it. The arsenic atoms are functionalized with aniline molecules and these organoarsenic groups (two of them being protonated to neutralize the negative charge of the POM) are arranged around the cluster in a tetrahedral manner. The introduction of silver ions is followed by the formation of 1D chains, where tetrahedral Ag links the amine nitrogen and oxo ligand of adjacent POMs (with two additional MeCN molecules). The second silver ion decorates the cluster as a $[Ag(MeCN)_3]^+$ group [301].

In the case of $[Ag_3(2,2'\text{-bipy})_4(\alpha\text{-}PMo_{12}O_{40})]\cdot 2H_2O$ the polyoxomolybdate clusters are linked via $Ag_3(2,2'\text{-bipy})_4$ motifs into 1D chains. The situation gets more complicated when V_2O_5 is added to the reaction mixture. A mono-substituted cluster is produced, that participates in the creation of both cationic chains and isolated anions for $[\{Ag(2,2'\text{-bipy})\}_2\{Ag_4(2,2'\text{-bipy})_6\}\alpha\text{-}PVMo_{11}O_{40}][\{Ag(2,2'\text{-bipy})\}_2\alpha\text{-}PVMo_{11}O_{40}]$. Supramolecular 3D assemblies are further developed by means of hydrogen bonds and π–π stacking [302].

The 2D arrays of $[Ag_4(Hfcz)_2(SiMo_{12}O_{40})]$ originate from POMs interconnecting Ag–organic chains. The bridging silver ions are in an unusual T-shaped coordination environment made by two nitrogens from 2 Hfcz molecules and one terminal oxygen from polyanion [303]. The polymeric $[Ag(MeCN)_4][Ag_3(MeCN)_8(SiMo_{12}O_{40})]$ forms a 2D right-hand screw helical network [304].

All types of Ag centers are involved in linking POM clusters in $[Ag_6(PV_2Mo_{10}O_{40})](CH_3COO)\cdot 8H_2O$. The overall coordination number/number of coordinated Mo clusters for Ag(1), Ag(2) and Ag(3) are: 8/2, 7/3 and 6/4, respectively. As a result the fascinating structure of a 3D macrocation is formed (see Fig. 62) [305].

8.2.5. Other polymolybdates

Recently new types of discreet and infinite Ag–POM architectures were reported. In neutral $[Ag_{40}(t\text{-}BuC{\equiv}C)_{20}(CF_3COO)_{12}(Mo_6O_{22})]$ the polyoxomolybdate is embedded in a giant cage made from 40 silver atoms held together by means of multiple argentophilic interactions, $Ag\text{–}O_{POM}$ bonding ($Ag\text{–}O_{bridging}$ bond lengths in the range of: 2.205(6)–2.691(7) Å and $Ag\text{–}O_{terminal}$ bond lengths in the range of: 2.304(6)–2.699(8) Å) and further stabilized by organic ligands coordinated to its outer surface. This compound is a result of reaction between (t-BuC≡C)Ag, CF_3COOH and $(Bu_4N)_2Mo_6O_{19}$ in MeOH and it is soluble in organic solvents [286]. Another example of this type, $[Ag_{60}(t\text{-}BuC{\equiv}C)_{38}(Mo_6O_{22})_2](CF_3SO_3)_6$, consists of two polyoxomolybdate clusters in a silver cage stabilized with t-BuC≡C ligands. Mo_6O_{22} units are made of 6 edge sharing octahedra. Ag–O bond lengths are in the range of: 2.039(6)–2.573(5) Å. Incorporation of polyoxometalate fragments makes the silver moiety light insensitive [307].

The compound $[Ag_7(C_2)Mo_6O_{22}]$ combines ethynediide $(C_2)^{2-}$ species entrapped in silver(I) cages: $(C_2)@Ag_7$ and a new type of Mo_6O_{22} polyanion, made from 2 MoO_4 tetrahedra and 4 MoO_6 octahedra, sharing edges and/or vertices. Silver cages in distorted monocapped square antiprism geometry form columns or chains that are cross-linked by POMs, thus creating a 3D network. Ag–O bond lengths are in the range of: 2.21(1)–2.567(9) Å [308].

8.3. Polytungstates

Some examples of compounds with Ag ions coordinated to iso- or hetero-polytungstate clusters are given in Table 3 .

Keggin-type polyoxotungstates linked to silver moieties or forming connections via silver linkers can be easily obtained by reactions between previously-made polyoxotungstate salts or their precursors (e.g. Na_2WO_4), $AgNO_3$ as silver source and additional ligands in H_2O or MeCN. The syntheses can be performed under ambient conditions [290,312,315,323] or hydrothermally, in sealed autoclaves [300,310,317,319].

The discreet motif of $[Ag_4(2,4'\text{-bipy})_4(SiW_{12}O_{40})]$ consists of a POM coordinated to a molecular square of $[Ag_4(2,4'\text{-bipy})_4]^{4+}$ through its 2 terminal oxygen atoms. Interestingly, it is the POM negative charge that, above all, influences the structure of the product – when in analogous reaction $[PMo_{12}O_{40}]^{3-}$ polyanion is used instead of $[SiW_{12}O_{40}]^{4-}$, see in the previous paragraph, the result is an infinite chain of alternating links [300]. The V-centered Keggin unit of $[\{VO_2Ag(phen)_3\}_2(VW_{12}O_{40})]$ supports two heterometallic complexes; the $[Ag(phen)]^+$ moiety binds to terminal oxygen of the cluster and to $[VO(phen)_2]^{3+}$ via an oxo bridge [309]. In another compound, $[\{Ag(2,2'\text{-bipy})\}_2\{Ag_2(2,2'\text{-bipy})_3\}_2(\alpha\text{-}PV_3W_9O_{40})]$, 4 (out of 6) Ag centers are coordinated to bridging oxygen atoms of one Keggin unit. Both types of Ag–bipy groups decorate the cluster and an extensive network of π–π interactions between aromatic ligands links the 0D building blocks into a 3D framework [310]. In $[\{Ag_3(2,2'\text{-bipy})_2(4,4'\text{-bipy})_2\}\{Ag(2,2'\text{-bipy})_2\}\{Ag(2,2'\text{-bipy})\}(AlW_{12}O_{40})]\cdot H_2O$ the Keggin units, monocapped with 2,2′-bipy, are inserted into channels of the 3D metallorganic framework [311].

The dimeric complex $K_{16}[\{Ag(H_2As_2W_9O_{33})(H_2AsW_9O_{33})(Mo_3S_4\{H_2O\}_5)\}_2]\cdot 48H_2O$ is the first combination of a trinuclear cluster $\{Mo_3S_4\}$, Ag ions and POMs. Two $\{As_2W_9O_{33}\}$ subunits with hanging $[AsOH]^{2+}$ group and $\{AsW_9O_{33}\}$ are linked through $\{Mo_3S_4\}$ into a monomer of the described compound. Then, silver binds to two terminal oxygen atoms of $\{AsW_9O_{33}\}$ and two sulphur atoms of two $\{Mo_3S_4\}$ clusters, one from the same monomer as $\{AsW_9O_{33}\}$, one from the adjacent one (see Fig. 63, on the left). The structure of a dimer holds then on 2 Ag–S bonds and is reinforced by 2 peripheral K^+ cations bonding to oxygen atoms of adjacent POMs, S···S interactions between 2 $\{Mo_3S_4\}$ clusters and a weak hydrogen bonding between aquo ligands of Mo atoms and terminal hydroxo groups. Interestingly, each Ag cation is dynamically delocalized over three available positions of

Table 3
Silver–polytungstates architectures. In the second column type and multiplicity of silver centers are given, followed by coordination number, geometry, type and origin of donor atoms in the third, e.g. "$1\times O_{POM\text{-}long}$" indicates coordination of a silver center to one oxygen originating from a polyoxometalate, with a bond classified as long (ca. 2.7–3.0 Å) and therefore weak. Priming results from more than one POM or L coordinated to a given center. Bond lengths in the fourth column and metallic Ag–Ag interactions in the fifth are given in Å. In the sixth column topology of Ag–POM moiety versus whole structure's dimensionality is shown.

Chemical formula	Type (multiplicity) of Ag centers	Coordination number; geometry/donor atoms$_{(\text{their -origin})}$	Bond length Ag–X (Å)	Ag···Ag distance (Å)	Topology: Ag–POM moiety/overall	Ref.
$[Ag_4(2,4'\text{-bipy})_4(SiW_{12}O_{40})]$	1 (×2)	3/1×O_{POM} 1×N_L 1×$N_{L'}$	Ag–O_{POM}: 2.38(3)–2.59(3) Ag–N_L: 2.20(3); 2.27(3)		0D/0D	[300]
	2 (×2)	2; linear/1×N_L 1×$N_{L'}$	Ag–N_L: 2.11(3)–2.17(3)			
$[VO_2Ag(phen)_3]_2[VW_{12}O_{40}]$	1 (×2)	4/1×O_{POM} 1×O_V 2×N_L	Ag–O_{POM}: 2.527(8) Ag–N_L: 2.302–2.391		0D/0D	[309]
$[\{Ag(2,2'\text{-bipy})\}_2\{Ag_2(2,2'\text{-bipy})_3\}_2(\alpha\text{-}PV_3W_9O_{40})]$	1 (×2)	4/2×O_{POM} 2×N_L	Ag–O_{POM}: 2.345(6); 2.579(6) Ag–N_L: 2.279(7); 2.326(8)		0D/3D	[310]
	2 (×2)	4/1×O_{POM} 2×N_L 1×$N_{L'}$	Ag–O_{POM}: 2.656(6) Ag–N_L: 2.241(6)–2.375(8)			
	3 (×2)	3; trigonal/2×N_L 1×$N_{L'}$	Ag–N_L: 2.263(7); 2.283(8)			
$\{Ag_3(2,2'\text{-bipy})_2(4,4'\text{-bipy})_2\}\{Ag(2,2'\text{-bipy})_2\}\{Ag(2,2'\text{-bipy})\}[AlW_{12}O_{40}]\cdot H_2O$	1 (×1)	6/4×O_{POM} 2×N_L	Ag–O_{POM}: 2.375(14)–2.866 Ag–N_L: 2.159(16)–2.373(18)		0D/3D	[311]
	2 (×1)	4; square planar/2×N_L 2×$N_{L'}$				
	3 (×2)	3; T-shaped/2×N_L 1×$N_{L'}$				
	4 (×1)	2; linear/1×N_L 1×$N_{L'}$				
$K_{16}[\{Ag(H_2As_2W_9O_{33})(H_2AsW_9O_{33})(Mo_3S_4\{H_2O\}_5)\}_2]\cdot 48H_2O$	1 (×2)	4/2×O_{POM} 1×$S_{\{MoS\}}$ 1×$S_{\{MoS\}'}$	Ag–O_{POM}: 2.220(13)–2.521(14) Ag–$S_{\{MoS\}}$: 2.463(5)–2.652(6)		0D/0D	[312]
$[Ag(phen)_2]_7[Ag\{Ag(phen)(VV_2W_{10}O_{40})\}_2]$	1 (×1)	8; square antiprism/4×O_{POM} 4×$O_{POM'}$	Ag–O_{POM}: 2.390–2.955	Ag 3···Ag 3 3.354–3.390	0D/2D	[313]
	2 (×2)	6/4×O_{POM} 2×N_L	Ag–N_L: 2.308–2.519			
	3 (×7)	4/2×N_L 2×$N_{L'}$				
$[Ag_3(bhepH)_6(\alpha\text{-}PW_{12}O_{40})(\alpha\text{-}Na_1PW_{11}O_{39})]\cdot 8H_2O$	1 (×1)	6; octahedral/1×O_{POM} 1×$O_{POM'}$ 1×O_L 1×N_L 1×$O_{L'}$ 1×$N_{L'}$	Ag–O_{POM}: 2.571(10) Ag–O_L: 2.633(10) Ag–N_L: 2.394(11)		0D/3D	[290]
	2 (×2)	5/1×O_{POM} 1×O_L 1×N_L 1×$O_{L'}$ 1×$N_{L'}$	Ag–O_{POM}: 2.552(9) Ag–O_L: 2.724 Ag–N_L: 2.3			
$Na_{19}[\{NaBi_2Ag_3(W_3O_{10})\}(BiW_9O_{33})_3]$	1 (×1)	8/3×O_{core} 2×O_{POM} 2×$O_{POM'}$ 1 × O_{H_2O}	Ag–O: 2.319(2)–2.59(2)		0D/0D	[314]
	2 (×1)	6/1×O_{core} 2×O_{POM} 2×$O_{POM'}$ 1 × O_{H_2O}				
	3 (×2)	5/1×O_{core} 2×O_{POM} 2×$O_{POM'}$				
$H_2Ag_{0.33}K_{3.67}[\alpha\text{-}AgPW_{11}O_{39}]\cdot 8.25H_2O\cdot CH_3OH$	1 (×1)	8; square antiprism/4×O_{POM} 4×$O_{POM'}$	Ag–O_{POM}: 2.39(2)–2.49(2) Ag–$O_{POM'}$: 2.56(2)–3.00(2)		1D/1D	[315]
$Na_8[\{Ag(4,4'\text{-bipy})\}_3(Ag_2PW_{10}O_{39})]\cdot 6H_2O$	1 (×2)	6; octahedral/5×O_{POM} 1× O_{apical}	Ag–O: 1.93(6)–2.59(4)		1D/3D	[316]
	2 (×1)	4; square planar/1×O_{POM} 1×$O_{POM'}$ 1×N_L 1×$N_{L'}$	Ag–$O_{POM\text{-terminal}}$: 2.792 Ag–N_L: 2.17(2)			
	3 (×2)	4/1×O_{POM} 1×$O_{POM\text{-long}}$ 1×N_L 1×$N_{L'}$	Ag–$O_{POM\text{-bridging}}$: 2.771 Ag–$O_{POM\text{-long}}$: 3.028(11) Ag–N_L: 2.180(18)			
$[\{Ag_2(bppy)_3\}\{Ag(bppy)_2\}\{Ag(bppy)\}_2(PW_{11}Co(bppy)O_{39})]\cdot 2H_2O$	1 (×2)	5; pyramidal/3×O_{POM} 1×$O_{POM\text{-long}}$ 1×N_L	Ag–O_{POM}: 2.337(8)–2.684(47) Ag–$O_{POM\text{-long}}$: 2.823(41); 3.015(34) Ag–N: 2.152(16)–2.181(13)		1D/3D	[317]
	2 (×3)	3; T-shaped/1×O_{POM} 1×N_L 1×$N_{L'}$	Ag–O_{POM}: 2.627(32)–2.665(38) Ag–N: 2.116(11)–2.227(12)			
$[\{Ag_3(H_2O)_2\}\{Ce_2(H_2O)_{12}\}H_5\{H_2W_{11}Ce(H_2O)_4O_{39}\}_2]\cdot 8H_2O$	1 (×1)	6/3×O_{POM} 3×$O_{POM'}$	Ag–O_{POM}: 2.362(13)–2.722(14)	Ag 2···Ag 2 2.365(13)	2D/3D	[318]
	2 (×2)	4/1×O_{POM} 1×$O_{POM'}$ 1×$O_{POM''}$ 1 × O_{H_2O}	Ag–O_{POM}: 2.472(13)–2.770(13) Ag–O_{H_2O} : 2.475(27)			
$[Ag(dafo)_2]_2[\{Ag(4,4'\text{-bipy})\}_2(\alpha\text{-}SiW_{12}O_{40})]$	1 (×2)	3; T-shaped/1×O_{POM} 1×N_L 1×$N_{L'}$	Ag–O_{POM}: 2.707(2)		2D/3D	[319]
	2 (×2)	4/2×N_L 2×$N_{L'}$	Ag–N: 2.147(1); 2.152(1)			
$[\{Ag(4,4'\text{-bipy})\}_3(HSiW_{12}O_{40})]\cdot(4,4'\text{-bipy})$	1 (×3)	4/1× O_{POM} 1×$O_{POM'}$ 1×N_L 1×$N_{L'}$	Ag–O_{POM}: 2.729–2.878 Ag–N: 2.144; 2.146		2D/3D	[320]

Table 3 (*Continued*)

Chemical formula	Type (multiplicity) of Ag centers	Coordination number; geometry/donor atoms$_{(\text{their -origin})}$	Bond length Ag–X (Å)	Ag···Ag distance (Å)	Topology: Ag–POM moiety/overall	Ref.
[{Ag_3(4,4′-bipy)$_2$(2,2′-bipy)$_2$}{Ag(2,2′-bipy)$_2$}{Ag(2,2′-bipy)(α-$HSiVW_{11}O_{40}$)}]	1 (×1)	4/2×O_{POM} 1×N_L 1×$N_{L'}$	Ag–$O_{POM\text{-long}}$: 2.844–2.976		2D/3D	[321]
	2 (×1)	4/1× $O_{POM\text{-long}}$ 1×$O_{POM'\text{-long}}$ 1×N_L 1×$N_{L'}$	Ag–N: 2.098(1)–2.383(2)			
	3 (×2)	4/1× $O_{POM\text{-long}}$ 2×N_L 1×$N_{L'}$				
	4 (×1)	4; square planar/2×N_L 2×$N_{L'}$				
$Na_4[Ag_6(nct)_4]H_2W_{12}O_{40}$	1 (×2)	5/1× O_{POM} 1×$O_{POM'\text{-long}}$ 1×O_L 1×$O_{L'}$ 1×$O_{L''}$	Ag–$O_{POM\text{-long}}$: 2.89(26)–2.96(20)	Ag 1···Ag 3 2.823(3)	2D/3D	[322]
	2 (×2)	4/1× $O_{POM\text{-long}}$ 1×$O_{POM'\text{-long}}$ 1×N_L 1×$N_{L'}$	Ag–O_L: 2.18(18)–2.22(16) Ag–N: 2.14(2)–2.15(2)			
	3 (×2)	4; tetrahedral/1×$O_{POM'\text{-long}}$ 1×O_L 1×$O_{L'}$ 1 × O_{H_2O}				
$[Ag(MeCN)_4]$ $[\{Ag(MeCN)_2\}_4(\alpha\text{-}H_3W_{12}O_{40})]$	1 (×4)	4/1×O_{POM} 1×$O_{POM'}$ 1×N_{MeCN} 1×$N_{MeCN'}$		Ag 1···Ag 1 2.9075(2)	3D/3D	[323]
	2 (×1)	4/1×N_{MeCN} 1×$N_{MeCN'}$ 1×$N_{MeCN''}$ 1×$N_{MeCN'''}$				
$[Ag_3(pz)_3(PW_{12}O_{40})]\cdot 0.5H_2O$	1 (×2)	6; octahedral/2×O_{POM} 2×$O_{POM'}$ 1×N_L 1×$N_{L'}$	Ag–O_{POM}: 3.011(14)–3.073(15) Ag–N: 2.158(18)		3D/3D	[324]
	2 (×1)	4; tetrahedral/1×O_{POM} 1×$O_{POM'}$ 1×N_L 1×$N_{L'}$	Ag–O_{POM}: 2.868(15) Ag–N: 2.161(18)			
[Ag(4,4′-bipy)](OH)[{Ag(4,4′-bipy)}$_2$($AgPW_{12}O_{40}$)]·3.5H_2O	1 (×1)	6; octahedral/2×O_{POM} 2×$O_{POM'}$ 1× $O_{POM\text{-long}}$ 1×$O_{POM'\text{-long}}$	Ag–O_{POM}: 2.446(8)–2.532(9) Ag–$O_{POM\text{-long}}$: 2.805	Ag 2···Ag 3 3.534	3D/3D	[325]
	2 (×1)	3; T-shaped/1×O_{POM} 1×N_L 1×$N_{L'}$	Ag–O_{POM}: 2.638 Ag–N: 2.143(7); 2.161(7)			
	3 (×1)	2; linear/1×N_L 1×$N_{L'}$	Ag–N_L: 2.131(7)			
[{Ag(4,4′-bipy)}$_2$($P_2W_{18}O_{62}$)]·2H_2bipy·4H_2O	1 (×2)	4/1×O_{POM} 1×$O_{POM'}$ 1×N_L 1×$N_{L'}$	Ag–O_{POM}: 2.841 Ag–N: 2.134–2.138		2D/3D	[326]
[{Ag(4,4′-bipy)}$_4$($P_2W_{18}O_{62}$)]·2Hbipy	1 (×1)	5; pyramidal/2×O_{POM} 1×$O_{POM'}$ 1×N_L1×$N_{L'}$	Ag–O_{POM}: 2.552–2.828 Ag–N: 2.134–2.138		2D/3D	
	2 (×2)	4; seesaw/1×O_{POM} 1×$O_{POM'}$ 1×N_L 1×$N_{L'}$				
	3 (×1)	3; T-shaped/1×O_{POM} 1×N_L 1×$N_{L'}$				
[{Ag(4,4′-bipy)}$_2${Ag(4,4′-bipy)(Hbipy)}($P_2W_{18}O_{62}$)]·H_2bipy	1 (×2)	4; seesaw/1×O_{POM} 1×$O_{POM'}$ 1×N_L 1×$N_{L'}$	Ag–O_{POM}: 2.508(10)–2.798(11)		2D/3D	[327]
	2 (×1)	4; square planar/1×O_{POM} 1×$O_{POM'}$ 1×N_L 1×$N_{L'}$	Ag–N: 2.151(13)–2.271(16)			
[{$Ag(H_2O)$(phnz)}{Ag(phnz)}$_5$($P_2W_{18}O_{62}$)]·(phnz)$_{0.5}$·4H_2O	1 (×2)	4/1×O_{POM} 1×$O_{POM'}$ 1×N_L 1×$N_{L'}$	Ag–O_{POM}: 2.268(14)–2.345(17) Ag–N: 2.24(7)–2.575(2)		3D/3D	[328]
	2 (×1)	4/1×O_{POM} 1 × O_{H_2O} 1×N_L 1×$N_{L'}$	Ag–O_{POM}: 2.318(17) Ag–N: 2.28(3)			
	3 (×1)	3; trigonal/1×O_{POM} 1×$O_{POM'}$ 1×$N_{L'}$	Ag–O_{POM}: 2.355(17) Ag–N: 2.14(4)			
	4 (×2)	3; T-shaped/1×O_{POM} 1×N_L 1×$N_{L'}$	Ag–O_{POM}: 2.672(2) Ag–N: 2.190			

bipy = bipyridine; bhep = N,N′-bis(2-hydroxyethyl)piperazine; bppy = 5-(4-bromophenyl)-2-(4-pyridinyl)pyridine; dafo = 4,5-diazafluoren-9-one; nct = nicotinate; pz = pyrazine; phnz = phenazine; Keggin structure $[XW_{12}O_{40}]^{n-}$.

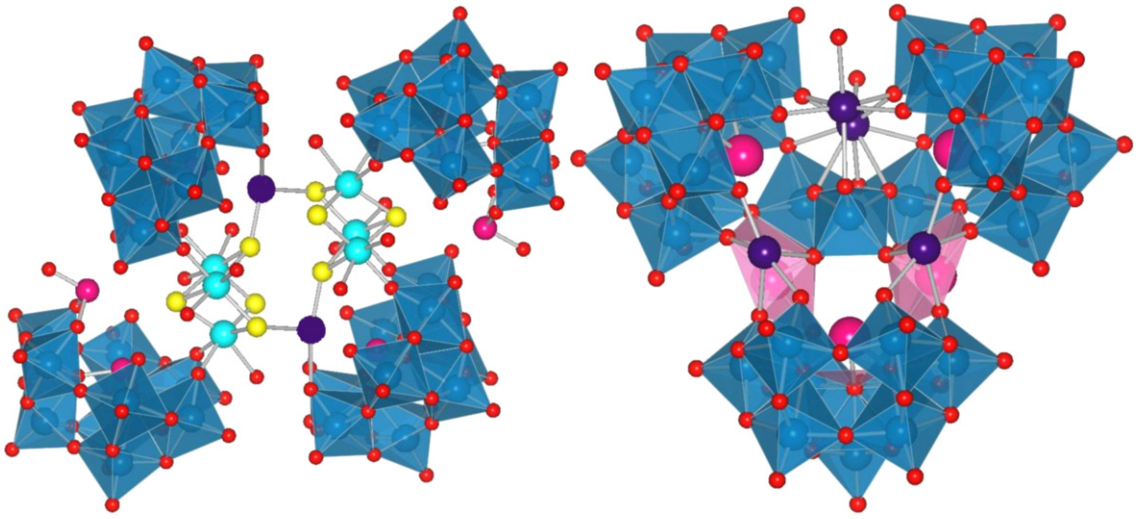

Fig. 63. Dimer of $[\{Ag(H_2As_2W_9O_{33})(H_2AsW_9O_{33})(Mo_3S_4\{H_2O\}_5)\}_2]^{16+}$ (left, Ref. [312]) and trimer of $Na_{19}[\{NaBi_2Ag_3(W_3O_{10})\}(BiW_9O_{33})_3]$ (right, Ref. [314]). Mo = light blue.

the POM, with occupancy factors 0.42, 0.15 and 0.42 and interacts with the lone-pair of the central As(III) atoms, as shown by a short Ag···As distance of 2.727(4)–2.770(5) Å [312].

The connection between two clusters in $\{Ag(phen)_2\}_7[Ag\{Ag(phen)(VV_2W_{10}O_{40})\}_2]$ is made by a single Ag^+ cation coordinating 8 oxygen atoms in a square antiprism geometry. The vanadium-centered tungstovanadate units are additionally decorated with one $[Ag(phen)]^+$ group. Seven $[Ag(phen)_2]^+$ complex cations help to develop a 2D connectivity by means of hydrogen bonds and π–π interactions [313]. $[Ag_3(bhepH)_6(\alpha\text{-}PW_{12}O_{40})(\alpha\text{-}NaPW_{11}O_{39})]\cdot 8H_2O$ is another example of dimeric structure. Two POM units are again joined by one Ag ion bound to their terminal oxygen atoms (only one from each unit) but in this case two single-protonated bhep ligands in bidentate mode complete the octahedral arrangement around silver. This species is also decorated with two non-bridging $[Ag(bhepH)_2]^{3+}$ groups [290].

$Na_{19}[\{NaBi_2Ag_3(W_3O_{10})\}(BiW_9O_{33})_3]$ is an example of a all-inorganic discreet trimeric structure. Three lacunary β-B-Keggin units are joined by a mixed Ag–Bi–W–O core (see Fig. 63, on the right) [314].

Ag cations occupying the lacuna of α-Keggin unit are the unique feature of $H_2Ag_{0.33}K_{3.67}[\alpha\text{-}AgPW_{11}O_{39}]\cdot 8.25H_2O\cdot CH_3OH$. Each silver is raised above the plane of four terminal oxygen atoms of the lacuna by ca. 1.2 Å. During crystallization the clusters organize in a head-to-tail manner and Ag bonds to 4 bridging oxygen atoms of adjacent POM. Four $Ag–O_{terminal}$ and four longer (ca. 2.5–3.0 Å) and therefore weaker $Ag–O_{bridging}$ bonds are arranged in a square antiprismatic manner. A weak 1D inorganic anionic chain is created by this way, see Fig. 64. Moreover, MAS ^{31}P NMR studies evidence that mechanical grinding reverses the self-assembly process and the spectra show the presence of independent anions in the structure [315].

In $Na_8[\{Ag(4,4'\text{-bipy})\}_3(Ag_2PW_{10}O_{39})]\cdot 6H_2O$ each divacant Keggin unit is substituted with two Ag^+ cations in octahedral coordination of 5 oxygen atoms from the lacuna and one apical O which is shared with another cluster. A 1D chain of polyoxometalates is then formed by this way. These chains are linked into a 3D network by means of $[Ag(4,4'\text{-bipy})]^+$ units [316].

The tungstophosphate unit in $[\{Ag_2(bppy)_3\}\{Ag(bppy)_2\}\{Ag(bppy)\}_2(PW_{11}Co(bppy)O_{39})]\cdot 2H_2O$ contains one Co(II) replacing one W=O group and coordinated to one terminal nitrogen of the bppy ligand. There are 5 silver species attached to each POM: 2 $[Ag(bppy)]^+$ groups via 3 $Ag–O_{bridging}$ bonds each, one $[Ag(bppy)_2]^+$ via sole $Ag–O_{terminal}$ bond and one $[Ag_2(bppy)_3]^{2+}$ again via sole $Ag–O_{terminal}$ bond. $[Ag_2(bppy)_3]^{2+}$ and $[Ag(bppy)_2]^+$ groups that belong to adjacent clusters share one bppy ligand providing connection into 1D chains. Double-strand ladder structure holds on Ag–Br interactions between parallel chains with Ag···Br = 3.179(51) Å, less than the sum of the van der Waals radii of Ag and Br (1.72 and 1.85 Å, respectively) [317].

In $[\{Ag_3(H_2O)_2\}\{Ce_2(H_2O)_{12}\}H_5\{H_2W_{11}Ce(H_2O)_4O_{39}\}_2]\cdot 8H_2O$ the overall purely inorganic 3D network results from combined effects of Ag– and Ce-based connectivity. Here, the α-metatungstate $[H_2W_{11}Ce(H_2O)_4O_{39}]^{7-}$ linked to a total number of 8 metal atoms (4 Ag and 4 Ce) is a basic building block. 2 units dimerize when Ce(1) centers form bonds with terminal oxygens of adjacent clusters. Chains of dimers are formed via 3 + 3 Ag–O bonds when one Ag(1) cation is sandwiched between dimers. Parallel chains are linked by Ce(2) cations into 2D sheets and sheets connect further through short Ag(2)–Ag(2) (Ag···Ag = 2.365 Å) bridges, with Ag(2) centers anchored on three clusters each, see Fig. 65 [318].

In $\{Ag(dafo)_2\}_2[\{Ag(4,4'\text{-bipy})\}_2(\alpha\text{-}SiW_{12}O_{40})]$ the disordered α-Keggin polyanion is coordinated to two Ag^+ ions from two parallel Ag–bipy chains by its terminal oxygens. Thus, the silver centers exhibit a T-shape coordination mode. Such double-stranded ladder structures are connected with each other via π–π stacking of the

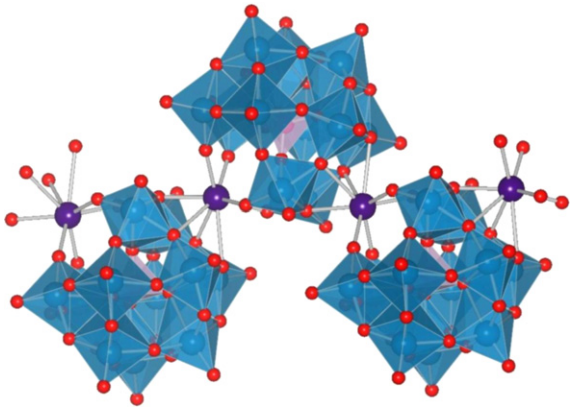

Fig. 64. Weak Ag–O interaction based chain of $H_2Ag_{0.33}K_{3.67}[\alpha\text{-}AgPW_{11}O_{39}]\cdot 8.25H_2O\cdot CH_3OH$ (Ref. [315]).

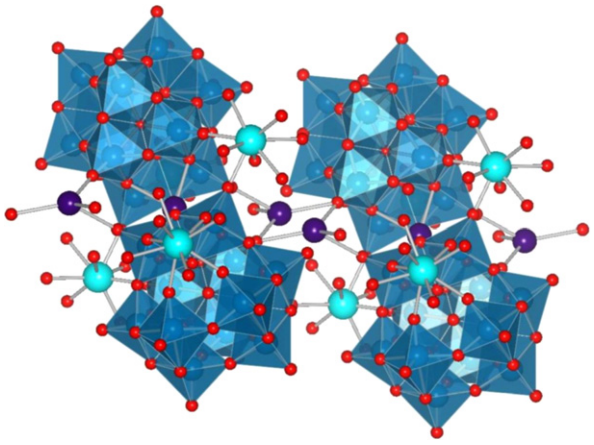

Fig. 65. Silver and cerium bridges in $[\{Ag_3(H_2O)_2\}\{Ce_2(H_2O)_{12}\}H_5\{H_2W_{11}Ce(H_2O)_4O_{39}\}_2]\cdot 8H_2O$ (Ref. [318]). Ce = light blue.

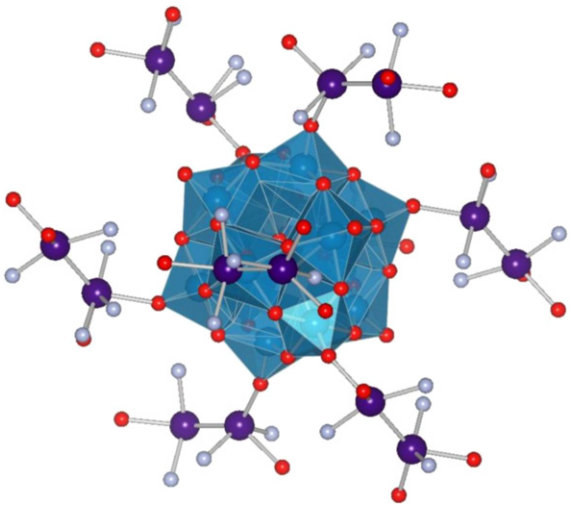

Fig. 66. $[Ag–Ag]^{2+}$ bridges coordinated to $[\alpha\text{-}H_3W_{12}O_{40}]^{5-}$ Keggin cluster. MeCN molecules reduced to their nitrogen atoms for clarity (Ref. [323]).

bipy aromatic rings. The $[Ag(dafo)_2]^+$ cations inserted between the so-created layers counterbalance their negative charge [319].

The overall 3D architecture of $[\{Ag(4,4'\text{-bipy})\}_3(HSiW_{12}O_{40})]\cdot(4,4'\text{-bipy})$ and of its germanotungstate isomorph is made of 2D Ag–POM layers and 1D Ag–bipy chains. In similar synthetic conditions, reaction with $H_4SiMo_{12}O_{40}$ resulted rather in Ag_2O deposition than incorporation of silver cations into the structure, due to the higher oxidizing ability of Mo-based polyanions compared to W-based ones [320].

From obvious reasons the use of 4,4′-bipy as a ligand favours the creation of infinite structures while use of the chelating 2,2′-bipy leads to more confined ones. Combining these two compounds together resulted in intermediate compounds such as $[\{Ag_3(4,4'\text{-bipy})_2(2,2'\text{-bipy})_2\}\{Ag(2,2'\text{-bipy})_2\}\{Ag(2,2'\text{-bipy})(\alpha\text{-}HSiVW_{11}O_{40})\}]$ and its isomorph $[\{Ag_3(4,4'\text{-bipy})_2(2,2'\text{-bipy})_2\}\{Ag(2,2'\text{-bipy})_2\}\{Ag(2,2'\text{-bipy})(\alpha\text{-}PVW_{11}O_{40})\}]$. These layered species are made of $[Ag_3(4,4'\text{-bipy})_2]^+$ chains, capped at the ends by 2,2′-bipy and thus restricted from further growth, that are connected to 4 POM clusters by means of long (>2.8 Å) and weak Ag–O bonds. In addition, the POM-supported $[Ag(2,2'\text{-bipy})]^+$ group and the $[Ag(2,2'\text{-bipy})_2]^+$ cation participate in extensive π–π bonding between 2D sheets [321].

The metatungstate Keggin units can coordinate up to 10 silver cations – which is the highest number reported so far, like for $Na_4[Ag_6(nct)_4]H_2W_{12}O_{40}$ [322]. Organometallic chains hold together on argentophilic interactions, weak Ag–O bonds and π–π stacking and are clipped by polyanions into 3D framework.

$\{Ag(MeCN)_4\}[\{Ag(MeCN)_2\}_4(\alpha\text{-}H_3W_{12}O_{40})]$ is a 3D network in which no organic linkers are present. The connection between metatungstate clusters is realized only by means of $[Ag–Ag]^{2+}$ bridges with argentophilic attractive interaction (Ag···Ag = 2.9075(2) Å). Each cluster coordinates 8 silver centers through its terminal oxygens, see Fig. 66. Each silver bridge links four different POMs. Two MeCN molecules per Ag are coordinated in a terminal mode and are distorted over two positions [323].

In the structure of $[Ag_3(pz)_3(PW_{12}O_{40})]\cdot 0.5H_2O$ the POM-based linking of the Ag–organic chains leads to a 3D architecture. Each polyanion is linked via its terminal oxygen atoms to 6 silver ions from 6 $[Ag(pz)]_n^{n+}$ chains. In this compound the silver atoms exhibit both tetrahedral and octahedral geometries [324].

$\{Ag(4,4'\text{-bipy})\}(OH)[\{Ag(4,4'\text{-bipy})\}_2\{AgPW_{12}O_{40}\}]\cdot 3.5H_2O$ combines already described structural features in a novel way. Two types of 1D chains, one inorganic, with one Ag ion sandwiched between two POMs and one of a mixed type (Ag–bipy) intertwine and are connected via Ag–O bonds to form arrays. The Ag(1) atom linking Keggin clusters is in a distorted octahedral geometry (when taking into account 4 $Ag–O_{bridging}$ and also two long and weak $Ag–O_{terminal}$ bonds), whereas the Ag(2) atom is in a T-shape coordination. The 3D structure is further reinforced by π–π stacking of the bipy aromatic rings and exhibits elliptic channels in which cationic $[Ag(4,4'\text{-bipy})]^+$ chains are embedded [325].

8.3.1. Wells-Dawson structure $[X_2W_{18}O_{62}]^{n-}$

Wells-Dawson-based architectures are obtained by hydrothermal syntheses from salts of the polyanion, Na_2WO_4, H_3PO_4, $AgNO_3$ and organic ligands. The influence of the synthesis pH on the structure of the final product can be illustrated by the two compounds: $[\{Ag(4,4'\text{-bipy})\}_2(P_2W_{18}O_{62})]\cdot 2(4,4'\text{-}H_2bipy)\cdot 4H_2O$ and $[\{Ag(4,4'\text{-bipy})\}_4(P_2W_{18}O_{62})]\cdot 2(4,4'\text{-Hbipy})$. In otherwise identical conditions the former is obtained at pH = 2.5, while the latter forms at pH = 3.5. These two compounds contain 2D silver–POM layers and Ag–bipy chains, that combine into overall 3D structures, but the more silver cations present the more sophisticated architecture becomes [326]. By varying the molar ratios of reagents and the pH new species from the same family such as $[\{Ag(4,4'\text{-bipy})\}_2\{Ag(4,4'\text{-bipy})(4,4'\text{-Hbipy})\}(P_2W_{18}O_{62})]\cdot(4,4'\text{-}H_2bipy)$ [327], $[\{Ag(4,4'\text{-bipy})\}_4(4,4'\text{-}H_2bipy)(P_2W_{18}O_{62})]\cdot 4H_2O$ and $[\{Ag(4,4'\text{-bipy})\}_4(H_2P_2W_{18}O_{62})]\cdot 7H_2O$ [316] can be obtained.

In $[\{Ag(H_2O)(phnz)\}\{Ag(phnz)\}_5(P_2W_{18}O_{62})]\cdot 0.5(phnz)\cdot 4H_2O$ each Dawson unit is surrounded be 9 Ag atoms – the highest number found to date – that display 4 different coordination modes. The connectivity into the 3D network is realized through linkage of POM–Ag–phnz layers and Ag–phnz chains [328].

8.3.2. Other polytungstates

$[As_4W_{40}O_{140}]^{28-}$ is made of four α-B-AsW_9O_{33} Keggin units that are joined by 4 WO_6 octahedra. Each octahedron shares its two *cis* oxygen atoms with two adjacent AsWO units. In the cavity of this macrocycle structure there are five possible coordination sites available of two distinct types called S1 and S2. S1 is made of 8 oxygen atoms belonging to WO_6 octahedra, while 4 equivalent S2 sites involve oxygen atoms from octahedra as well as AsWO subunits (2 + 2 mode). The S1 "cryptate" site is preferentially occupied by alkaline or alkaline-earth cations, like in $[KAs_4W_{40}O_{140}]^{27-}$. Ag^+ is able to substitute Na^+ in this site, although it is replaced by K^+ or Ba^{2+}. The S2 sites could be occupied by 4 Ag^+ cations exclusively or in combination (2 + 2) with ions of the first transition series (Mn^{2+}, Co^{2+}, Ni^{2+}, Cu^{2+}, Zn^{2+}). It was shown that the Ag^+ ions do not

substitute the Co^{2+} ones:

$$2\,Ag^{+} + [KAs_4W_{40}O_{140}Co_2]^{23-} \rightarrow [KAs_4W_{40}O_{140}Co_2Ag_2]^{21-}$$

but Co^{2+} will substitute Ag^{+} according to the reaction:

$$2\,Co^{2+} + [KAs_4W_{40}O_{140}\,Ag_4]^{23-} \rightarrow [KAs_4W_{40}O_{140}Co_2Ag_2]^{21-} + 2\,Ag^{+}$$

This preferential binding is a result of major changes of the S2 sites geometry upon incorporating the first Co^{2+} cation (inorganic allosteric effect), while coordination of Ag^{+} alone does not modify it strongly.

$[KAs_4W_{40}O_{140}]^{27-}$ reacts with tungstate and vanadate ions at pH < 3 leading to the synthesis of $[KAs_4W_{42}O_{144}]^{23-}$ and $[KAs_4V_2W_{40}O_{144}]^{25-}$ which can also form the $[KAs_4W_{42}O_{144}Ag_2]^{21-}$ and $[KAs_4V_2W_{40}O_{144}Ag_2]^{23-}$ complexes with silver [329,330].

8.4. Applications in catalysis

Synergistic effects between Ag^{I} and V^{V} – both redox active species – have been postulated to be responsible for the catalytic activity of Ag–(vanadium heterogenized) polymolybdate systems. For example $Ag_{10.4}P_2V_4Mo_{20}O_{80}(NO_3)_{0.4}\cdot(MeCN)_{17.3}\cdot(H_2O)_{1.5}$ can catalyze the selective O_2 sulfoxidation of 2-chloroethyl ethyl sulfide (CEES) to a far less toxic sulfoxide (CEESO) in the ambient environment (room temperature and 1.0 atm of air). The studies indicated that the catalytic cycle involves the reduction of the d^0 V(V) center, followed by a reoxidation process, as for other thioether oxidations catalyzed by vanadium-containing POMs. Far less labile polytungstates such as the corresponding analogue $Ag_5PV_2W_{10}O_{40}$ and the Wells-Dawson complex $Ag_9P_2V_3W_{15}O_{62}$, are both inactive under ambient conditions [298].

Preliminary results on the use of $[Ag_6(PV_2Mo_{10}O_{40})](CH_3COO)\cdot 8H_2O$ in the oxidation of *p*-methoxytoluene by air were rather promising compared to those achieved with $H_5[PV_2Mo_{10}O_{40}]\cdot 23H_2O$. The replacement of the counterions H^{+} by Ag^{+} increased noticeably the yield to oxidation products from 4.3% to 11.4% due to an enhancement in selectivity, despite a decrease of the conversion [305].

Various Ag-containing POMs with the 4,4′-bipy or 2,2′-bipy ligands ($[Ag_3(2,2'\text{-bipy})_4(\alpha\text{-}PMo_{12}O_{40})]\cdot 2H_2O$, $[\{Ag(2,2'\text{-bipy})\}_2\{Ag_4(2,2'\text{-bipy})_6\}\alpha\text{-}PVMo_{11}O_{40}]$, $[\{Ag(2,2'\text{-bipy})\}_2\alpha\text{-}PVMo_{11}O_{40}]$ [302], $[\{Ag(4,4'\text{-bipy})\}_3(HSiW_{12}O_{40})]\cdot(4,4'\text{-bipy})$ [320] and $[\{Ag(4,4'\text{-bipy})\}_2\{Ag(4,4'\text{-bipy})(Hbipy)\}(P_2W_{18}O_{62})]\cdot H_2bipy$ [327]) were used to fabricate modified carbon paste electrodes (CPE) and were tested in the electrochemical reduction of nitrite (to ammonia) and bromate in acidic solutions.

9. Polyoxometalates containing gold

Up to now there are only two reports of polyoxometalates with gold [331]. Quite the same strategy that for the Pd and Pt compounds [284,238] was used to obtain $[Au(O)(OH_2)(A\text{-}PW_9O_{34})_2]^{17-}$ (**1**) and $[Au(O)(OH_2)P_2W_{20}O_{70}(OH_2)_2]^{9-}$ (**2**) from aqueous solutions of $AuCl_3$ and salts of polytungstates. In the case of (**1**), the polytungstate ligand had to be prepared *in situ* due to its instability in low pH solutions. The two complexes were characterized by various physico-chemical methods such as multinuclear NMR, X-ray and neutron diffraction, optical spectroscopy, X-ray absorption spectroscopy. They were evidenced to contain Au(III) centers in an octahedral coordination formed by 4 oxygen atoms of the polytungstate units in an equatorial plane, one terminal oxo ligand and one water molecule in *trans* conformation. The oxo moieties are situated outwards the inter-cluster areas. The Au–O_{oxo} multiple bond of 1.763(17) Å. was reported as the shortest gold–oxygen bond in the literature. The polyanionic lacunary Keggin unit in (**1**) is disorder-free whereas (**2**) shows some disorder (crystallographically imposed D_{3h} symmetry instead of the expected C_{2v} group) which has already been observed for the isostructural all-tungsten complex $[P_2W_{21}O_{71}(OH_2)_3]^{6-}$. (**2**) can stoichiometrically transfer the oxo ligand to PPh_3, creating triphenylphosphine oxide $PPh_3{=}O$, with concomitant reduction of Au(III) to Au(I). Attempts to model the ^{17}O and ^{183}W NMR spectra of this compound by means of relativistic DFT calculations did not provide conclusive evidence for or against the proposed structural model [255].

10. Conclusion

This review has shown that the number of compounds which can be prepared from a noble metal and a polyoxometalate is very high with a great variety of structures and applications. When looking at their repartition as a function of the noble metal it is evident that there is a discrepancy between some metals for which there are numerous reports (typically ruthenium and silver) and gold and osmium for which there are only few reports. However a simple survey of the literature data shows that the use of gold in catalysis is actually exploding and one can think that a lot of papers on the synthesis and characterization of polyoxometalates containing this metal should appear in the future.

An other comment when looking at the literature about these species is that there are sometimes controversies (for example in the case of di-ruthenium complexes or high valent oxo compounds of Pd, Pt and Au). These controversies are probably related to slight differences in the experimental methods. This shows that precise descriptions of the synthesis conditions are required for the preparations of these complexes and a simple survey of the literature published during the course of the redaction of this review shows that there are numerous structures which can be synthesized.

From the point of view of the catalytic applications of these compounds, it is clear that most of the reactions catalyzed by noble metal complexes which could be made by replacing one or more ligands by polyoxometalates. This could lead to unexpected activities and/or selectivities.

Finally, a new field in this domain has recently be opened by Kortz et al. who synthesized oxo clusters of noble metals without vanadium, tungsten or molybdenum. Some typical examples are $[Au^{III}{}_4As^{V}{}_4O_{20}]^{8-}$ [332] or $[Pd_{13}(As^{V}Ph)_8O_{32}]^{6-}$ [333]. Such systems could also be very useful not only in catalysis but also for fundamental studies on nanoparticles of oxides.

References

[1] J.J. Berzelius, Poggendorffs Ann. Phys. Chem. 6 (1826) 369.
[2] J.F. Keggin, Nature 131 (1933) 908.
[3] B.L.W.J.T. Conley III, K.J.H. Young, S.K. Ganesh, S.K. Meier, V.R. Ziatdinov, O. Mironov, J. Oxgaard, J.W.A.G. Gonzales III, R.A. Periana, J. Mol. Catal. A: Chem. 251 (2006) 8.
[4] E. Coronado, C. Gimenez-Saiz, C.J. Gomez-Garcia, Coord. Chem. Rev. 249 (2005) 1776.
[5] E. Coronado, C.J. Gomez-Garcia, Chem. Rev. 98 (1998) 273.
[6] P. Gouzerh, A. Proust, Chem. Rev. 98 (1998) 77.
[7] Z. Helwani, M.R. Othman, N. Aziz, J. Kim, W.J.N. Fernando, Appl. Catal. A: Gen. 363 (2009) 1.
[8] C.L. Hill, J. Mol. Catal. A: Chem. 262 (2007) 2.
[9] B. Keita, L. Nadjo, J. Mol. Catal. A: Chem. 262 (2007) 190.
[10] I.V. Kozhevnikov, Chem. Rev. 98 (1998) 171.
[11] I.V. Kozhevnikov, J. Mol. Catal. A: Chem. 305 (2009) 104.
[12] M. Misono, Catal. Rev. Sci. Eng. 29 (1987) 269.
[13] M. Misono, Chem. Commun. (2001) 1141.
[14] M. Misono, Catal. Today 144 (2009) 285.
[15] N. Mizuno, M. Misono, Chem. Rev. 98 (1998) 199.
[16] N. Mizuno, S. Uchida, Chem. Lett. 35 (2006) 688.
[17] J.T. Rhule, C.L. Hill, D.A. Judd, R.F. Schinazi, Chem. Rev. 98 (1998) 327.
[18] M.N. Timofeeva, Appl. Catal. A: Gen. 256 (2003) 19.
[19] T. Yamase, Chem. Rev. 98 (1998) 307.
[20] N. Essayem, Y. Ben Taârit, C. Feche, P.Y. Gayraud, G. Sapaly, C. Naccache, J. Catal. 219 (2003) 97.

[21] A.V. Ivanov, T.V. Vasina, V.D. Nissenbaum, L.M. Kustov, M.N. Timofeeva, J.I. Houzvicka, Appl. Catal. A: Gen. 259 (2004) 65.
[22] W. Kuang, A. Rives, B.O.B. Tayeb, M. Fournier, R. Hubaut, J. Colloid Interface Sci. 248 (2002) 123.
[23] A. Oulmekki, F. Lefebvre, React. Kinet. Catal. Lett. 48 (1992) 607.
[24] A. Oulmekki, F. Lefebvre, React. Kinet. Catal. Lett. 48 (1992) 601.
[25] A. Oulmekki, F. Lefebvre, React. Kinet. Catal. Lett. 48 (1992) 593.
[26] J.R. Satam, R.V. Jayaram, Catal. Commun. 9 (2008) 2365.
[27] N. Seifi, M.H. Zahedi-Niaki, M.R. Barzegari, A. Davoodnia, R. Zhiani, A.A. Kaju, J. Mol. Catal. A: Chem. 260 (2006) 77.
[28] K.A. da Silva, P.A. Robles-Dutenhefner, E.M.B. Sousa, E.F. Kozhevnikova, I.V. Kozhevnikov, E.V. Gusevskaya, Catal. Commun. 5 (2004) 425.
[29] K. Srilatha, N. Lingaiah, B.L.A.P. Devi, R.B.N. Prasad, S. Venkateswar, P.S.S. Prasad, Appl. Catal. A: Gen. 365 (2009) 28.
[30] G.-W. Wang, Y.-B. Shen, X.-L. Wu, L. Wang, Tetrahedron Lett. 49 (2008) 5090.
[31] G.D. Yadav, G. George, Catal. Today 141 (2009) 130.
[32] A.C. Estrada, M.M.Q. Simões, I.C.M.S. Santos, M.G.P.M.S. Neves, A.M.S. Silva, J.A.S. Cavaleiro, A.M.V. Cavaleiro, Appl. Catal. A: Gen. 366 (2009) 275.
[33] Y. Matsumoto, M. Asami, M. Hashimoto, M. Misono, J. Mol. Catal. A: Chem. 114 (1996) 161.
[34] V. Mirkhani, M. Moghadam, S. Tangestaninejad, I. Mohammadpoor-Baltork, N. Rasouli, Catal. Commun. 9 (2008) 2171.
[35] N. Mizuno, C. Nozaki, T.-O. Hirose, M. Tateishi, M. Iwamoto, J. Mol. Catal. A: Chem. 117 (1997) 159.
[36] R. Neumann, A.M. Khenkin, Chem. Commun. (2006) 2529.
[37] I.C.M.S. Santos, J.A.F. Gamelas, M.S.S. Balula, M.M.Q. Simoes, M.G.P.M.S. Neves, J.A.S. Cavaleiro, A.M.V. Cavaleiro, J. Mol. Catal. A: Chem. 262 (2007) 41.
[38] S. Shinachi, M. Matsushita, K. Yamaguchi, N. Mizuno, J. Catal. 233 (2005) 81.
[39] D. Attanasio, F. Bachechi, L. Suber, J. Chem. Soc. Dalton Trans. (1993) 2373.
[40] G. Süss-Fink, L. Plasseraud, V. Ferrand, S. Stanislas, A. Neels, H. Stoeckli-Evans, M. Henry, G. Laurenczy, R. Roulet, Polyhedron 17 (1998) 2817.
[41] K. Momma, F. Izumi, J. Appl. Cryst. 41 (2008) 653.
[42] L. Bi, S.S. Mal, N.H. Nsouli, M.H. Dickman, U. Kortz, S. Nellutla, N.S. Dalal, M. Prinz, G. Hofmann, M. Neumann, J. Cluster Sci. 19 (2008) 259.
[43] D. Laurencin, R. Thouvenot, K. Boubekeur, A. Proust, J. Chem. Soc. Dalton Trans. (2007) 1334.
[44] G. SüssFink, L. Plasseraud, V. Ferrand, H. StoeckliEvans, Chem. Commun. (1997) 1657.
[45] V. Artero, A. Proust, P. Herson, R. Thouvenot, P. Gouzerh, Chem. Commun. (2000) 883.
[46] V. Artero, A. Proust, P. Herson, P. Gouzerh, Chem. Eur. J. 7 (2001) 3901.
[47] D. Laurencin, E.G. Fidalgo, R. Villanneau, F. Villain, P. Herson, J. Pacifico, H. Stoeckli-Evans, M. Benard, M.-M. Rohmer, G. Süss-Fink, A. Proust, Chem. Eur. J. 10 (2004) 208.
[48] D. Laurencin, R. Thouvenot, K. Boubekeur, F. Villain, R. Villanneau, M.M. Rohmer, M. Benard, A. Proust, Organometallics 28 (2009) 3140.
[49] D. Laurencin, R. Villanneau, A. Proust, A. Brethon, I.W.C.E. Arends, R.A. Sheldon, Tetrahedron 18 (2007) 367.
[50] L. Plasseraud, H. Stoeckli-Evans, G. Süss-Fink, Inorg. Chem. Commun. 2 (1999) 344.
[51] R. Villanneau, V. Artero, D. Laurencin, P. Herson, A. Proust, P. Gouzerh, J. Mol. Struct. 656 (2003) 67.
[52] M. Bonchio, G. Scorrano, P. Toniolo, A. Proust, V. Artero, V. Conte, Adv. Synth. Catal. 344 (2002) 841.
[53] R. Neumann, M. Dahan, J. Chem. Soc. Chem. Commun. (1995) 171.
[54] R. Neumann, M. Dahan, Polyhedron 17 (1998) 3557.
[55] K. Nomiya, H. Torii, K. Nomura, Y. Sato, J. Chem. Soc. Dalton Trans. (2001) 1506.
[56] A.M. Khenkin, L.J.W. Shimon, R. Neumann, Inorg. Chem. 42 (2003) 3331.
[57] V.W. Day, T.A. Eberspacher, W.G. Klemperer, R.P. Planalp, P.W. Schiller, A. Yagasaki, B. Zhong, Inorg. Chem. 32 (1993) 1629.
[58] W.G. Klemperer, B. Zhong, Inorg. Chem. 32 (1993) 5821.
[59] C. Rong, M.T. Pope, J. Am. Chem. Soc. 114 (1992) 2932.
[60] X.R. Lin, J.Y. Xu, H.Z. Liu, B. Yue, S.L. Jin, G.Y. Xie, J. Mol. Catal. A Chem. 161 (2000) 163.
[61] J.C. Bart, F.C. Anson, J. Electroanal. Chem. 390 (1995) 11.
[62] M. Bressan, A. Morvillo, G. Romanello, J. Mol. Catal. 77 (1992) 283.
[63] M.S.S. Balula, I. Santos, J.A.F. Gamelas, A.M.V. Cavaleiro, N. Binsted, W. Schlindwein, Eur. J. Inorg. Chem. (2007) 1027.
[64] L.I. Kuznetsova, V.A. Likholobov, L.G. Detusheva, Kinet. Catal. 34 (1993) 914.
[65] L.I. Kuznetsova, L.G. Detusheva, N.I. Kuznetsova, M.A. Fedotov, V.A. Likholobov, J. Mol. Catal. A Chem. 117 (1997) 389.
[66] P. Shringarpure, A. Patel, Inorg. Chim. Acta 362 (2009) 3796.
[67] C. Besson, S.W. Chen, R. Villanneau, G. Izzet, A. Proust, Inorg. Chem. Commun. 12 (2009) 1038.
[68] A. Bagno, M. Bonchio, A. Sartorel, G. Scorrano, Eur. J. Inorg. Chem. (2000) 17.
[69] M. Bonchio, M. Carraro, A. Sartorel, G. Scorrano, U. Kortz, J. Mol. Catal. A: Chem. 251 (2006) 93.
[70] A. Bagno, M. Bonchio, Eur. J. Inorg. Chem. (2002) 1475.
[71] A. Bagno, M. Bonchio, Magn. Res. Chem. 42 (2004) S79.
[72] A. Bagno, M. Bonchio, A. Sartorel, G. Scorrano, ChemPhysChem 4 (2003) 517.
[73] D. Laurencin, R. Villanneau, H. Gérard, A. Proust, J. Phys. Chem. A 110 (2006) 6345.
[74] C.C. Rong, H. So, M.T. Pope, Eur. J. Inorg. Chem. (2009) 5211.
[75] V. Artero, D. Laurencin, R. Villanneau, R. Thouvenot, P. Herson, P. Gouzerh, A. Proust, Inorg. Chem. 44 (2005) 2826.
[76] K. Nomiya, K. Hayashi, Y. Kasahara, T. Iida, Y. Nagaoka, H. Yamamoto, T. Ueno, Y. Sakai, Bull. Chem. Soc. Jpn. 80 (2007) 724.
[77] V. Lahootun, C. Besson, R. Villanneau, F. Villain, L.-M. Chamoreau, K. Boubekeur, S. Blanchard, R. Thouvenot, A. Proust, J. Am. Chem. Soc. 129 (2007) 7127.
[78] C. Besson, Y.V. Geletii, F. Villain, R. Villanneau, C.L. Hill, A. Proust, Inorg. Chem. 48 (2009) 9436.
[79] S. Romo, N.S. Antonova, J.J. Carbo, J.M. Poblet, Dalton Trans. (2008) 5166.
[80] C.G. Liu, Z.M. Su, W. Guan, L.K. Yan, Inorg. Chem. 48 (2009) 541.
[81] C.G. Liu, W. Guan, L.K. Yan, P. Song, Z.M. Su, Dalton Trans. (2009) 6208.
[82] S.-W. Chen, R. Villanneau, Y. Li, L.-M. Chamoreau, K. Boubekeur, R. Thouvenot, P. Gouzerh, A. Proust, Eur. J. Inorg. Chem. (2008) 2137.
[83] L.D. Dingwall, C.M. Corcoran, A.F. Lee, L. Olivi, J.M. Lynam, K. Wilson, Catal. Commun. 10 (2008) 53.
[84] R. Neumann, C. Abu-Gnim, Chem. Commun. (1989) 1324.
[85] R. Neumann, C. Abu-Gnim, J. Am. Chem. Soc. 112 (1990) 6025.
[86] K. Yamaguchi, N. Mizuno, New J. Chem. 26 (2002) 972.
[87] W.J. Randall, T.J.R. Weakley, R.G. Finke, Inorg. Chem. 32 (1993) 1068.
[88] E.A. Seddon, K.R. Seddon, The Chemistry of Ruthenium, Elsevier, New York, 1984, p. 156.
[89] K. Filipek, Inorg. Chim. Acta 231 (1995) 237.
[90] Y.Y. Matsumoto, M. Asami, M. Hashimoto, M. Misono, J. Mol. Catal. A: Chem. 114 (1996) 161.
[91] E. Steckhan, C. Kandzia, Synlett (1992) 139.
[92] W.L. Sun, Y. Xie, H.Z. Liu, J.L. Kong, S.L. Jin, G.Y. Xie, J.Q. Deng, Indian J. Chem. A: Inorg. Bio-Inorg. Phys. Theor. Anal. Chem. 36 (1997) 1023.
[93] M. Higashijima, Chem. Lett. (1999) 1093.
[94] M. Sadakane, M. Higashijima, J. Chem. Soc. Dalton Trans. (2003) 659.
[95] A.M. Khenkin, I. Efremenko, L. Weiner, J.M.L. Martin, R. Neumann, Chem. Eur. J. 16 (2010) 1356.
[96] M. Sadakane, D. Tsukuma, M.H. Dickman, B. Bassil, U. Kortz, M. Higashijima, W. Ueda, J. Chem. Soc. Dalton Trans. (2006) 4271.
[97] L.H. Bi, U. Kortz, B. Keita, L. Nadjo, J. Chem. Soc. Dalton Trans. (2004) 3184.
[98] M. Sadakane, D. Tsukuma, M.H. Dickman, B. Bassil, U. Kortz, M. Capron, W. Ueda, J. Chem. Soc. Dalton Trans. (2007) 2833.
[99] M. Sadakane, Y. Iimuro, D. Tsukuma, B. Bassil, M.H. Dickman, U. Kortz, Y. Zhang, S. Ye, W. Ueda, J. Chem. Soc. Dalton Trans. (2008) 6692.
[100] L. Bi, U. Kortz, M.H. Dickman, B. Keita, L. Nadjo, Inorg. Chem. 44 (2005) 7485.
[101] L. Bi, E.V. Chubarova, N.H. Nsouli, M.H. Dickman, U. Kortz, B. Keita, L. Nadjo, Inorg. Chem. 45 (2006) 8575.
[102] C. Besson, D.G. Musaev, V. Lahootun, R. Cao, L.M. Chamoreau, R. Villanneau, F. Villain, R. Thouvenot, Y.V. Geletii, C.L. Hill, A. Proust, Chem. Eur. J. 15 (2009) 10233.
[103] D. Laurencin, A. Proust, H. Gerard, Inorg. Chem. 47 (2008) 7888.
[104] D. Quinonero, Y. Wang, K. Morokuma, L.A. Khavrutskii, B. Botar, Y.V. Geletii, C.L. Hill, D.G. Musaev, J. Phys. Chem. B 110 (2006) 170.
[105] D. Quinonero, K. Morokuma, Y.V. Geletii, C.L. Hill, D.G. Musaev, J. Mol. Catal. A: Chem. 262 (2007) 227.
[106] A.E. Kuznetsov, Y.V. Geletii, C.L. Hill, K. Morokuma, D.G. Musaev, J. Am. Chem. Soc. 131 (2009) 6844.
[107] S. Yamaguchi, K. Uehara, K. Kamata, K. Yamaguchi, N. Mizuno, Chem. Lett. 37 (2008) 328.
[108] A. Sartorel, M. Carraro, G. Scorrano, R. De Zorzi, S. Geremia, N.D. McDaniel, S. Bernhard, M. Bonchio, J. Am. Chem. Soc. 130 (2008) 5006.
[109] Y.V. Geletii, B. Botar, P. Kögerler, D.A. Hillesheim, D.G. Musaev, C.L. Hill, Angew. Chem. Int. Ed. 47 (2008) 3896.
[110] A. Sartorel, P. Miro, E. Salvadori, S. Romain, M. Carraro, G. Scorrano, M. Di Valentin, A. Llobet, C. Bo, M. Bonchio, J. Am. Chem. Soc. 131 (2009) 16051.
[111] M. Orlandi, A. Sartorel, M. Carraro, G. Scorrano, M. Bonchio, F. Scandola, Chem. Commun. 46 (2010) 3152.
[112] C. Besson, Z.Q. Huang, Y.V. Geletii, S. Lense, K.I. Hardcastle, D.G. Musaev, T.Q. Lian, A. Proust, C.L. Hill, Chem. Commun. 46 (2010) 2784.
[113] L.H. Bi, G.F. Hou, B. Li, L.X. Wu, U. Kortz, Dalton Trans. (2009) 6345.
[114] V. Artero, A. Proust, P. Herson, F. Villain, C. Cartier dit Moulin, P. Gouzerh, J. Am. Chem. Soc. 125 (2003) 11156.
[115] R. Neumann, A.M. Khenkin, Inorg. Chem. 34 (1995) 5753.
[116] R. Neumann, A.M. Khenkin, M. Dahan, Angew. Chem. Int. Ed. Engl. 34 (1995) 1587.
[117] R. Neumann, M. Dahan, Nature 388 (1997) 353.
[118] R. Neumann, M. Dahan, J. Am. Chem. Soc. 120 (1998) 11969.
[119] H. Weiner, R.G. Finke, J. Am. Chem. Soc. 121 (1999) 9831.
[120] C.X. Yin, R.G. Finke, Inorg. Chem. 44 (2005) 4175.
[121] A.M. Morris, O.P. Anderson, R.G. Finke, Inorg. Chem. 48 (2009) 4411.
[122] R. Neumann, A.M. Khenkin, D. Juwiler, H. Miller, M. Gara, J. Mol. Catal. A: Chem. 117 (1997) 169.
[123] W. Adam, P.L. Alsters, R. Neumann, C.R. Saha-Möller, D. Sloboda-Rozner, R. Zhang, Synlett (2002) 2011.
[124] W. Adam, P.L. Alsters, R. Neumann, C.R. Saha-Möller, D. Sloboda-Rozner, R. Zhang, J. Org. Chem. 68 (2003) 1721.
[125] W. Adam, P.L. Alsters, R. Neumann, C.R. Saha-Möller, D. Seebach, A.K. Beck, R. Zhang, J. Org. Chem. 68 (2003) 8222.
[126] A.R. Howells, A. Sankarraj, C. Shannon, J. Am. Chem. Soc. 126 (2004) 12258.
[127] D. Laurencin, R. Villanneau, P. Herson, R. Thouvenot, Y. Jeannin, A. Proust, Chem. Commun. (2005) 5524.

[128] L.H. Bi, G. Al-Kadamany, E.V. Chubarova, M.H. Dickman, L.F. Chen, D.S. Gopala, R.M. Richards, B. Keita, L. Nadjo, H. Jaensch, G. Mathys, U. Kortz, Inorg. Chem. 48 (2009) 10068.
[129] L.H. Bi, L. Bao, S. Bi, L.-X. Wu, J. Solid State Chem. 182 (2009) 1401.
[130] L.H. Bi, F. Hou, L.X. Wu, U. Kortz, CrystEngComm 11 (2009) 1532.
[131] H. Weiner, J.D. Aiken, R.G. Finke, Inorg. Chem. 35 (1996) 7905.
[132] D.J. Edlund, R.J. Saxton, D.K. Lyon, R.G. Finke, Organometallics 7 (1988) 1692.
[133] M. Pohl, Y. Lin, T.J.R. Weakley, K. Nomiya, M. Kaneko, H. Weiner, R.G. Finke, Inorg. Chem. 34 (1995) 767.
[134] N. Mizuno, D.K. Lyon, R.G. Finke, J. Catal. 128 (1991) 84.
[135] K. Nomiya, Y. Kasahara, Y. Sado, A. Shinohara, Inorg. Chim. Acta 360 (2007) 2313.
[136] H.Z. Liu, B. Yue, W.L. Sun, Z.J. Chen, S.L. Jin, J.Q. Deng, G.Y. Xie, Q.F. Shao, T.L. Wu, Trans. Met. Chem. 22 (1997) 321.
[137] Y. Sakai, A. Shinohara, K. Hayashi, K. Nomiya, Eur. J. Inorg. Chem. (2006) 163.
[138] C.N. Kato, A. Shinohara, N. Moriya, K. Nomiya, Catal. Commun. 7 (2006) 413.
[139] T.L. Jorris, M. Kozik, L.C.W. Baker, Inorg. Chem. 29 (1990) 4584.
[140] R. Ben-Daniel, A.M. Khenkin, R. Neumann, Chem. Eur. J. 6 (2000) 3722.
[141] L.H. Bi, F. Hussain, U. Kortz, M. Sadakane, M.H. Dickman, Chem. Commun. (2004) 1420.
[142] B. Krebs, I. Loose, L. Boesing, A. Noeh, E. Droste, C. R. Acad. Sci. Paris (1998) 351.
[143] L. Bi, M.H. Dickman, U. Kortz, I. Dix, Chem. Commun. (2005) 3962.
[144] S.S. Mal, N.H. Nsouli, M.H. Dickman, U. Kortz, J. Chem. Soc. Dalton Trans. (2007) 2627.
[145] H. Kwen, S. Tomlinson, E.A. Maatta, C. Dablemont, R. Thouvenot, A. Proust, P. Gouzerh, Chem. Commun. (2002) 2970.
[146] L.K. Yan, Z. Dou, W. Guan, S.-Q. Shi, Z.-M. Su, Eur. J. Inorg. Chem. (2006) 5126.
[147] C. Dablemont, C.G. Hamaker, R. Thouvenot, Z. Sojka, M. Che, E.A. Maatta, A. Proust, Chem. Eur. J. 12 (2006) 9150.
[148] L.H. Bi, B. Li, L.X. Wu, K.Z. Shao, Z.M. Su, J. Solid State Chem. 182 (2009) 83.
[149] H. Akashi, K. Isobe, Y. Ozawa, A. Yagasaki, J. Cluster Sci. 2 (1991) 291.
[150] M. Abe, K. Isobe, K. Kida, A. Yagasaki, Inorg. Chem. 35 (1996) 5114.
[151] M. Abe, H. Akashi, K. Isobe, A. Nakanishi, A. Yagasaki, J. Cluster Sci. 7 (1996) 103.
[152] M. Abe, K. Isobe, K. Kida, Y. Nagasawa, A. Yagasaki, J. Cluster Sci. 5 (1994) 565.
[153] Y. Hayashi, Y. Ozawa, K. Isobe, Chem. Lett. (1989) 425.
[154] H.K. Chae, W.G. Klemperer, V.W. Day, Inorg. Chem. 28 (1989) 1423.
[155] Y. Hayashi, Y. Ozawa, K. Isobe, Inorg. Chem. 30 (1991) 1025.
[156] C.J. Zhang, Y. Ozawa, Y. Hayashi, K. Isobe, J. Organomet. Chem. 373 (1989) C21.
[157] K. Takahashi, M. Yamaguchi, T. Shido, H. Ohtani, K. Isobe, M. Ichikawa, J. Chem. Soc. Chem. Commun. (1995) 1301.
[158] M. Ichikawa, W. Pan, Y. Imada, M. Yamaguchi, K. Isobe, T. Shido, J. Mol. Catal. A: Chem. 107 (1996) 23.
[159] M. Yamaguchi, T. Shido, H. Ohtani, K. Isobe, M. Ichikawa, Chem. Lett. (1995) 717.
[160] Y. Hayashi, K. Toriumi, K. Isobe, J. Am. Chem. Soc. 110 (1988) 3666.
[161] Y.K. Do, X.Z. You, C.J. Zhang, Y. Ozawa, K.Y. Isobe, J. Am. Chem. Soc. 113 (1991) 5892.
[162] R.M. Xi, B. Wang, M. Abe, Y. Ozawa, K. Isobe, Chem. Lett. (1994) 1177.
[163] R.M. Xi, B. Wang, Y. Ozawa, M. Abe, K. Isobe, Chem. Lett. (1994) 323.
[164] R.M. Xi, B.T. Wang, K. Isobe, T. Nishioka, K. Toriumi, Y. Ozawa, Inorg. Chem. 33 (1994) 833.
[165] R.M. Xi, B.T. Wang, M. Abe, Y. Ozawa, I. Kinoshita, K. Isobe, Bull. Chem. Soc. Jpn. 72 (1999) 1985.
[166] R.M. Xi, M. Abe, T. Suzuki, T. Nishioka, K. Isobe, J. Organomet. Chem. 549 (1997) 117.
[167] S. Takara, T. Nishioka, I. Kinoshita, K. Isobe, Chem. Commun. (1997) 891.
[168] S. Takara, S. Ogo, Y. Watanabe, K. Nishikawa, I. Kinoshita, K. Isobe, Angew. Chem. Int. Ed. 38 (1999) 3051.
[169] Y. Imada, T. Shido, R. Ohnishi, K. Isobe, M. Ichikawa, Catal. Lett. 38 (1996) 101.
[170] A. Proust, P. Gouzerh, F. Robert, Angew. Chem. Int. Ed. Engl. 32 (1993) 115.
[171] R. Villanneau, A. Proust, F. Robert, F. Villain, M. Verdaguer, P. Gouzerh, Polyhedron 22 (2003) 1157.
[172] Y. Ozawa, Y. Hayashi, K. Isobe, Acta Cryst. C 47 (1991) 637.
[173] C.I. Cabello, I.L. Botto, M. Munoz, H.J. Thomas, Scientific Bases for the Preparation of Heterogeneous Catalysts, 143, 2002, p. 565.
[174] C.I. Cabello, M. Munoz, I.L. Botto, E. Payen, Thermochim. Acta 447 (2006) 22.
[175] A.M. Kijak, R.K. Perdue, J.A. Cox, J. Solid State Electrochem. 8 (2004) 376.
[176] H.K. Chae, W.G. Klemperer, D.E. Paez-Loyo, V.W. Day, T.A. Eberspacher, Inorg. Chem. 31 (1992) 3187.
[177] K. Nishikawa, K. Kido, J. Yoshida, T. Nishioka, I. Kinoshita, B.K. Breedlove, Y. Hayashi, A. Uehara, K. Isobe, Appl. Organomet. Chem. 17 (2003) 446.
[178] C.J. Besecker, W.G. Klemperer, V.W. Day, J. Am. Chem. Soc. 104 (1982) 6158.
[179] W.G. Klemperer, D.J. Main, Inorg. Chem. 29 (1990) 2355.
[180] C.J. Besecker, V.W. Day, W.G. Klemperer, M.R. Thompson, J. Am. Chem. Soc. 106 (1984) 4125.
[181] W.H. Knoth, J. Am. Chem. Soc. 101 (1979) 2211.
[182] F. Zonnevijlle, C.M. Tourné, G.F. Tourné, Inorg. Chem. 21 (1982) 2751.
[183] X. Wei, R.E. Bachman, M.T. Pope, J. Am. Chem. Soc. 120 (1998) 10248.
[184] X. Wei, M.H. Dickman, M.T. Pope, J. Am. Chem. Soc. 120 (1998) 10254.
[185] Z.Y. Wei, M.H. Dickman, M.T. Pope, Inorg. Chem. 36 (1997), 130-&.
[186] M.E. Tess, J.A. Cox, Electroanalysis 10 (1998) 1237.
[187] J.A. Cox, S.D. Holmstrom, M.E. Tess, Talanta 52 (2000) 1081.
[188] N.N. Sveshnikov, M.H. Dickman, M.T. Pope, Inorg. Chim. Acta 359 (2006) 2721.
[189] N. Ban, B. Freeborn, P. Nissen, P. Penczek, R.A. Grassucci, R. Sweet, J. Frank, P.B. Moore, T.A. Steitz, Cell 93 (1998) 1105.
[190] N. Ban, P. Nissen, J. Hansen, M. Capel, P.B. Moore, T.A. Steitz, Nature 400 (1999) 841.
[191] R.G. Finke, M.W. Droege, J. Am. Chem. Soc. 106 (1984) 7274.
[192] K. Nomiya, C. Nozaki, A. Kano, T. Taguchi, K. Ohsawa, J. Organomet. Chem. 533 (1997) 153.
[193] K. Nomiya, Y. Sakai, Y. Yamada, T. Hasegawa, J. Chem. Soc. Dalton Trans. (2001) 52.
[194] R.L. Augustine, S. Tanielyan, S. Anderson, H. Yang, Chem. Commun. (1999) 1257.
[195] R.L. Augustine, S.K. Tanielyan, N. Mahata, Y. Gao, A. Zsigmond, H. Yang, Appl. Catal. A: Gen. 256 (2003) 69.
[196] R.L. Augustine, P. Goel, N. Mahata, C. Reyes, S.K. Tanielyan, J. Mol. Catal. A: Chem. 216 (2004) 189.
[197] A. Zsigmond, K. Bogar, F. Notheisz, J. Catal. 213 (2003) 103.
[198] I. Bar-Nahum, R. Neumann, Chem. Commun. (2003) 2690.
[199] R. Neumann, A.M. Khenkin, J. Mol. Catal. A: Chem. 114 (1996) 169.
[200] C.A. Ciocan, G.L. Turdean, C. Rosu, M. Rusu, Rev. Roum. Chim. 49 (2004) 279.
[201] K. Nomiya, C. Nozaki, M. Kaneko, R.G. Finke, M. Pohl, J. Organomet. Chem. 505 (1995) 23.
[202] M. Pohl, D.K. Lyon, N. Mizuno, K. Nomiya, R.G. Finke, Inorg. Chem. 34 (1995) 1413.
[203] T. Nagata, M. Pohl, H. Weiner, R.G. Finke, Inorg. Chem. 36 (1997) 1366.
[204] K. Nomiya, T. Hasegawa, Chem. Lett. (2000) 410.
[205] K. Nomiya, Y. Sakai, T. Hasegawa, J. Chem. Soc. Dalton Trans. (2002) 252.
[206] V.W. Day, W.G. Klemperer, A. Yagasaki, Chem. Lett. (1990) 1267.
[207] Y. Hayashi, F. Müller, Y. Lin, S.M. Miller, O.P. Anderson, R.G. Finke, J. Am. Chem. Soc. 119 (1997) 11401.
[208] W.G. Klemperer, A. Yagasaki, Chem. Lett. (1989) 2041.
[209] V.W. Day, W.G. Klemperer, D.J. Main, Inorg. Chem. 29 (1990) 2345.
[210] Y. Lin, K. Nomiya, R.G. Finke, Inorg. Chem. 32 (1993) 6040.
[211] H.Z. Liu, W.L. Sun, B. Yue, S.L. Jin, J.Q. Deng, G.Y. Xie, Synth. React. Inorg. Met. Org. Chem. 27 (1997) 551.
[212] W.L. Sun, H.Z. Liu, J.L. Kong, G.Y. Xie, J.Q. Deng, J. Electroanal. Chem. 437 (1997) 67.
[213] R.G. Finke, D.K. Lyon, K. Nomiya, T.J.R. Weakley, Acta Cryst. C 46 (1990) 1592.
[214] R.G. Finke, D.K. Lyon, K. Nomiya, S. Sur, N. Mizuno, Inorg. Chem. 29 (1990) 1784.
[215] M. Pohl, R.G. Finke, Organometallics 12 (1993) 1453.
[216] A. Trovarelli, R.G. Finke, Inorg. Chem. 32 (1993) 6034.
[217] D.K. Lyon, R.G. Finke, Inorg. Chem. 29 (1990) 1787.
[218] Y. Lin, R.G. Finke, J. Am. Chem. Soc. 116 (1994) 8335.
[219] H. Weiner, A. Trovarelli, R.G. Finke, J. Mol. Catal. A: Chem. 191 (2003) 217.
[220] H. Weiner, A. Trovarelli, R.G. Finke, J. Mol. Catal. A: Chem. 191 (2003) 253.
[221] N. Mizuno, H. Weiner, R.G. Finke, J. Mol. Catal. A: Chem. 114 (1996) 15.
[222] W.L. Sun, F. Yang, H.Z. Liu, J.L. Kong, S.L. Jin, G.Y. Xie, J.Q. Deng, J. Electroanal. Chem. 451 (1998) 49.
[223] R. Cao, H.Y. Ma, Y.V. Geletii, K.I. Hardcastle, C.L. Hill, Inorg. Chem. 48 (2009) 5596.
[224] Y. Hayashi, N. Miyakoshi, T. Shinguchi, A. Uehara, Chem. Lett. (2001) 170.
[225] T. Kurata, A. Uehara, Y. Hayashi, K. Isobe, Inorg. Chem. 44 (2005) 2524.
[226] S. Angus-Dunne, R.C. Burns, D.C. Craig, G.A. Lawrance, Z. anorg. allg. Chem. 636 (2010) 727.
[227] L.G. Detusheva, L.I. Kuznetsova, M.A. Fedotov, L.S. Dovlitova, A.A. Vlasov, V.A. Likholobov, V.V. Malakhov, Russian J. Inorg. Chem. 48 (2003) 1685.
[228] S.J. Angus-Dunne, R.C. Burns, D.C. Craig, G.A. Lawrance, Chem. Commun. (1994) 523.
[229] N.I. Kuznetsova, L.G. Detusheva, L.I. Kuznetsova, M.A. Fedotov, V.A. Likholobov, J. Mol. Catal. A: Chem. 114 (1996) 131.
[230] N.I. Kuznetsova, L.I. Kuznetsova, L.G. Detusheva, V.A. Likholobov, M.A. Fedotov, S.V. Koscheev, E.B. Burgina, in: R.K. Grasselli, S.T. Oyama, A.M. Gaffney, J.E. Lyons (Eds.), O-2/H-2 oxidation of hydrocarbons on the catalysts prepared from Pd(II) complexes with heteropolytungstates, Elsevier Science Publ. B.V., San Diego, CA, 1997, p. 1203.
[231] V. Kogan, Z. Aizenshtat, R. Neumann, New J. Chem. 26 (2002) 272.
[232] V. Kogan, Z. Aizenshtat, R. Popovitz-Biro, R. Neumann, Org. Lett. 4 (2002) 3529.
[233] P.A. Korovchenko, R.A. Gazarov, A.Y. Stakheev, L.M. Kustov, Russian Chem. Bull. 48 (1999) 1261.
[234] N.A. Vladimirov, P.A. Korovchenko, R.A. Gazarov, L.M. Kustov, A.V. Ivanov, Russian Chem. Bull. 52 (2003) 2382.
[235] Y. Xie, W.L. Sun, H.Z. Liu, J.L. Kong, G.Y. Xie, J.Q. Deng, Anal. Lett. 31 (1998) 2009.
[236] W.L. Sun, S. Zhang, H.Z. Liu, L.T. Jin, J. Kong, Anal. Chim. Acta 388 (1999) 103.
[237] I. Bar-Nahum, H. Cohen, R. Neumann, Inorg. Chem. 42 (2003) 3677.
[238] T.M. Anderson, R. Cao, E. Slonkina, B. Hedman, K.O. Hodgson, K.I. Hardcastle, W.A. Neiwert, S. Wu, M.L. Kirk, S. Knottenbelt, E.C. Depperman, B. Keita, D.G. Musaev, K. Morokuma, C.L. Hill, J. Am. Chem. Soc. 127 (2005) 11948.
[239] T.M. Anderson, R. Cao, E. Slonkina, B. Hedman, K.O. Hodgson, K.I. Hardcastle, W.A. Neiwert, S.X. Wu, M.L. Kirk, S. Knottenbelt, E.C. Depperman, B. Keita, L. Nadjo, D.G. Musaev, K. Morokuma, C.L. Hill, J. Am. Chem. Soc. 130 (2008) 2877.
[240] U. Kortz, U. Lee, H.-C. Joo, K.-M. Park, S.S. Mal, M.H. Dickman, G.B. Jameson, Angew. Chem. 47 (2008) 9383.
[241] W.H. Knoth, P.J. Domaille, R.D. Farlee, Organometallics 4 (1985) 62.
[242] W.H. Knoth, P.J. Domaille, R.L. Harlow, Inorg. Chem. 25 (1986) 1577.

[243] L.G. Detusheva, L.I. Kuznetsova, M.A. Fedotov, V.A. Likholobov, L.S. Dovlitova, A.A. Vlasov, V.V. Malakhov, Russian J. Coord. Chem. 27 (2001) 838.
[244] L.I. Kuznetsova, N.I. Kuznetsova, L.G. Detusheva, M.A. Fedotov, V.A. Likholobov, J. Mol. Catal. A: Chem. 158 (2000) 429.
[245] R. Villanneau, S. Renaudineau, P. Herson, K. Boubekeur, R. Thouvenot, A. Proust, Eur. J. Inorg. Chem. (2009) 479.
[246] L. Bi, U. Kortz, B. Keita, L. Nadjo, H. Borrmann, Inorg. Chem. 43 (2004) 8367.
[247] C.M. Tourné, G.F. Tourné, F. Zonnevijlle, J. Chem. Soc. Dalton Trans. (1991) 143.
[248] D. Barats, R. Neumann, Adv. Synth. Catal. 352 (2010) 293.
[249] L. Bi, M. Reicke, U. Kortz, B. Keita, L. Nadjo, R.J. Clark, Inorg. Chem. 43 (2004) 3915.
[250] L. Bi, U. Kortz, B. Keita, L. Nadjo, L. Daniels, Eur. J. Inorg. Chem. (2005) 3034.
[251] L.G. Detusheva, L.I. Kuznetsova, N.I. Kuznetsova, L.S. Dovlitova, A.A. Vlasov, V.A. Likholobov, Russian J. Inorg. Chem. 53 (2008) 690.
[252] L.H. Bi, M.H. Dickman, U. Kortz, CrystEngComm 11 (2009) 965.
[253] U. Lee, H.-C. Joo, K.-M. Park, S.S. Mal, U. Kortz, B. Keita, L. Nadjo, Angew. Chem. 47 (2008) 793.
[254] R. Cao, T.M. Anderson, D.A. Hillesheim, P. Koegerler, K.I. Hardcastle, C.L. Hill, Angew. Chem. 47 (2008) 9380.
[255] A. Bagno, R. Bini, Angew. Chem. Int. Ed. 49 (2010) 1083.
[256] N. Vankova, T. Heine, U. Kortz, Eur. J. Inorg. Chem. 2009 (2009) 5102.
[257] U. Kortz, U. Lee, H.C. Joo, K.M. Park, S.S. Mal, M.H. Dickman, G.B. Jameson, Angew. Chem. Int. Ed. 47 (2008) 9383.
[258] V.W. Day, J.C. Goloboy, W.G. Klemperer, Eur. J. Inorg. Chem. (2009) 5079.
[259] T. Liu, K. Asakura, U. Lee, Y. Matsui, Y. Iwasawa, J. Catal. 135 (1992) 367.
[260] D.I. Kondarides, K. Tomishige, Y. Nagasawa, U. Lee, Y. Iwasawa, J. Mol. Catal. A: Chem. 111 (1996) 145.
[261] U. Lee, H.C. Joo, Acta Cryst. E 60 (2004) I61.
[262] U. Lee, H.C. Joo, Acta Cryst. C 56 (2000) E311.
[263] U. Lee, Bull. Korean Chem. Soc. 9 (1988) 256.
[264] H.C. Joo, K.M. Park, U. Lee, Acta Cryst. C 50 (1994) 1659.
[265] U. Lee, Y. Sasaki, Chem. Lett. (1984) 1297.
[266] U. Lee, Y. Sasaki, Bull. Korean Chem. Soc. 15 (1994) 37.
[267] U. Lee, H.C. Joo, Acta Cryst. E 63 (2007) I11.
[268] U. Lee, H.C. Joo, Acta Cryst. E 62 (2006) I241.
[269] U. Lee, Acta Cryst. C 50 (1994) 1657.
[270] U. Lee, H.C. Joo, Acta Cryst. E 62 (2006) I231.
[271] U. Lee, S.J. Jang, H.C. Joo, K.M. Park, Acta Cryst. E 59 (2003) M116.
[272] U. Lee, H. Ichida, A. Kobayashi, Y. Sasaki, Acta Cryst. C 40 (1984) 5.
[273] U. Lee, H.C. Joo, Acta Cryst. E 60 (2004) I86.
[274] U. Lee, H.C. Joo, K.M. Park, Acta Cryst. E 60 (2004) I55.
[275] U. Lee, H.C. Joo, Acta Cryst. E 60 (2004) I33.
[276] U. Lee, A. Kobayashi, Y. Sasaki, Acta Cryst. C 39 (1983) 817.
[277] U. Lee, Acta Cryst. E 58 (2002) I130.
[278] U. Lee, Y. Sasaki, J. Korean Chem. Soc. 31 (1987) 118.
[279] H. Nakajima, I. Honma, Electrochem. Solid State Lett. 7 (2004) 135.
[280] P.A. Korovchenko, N.A. Vladimirov, R.A. Gazarov, L.M. Kustov, Russian Chem. Bull. 52 (2003) 2376.
[281] U. Lee, H.C. Joo, K.M. Park, T. Ozeki, Acta Cryst. C 59 (2003) M152.
[282] A. Thomas, PhD Thesis, Université Claude Bernard, Lyon 1, Lyon, France, 2007.
[283] N. Legagneux, PhD Thesis, Université Claude Bernard, Lyon 1, Lyon, France, 2009.
[284] T.M. Anderson, W.A. Neiwert, M.L. Kirk, P.M.B. Piccoli, A.J. Schultz, T.F. Koetzle, D.G. Musaev, K. Morokuma, R. Cao, C.L. Hill, Science 306 (2004) 2074.
[285] K. Nomiya, H. Torii, C.N. Kato, Y. Sado, Chem. Lett. 32 (2003) 664.
[286] G.G. Gao, P.S. Cheng, T.C.W. Mak, J. Am. Chem. Soc. 131 (2009) 18257.
[287] C. Streb, R. Tsunashima, D.A. MacLaren, T. McGlone, T. Akutagawa, T. Nakamura, A. Scandurra, B. Pignataro, N. Gadegaard, L. Cronin, Angew. Chem. Int. Ed. 48 (2009) 6490.
[288] R. Villanneau, A. Proust, F. Robert, P. Gouzerh, Chem. Commun. (1998) 1491.
[289] H.Y. An, Y.G. Li, E.B. Wang, D.R. Xiao, C.Y. Sun, L. Xu, Inorg. Chem. 44 (2005) 6062.
[290] Y.F. Song, H. Abbas, C. Ritchie, N. McMillian, D.-L. Long, N. Gadegaard, L. Cronin, J. Mater. Chem. 17 (2007) 1903.
[291] F.X. Liu, C. Marchal-Roch, D. Dambournet, A. Acker, J. Marrot, F. Sécheresse, Eur. J. Inorg. Chem. (2008) 2191.
[292] H.Y. An, Y.G. Li, D.R. Xiao, E.B. Wang, C.Y. Sun, Cryst. Growth Des. 6 (2006) 1107.
[293] H. Abbas, A.L. Pickering, D.L. Long, P. Kögerler, L. Cronin, Chem. Eur. J. 11 (2005) 1071.
[294] S.M. Chen, C.Z. Lu, Y.Q. Yu, Q.Z. Zhang, X. He, Inorg. Chem. Commun. 7 (2004) 1041.
[295] H. Abbas, C. Streb, A.L. Pickering, A.R. Neil, D.-L. Long, L. Cronin, Cryst. Growth Des. 8 (2008) 635.
[296] Q.-G. Zhai, X.-Y. Wu, S.-M. Chen, Z.-G. Zhao, C.-Z. Lu, Inorg. Chem. 46 (2007) 5046.
[297] E. Burkholder, J. Zubieta, Solid State Sci. 6 (2004) 1421.
[298] J.T. Rhule, W.A. Neiwert, K.I. Hardcastle, B.T. Do, C.L. Hill, J. Am. Chem. Soc. 123 (2001) 12101.
[299] J. Lu, F.-X. Xiao, L.-X. Shi, R. Cao, J. Solid State Chem. 181 (2008) 313.
[300] Y.P. Ren, X.J. Kong, L.S. Long, R.B. Huang, L.S. Zheng, Cryst. Growth Des. 6 (2006) 572.
[301] B.J.S. Johnson, R.C. Schroden, C.C. Zhu, V.G. Young, A. Stein, Inorg. Chem. 41 (2002) 2213.
[302] L.M. Dai, W.S. You, E.B. Wang, S.X. Wu, Z.M. Su, Q.H. Du, Y. Zhao, Y. Fang, Cryst. Growth Des. 9 (2009) 2110.
[303] Y.-Q. Lan, S.-L. Li, K.-Z. Shao, X.-L. Wang, Z.-M. Su, J. Chem. Soc. Dalton Trans. (2008) 3824.
[304] D.B. Dang, H. Gao, Y. Bai, X.F. Hu, F. Yang, Y. Chen, J.Y. Niu, Inorg. Chem. Commun. 13 (2010) 37.
[305] F.-X. Liu, C. Marchal-Roch, P. Bouchard, J. Marrot, J.-P. Simonato, G. Hervé, F. Sécheresse, Inorg. Chem. 43 (2004) 2240.
[306] E.F. Wilson, H. Abbas, B.J. Duncombe, C. Streb, D.L. Long, L. Cronin, J. Am. Chem. Soc. 130 (2008) 13876.
[307] J. Qiao, K. Shi, Q.M. Wang, Angew. Chem. Int. Ed. 49 (2010) 1765.
[308] X.L. Zhao, T.C.W. Mak, Inorg. Chem. 49 (2010) 3676.
[309] M.X. Yang, S. Lin, L.J. Chen, X.F. Zhang, H.H. Xu, Inorg. Chem. Commun. 12 (2009) 566.
[310] G. Luan, Y. Li, S. Wang, E. Wang, Z. Han, C. Hu, N. Hu, H. Jia, J. Chem. Soc. Dalton Trans. (2003) 233.
[311] L. Yuan, C. Qin, X.L. Wang, Y.G. Li, E.B. Wang, Dalton Trans. (2009) 4169.
[312] S. Duval, A.-M. Pilette, J. Marrot, C. Simonnet-Jegat, M. Sokolov, E. Cadot, Chem. Eur. J. 14 (2008) 3457.
[313] H.J. Pang, J. Chen, J. Peng, J. Sha, Z.-Y. Shi, A.-X. Tian, P.-P. Zhang, Solid State Sci. 11 (2009) 824.
[314] L. Zeng, Y.Q. Chen, G.C. Liu, J.X. Zhang, J. Mol. Struct. 930 (2009) 176.
[315] H.I.S. Nogueira, F.A.A. Paz, P.A.F. Teixeira, J. Klinowski, Chem. Commun. (2006) 2953.
[316] H.X. Yang, S.Y. Gao, J. Lu, B. Xu, J.X. Lin, R. Cao, Inorg. Chem. 49 (2010) 736.
[317] Z.G. Han, Y.L. Zhao, J. Peng, H.Y. Ma, Q. Liu, E.B. Wang, N.H. Hu, H.Q. Jia, Eur. J. Inorg. Chem. (2005) 264.
[318] H. Pang, C. Zhang, D. Shi, Y. Chen, Cryst. Growth Des. 8 (2008) 4476.
[319] J. Meng, X. Wang, Y. Ma, E. Wang, X. Xu, J. Coord. Chem. 61 (2008) 2853.
[320] J.Q. Sha, J. Peng, H.J. Pang, A.X. Tian, J. Chen, P.P. Zhang, M. Zhu, Solid State Sci. 10 (2008) 1491.
[321] J. Chen, J.Q. Sha, J. Peng, Z.Y. Shi, A.X. Tian, P.P. Zhang, J. Mol. Struct. 917 (2009) 10.
[322] C.J. Zhang, Y.G. Chen, H.J. Pang, D.M. Shi, M.X. Hu, J. Li, Inorg. Chem. Commun. 11 (2008) 765.
[323] C. Streb, C. Ritchie, D.-L. Long, P. Koegerler, L. Cronin, Angew. Chem. Int. Ed. 46 (2007) 7579.
[324] Y.-P. Ren, X.-J. Kong, X.-Y. Hu, M. Sun, L.-S. Long, R.-B. Huang, L.-S. Zheng, Inorg. Chem. 45 (2006) 4016.
[325] J.X. Chen, T.Y. Lan, Y.B. Huang, C.X. Wei, Z.S. Li, Z.C. Zhang, J. Solid State Chem. 179 (2006) 1904.
[326] J.Q. Sha, J. Peng, Y.A. Lan, Z.M. Su, H.J. Pang, A.X. Tian, P.P. Zhang, M. Zhu, Inorg. Chem. 47 (2008) 5145.
[327] H.J. Pang, J. Peng, J.Q. Sha, A.X. Tian, P.P. Zhang, Y. Chen, M. Zhu, J. Mol. Struct. 921 (2009) 289.
[328] J.Q. Sha, J. Peng, Y.G. Li, P.P. Zhang, H.J. Pang, Inorg. Chem. Commun. 11 (2008) 907.
[329] M. Leyrie, G. Hervé, New J. Chem. 2 (1978) 233.
[330] F. Robert, M. Leyrie, G. Hervé, A. Tézé, Y. Jeannin, Inorg. Chem. 19 (1980) 1746.
[331] R. Cao, T.M. Anderson, P.M.B. Piccoli, A.J. Schultz, T.F. Koetzle, Y.V. Geletii, E. Slonkina, B. Hedman, K.O. Hodgson, K.I. Hardcastle, X. Fang, M.L. Kirk, S. Knottenbelt, P. Kögerler, D.G. Musaev, K. Morokuma, M. Takahashi, C.L. Hill, J. Am. Chem. Soc. 129 (2007) 11118.
[332] N.V. Izarova, N. Vankova, T. Heine, R.N. Biboum, B. Keita, L. Nadjo, U. Kortz, Angew. Chem. Int. Ed. 49 (2010) 1886.
[333] N.V. Izarova, M.H. Dickman, R.N. Biboum, B. Keita, L. Nadjo, V. Ramachandran, N.S. Dalal, U. Kortz, Inorg. Chem. 48 (2009) 7504.